# Ultraviolet radiation and primary production by Lake Erie phytoplankton communities

by

Véronique P. Hiriart

A thesis

presented to the University of Waterloo

in fulfilment of the

thesis requirement for the degree of

Doctor of Philosophy

in

Biology

Waterloo, Ontario, Canada, 2000

©Véronique P. Hiriart, 2000

National Library of Canada
Acquisitions and Bibliographic Services
395 Wellington Street
Ottawa ON K1A 0N4
Canada

Bibliothèque nationale du Canada
Acquisitions et services bibliographiques
395, rue Wellington
Ottawa ON K1A 0N4
Canada

*Your file Votre référence*

*Our file Notre référence*

The author has granted a non-exclusive licence allowing the National Library of Canada to reproduce, loan, distribute or sell copies of this thesis in microform, paper or electronic formats.

L'auteur a accordé une licence non exclusive permettant à la Bibliothèque nationale du Canada de reproduire, prêter, distribuer ou vendre des copies de cette thèse sous la forme de microfiche/film, de reproduction sur papier ou sur format électronique.

The author retains ownership of the copyright in this thesis. Neither the thesis nor substantial extracts from it may be printed or otherwise reproduced without the author's permission.

L'auteur conserve la propriété du droit d'auteur qui protège cette thèse. Ni la thèse ni des extraits substantiels de celle-ci ne doivent être imprimés ou autrement reproduits sans son autorisation.

0-612-53496-0

Canada

The University of Waterloo requires the signatures of all persons using or photocopying this thesis. Please sign below, and give address and date.

## General Abstract

The aim of this work was to investigate and quantify the effects of ultraviolet radiation (UVR) in L. Erie phytoplankton communities. Briefly, primary production, measured as $^{14}C$ incorporation over time, was determined during the late spring and summer months of 1997 and 1998. While all three basins of L. Erie were sampled, the East basin was under represented relative to both the Central and West basins. In all experiments, determination of the effects of UVR on primary production was carried out using natural solar radiation which was selectively screened by various optical filters or modified using ultraviolet B (UVB) lamps.

In L. Erie, UVB inhibited primary production severely (58%) but only in very severe exposures, as would be experienced at the surface. The kinetics of inhibition were, however, rapid suggesting that short exposures, as would occur under mixing, could result in significant inhibition. No simple and strong relationships could be identified between the efficiency of UVB in inducing photoinhibition and measures of phytoplankton light history or micro- and nanoplankton dominant genera. However, UVB inhibition efficiency was higher for phosphorus (P) deficient than P-replete algal assemblages. UVR significantly affected the proportion of production in the particulate (POC; <2 and >2 μm) and dissolved (DOC) organic carbon pools resulting in higher production of DOC and reduced production in the small particulate carbon fraction (i.e. picoplankton). UVR may, therefore, have important effects on the carbon flow dynamics of for near-surface populations of L. Erie. Additionally, basin-specific PAR and UVR transmission properties showed that the West basin of L. Erie is potentially more susceptible to UVR photoinhibition than either the East or Central basins. However, predictions of the effects of UVR on primary production remain elusive without

further model development. Furthermore, evidence of a significant role for UVA as an inhibitor of primary production underscores the need for a more inclusive approach, that is modelling photoinhibition in terms of total spectral effects.

A new model (the R model) for the response of photosynthetic carbon fixation to UVR was formulated, allowing finite rates of recovery and the incorporation of wavelength interactions, and was tested against observations on phytoplankton communities in L. Erie. Additionally, biological weighting functions (BWFs), the first for freshwater phytoplankton assemblages, were determined. The application of both the R model and the BWFs successfully described the kinetics of UVR- and PAR-dependent photoinhibition in L. Erie. These results indicated that, in this large lake, recovery rate processes were active yet not in equilibrium with damage rate processes and that variations both in spectral sensitivity (expressed by the BWFs) and recovery rate constants were important determinants of phytoplankton response to UVR.

Possessing both measures of spectral sensitivity and recovery rates, losses of daily production were calculated under mixing and water transparency scenarios that span the common range of conditions in L. Erie. Predictions of daily integrated photoinhibition ($PI_{int}$) were insensitive to variations in mixing rates, although, simulated mixed conditions always resulted in higher daily losses of production than simulated motionless water column. The contribution of each spectral waveband to $PI_{int}$ also varied little with mixing scenarios. Unexpectedly, $PI_{int}$ was always highest in the relatively turbid, and shallow West basin, regardless of the mixing scenario. Furthermore, this inhibition was enhanced when the presence of shallow 'temporary' thermoclines, which frequently develop in this basin, was simulated. Although ozone depletion is a major concern, a simulated 20% reduction of ozone over L. Erie

resulted in a minimal increase of $PI_{int}$ even in the relatively sensitive West basin. Sensitivity analysis revealed that variations of phytoplankton susceptibility to UVR, and of their recovery rates, over the ranges observed to date in L. Erie, could lead to 5% to 20% loss of production under normal mixing conditions.

Overall, UVA, rather than UVB or PAR, appears to be the major waveband responsible for photoinhibition of primary production in L. Erie. The impacts of climate change and human activity on transmission of UVA are therefore more of a concern than ozone-related variations of UVB for primary production in the Laurentian Great Lakes.

Acknowledgments

I would like to thank my supervisor, Ralph Smith, for his patience and support. Under his guidance I learned to think critically and I will always be thankful for that. I would like to thank my committee members Drs. Bruce Greenberg and Bill Taylor. I would like to thank Jenni Kerteston for her invaluable help on the boat and in the laboratory and also for putting up with me. I would like to thank the captain and crew of the Limnos for their help and flexibility in the field. I would like to thank all the friends (John, Lisa, Steve, Chris A., Chris M., Chris S., Mark H., Mark L., Jenny, Rachael, Jim, Janet, Karin, Andrea, Sherwin, Leo1, Leo2, Neil, Gen, Jane, Yuxiang, insert name I forgot here) I've made in Waterloo, you kept me sane when you weren't driving me crazy. Last but not least I'd like to thank Bill Baer for being there for me when I needed support, and for believing in me when I had lost faith.

I dedicate this thesis to my mother who supported me through all my ups and downs. Without her support I wouldn't have made it.

Véronique

# Table of Contents

General Abstract . . . . . iv

Acknowledgments . . . . . vii

Dedication. . . . . viii

Table of Contents . . . . . ix

List of Tables . . . . . xiii

List of Figures . . . . . xv

Chapter 1

Introduction . . . . . 1

Primary Production . . . . . 2

Light Availability . . . . . 5

Ultraviolet Radiation in the Environment . . . . . 7

Mechanisms of Action of UVR . . . . . 10

Changes in the Chemical Environment . . . . . 10

Biological Effects . . . . . 10

Protection and Repair Mechanisms . . . . . 13

Protection . . . . . 13

Repair . . . . . 14

Biological Weighting Functions . . . . . 16

Objectives . . . . . 17

Chapter 2

Effects of ultraviolet B radiation on rates and size distribution of primary production

by Lake Erie phytoplankton ..... 19

Abstract ..... 20

Introduction ..... 22

Materials and Methods ..... 25

Study Site ..... 25

Experimental Design and Sampling Protocol ..... 25

Measures of response to UVR and PAR ..... 33

Nutrient Status ..... 34

Statistical Analysis ..... 35

Results ..... 36

Limnological Conditions ..... 36

Phytoplankton Characteristics ..... 38

Time Course and Extent of UVB Inhibition ..... 41

Inhibition Efficiency of UVB ..... 47

UVB Effects on Particulate and Dissolved Organic Carbon Production ..... 52

Expected UVB Impacts in L. Erie ..... 54

Discussion ..... 57

Chapter 3

Models for UVR-dependent photoinhibition of Lake Erie phytoplankton ..... 65

Abstract ..... 66

Introduction ..... 67

Materials and methods ..... 71

Theory ..... 71

Statistical Analysis ..... 75

Biological Weighting Functions ..... 77

Study Site ..... 78

Experimental Procedures ..... 81

Results ..... 83

Limnological conditions ..... 83

Performance of limiting case models in 1997 ..... 86

Calibration of the R model and BWF derivation ..... 90

Application of the R model to 1997 observations ..... 100

Discussion ..... 104

Chapter 4

The impact of ultraviolet radiation onvertically-integrated primary production in L. Erie:

The role of recovery and mixing processes ..... 113

Abstract ..... 114

Introduction ..... 116

Methods and Materials ..... 119

Theory ..... 119

Experimental Procedures ..... 120

Modelling of Lake Erie ..... 121

Statistical Analysis . . . . . 125

Results . . . . . 128

Limnological Conditions . . . . . 128

UVR-Dependent Inhibition and Recovery of Photosynthesis . . . . . 128

Recovery Rate Constants and Associated Recovery Times . . . . . 132

Modelling Inhibition of Integrated Primary Production

in a Mixed Water Column . . . . . 135

Discussion . . . . . 144

Chapter 5

Conclusions . . . . . 154

General Conclusions. . . . . 155

Future Directions. . . . . .159

Chapter 6

Reference List . . . . . 161

## List of Tables

Table 2.1: Summary of limnological variables of the stations sampled for time-series experiments conducted on L. Erie between the months of May and August 1997 . . . . . 28

Table 2.2: Percent photosynthetically active radiation (PAR), ultraviolet A (UVA) and ultraviolet B (UVB) radiation in the different spectral treatments of the time series experiments . . . . . 32

Table 2.3: Dominant nano- and microphytoplankton genera, photosynthesis parameters, nutrient status and $UVB_{inh\,eff}$ for the different stations sampled in L. Erie . . . . . 42

Table 2.4: Average percent UVB-dependent inhibition of cumulative photosynthesis (PS) found following 1h and 8h of exposure to different spectral treatments and the 1h and 8h $UVB_{inh\,eff}$ values for the different UVB exposure levels . . . . . 46

Table 2.5: Average percent partial UVA-dependent inhibition of cumulative photosynthesis (PS) found following 1h and 8h exposure to different spectral treatments . . . . . 48

Table 2.6: Average percent of total organic production (% TO$^{14}$C) of eight experiments (May 7 and July 1 not included in analysis) in the different carbon pools for each treatment . . . . . 53

Table 2.7: Water column depths represented by each UVB exposure level treatment, calculated using basin specific median PAR, UVA and UVB broadband attenuation coefficients . . . . . 55

Table 3.1: Summary of limnological variables of the stations sampled for time-series experiments conducted on L. Erie between the months of May and August 1997 and June and August 1998 ..... 84

Table 3.2: Nutrient status and light history/adaptation indicators for the algal assemblages sampled in 1997 and the amount of variance in photosynthesis explained by the E and H models ..... 89

Table 3.3: Summary of the statistical analysis of algal photoinhibition using the repair model for L. Erie phytoplankton ..... 91

Table 4.1: Summary of the limnological variables of the stations sampled for time-series recovery experiments conducted on L. Erie in the summers of 1997 and 1998 ..... 129

Table 4.2: Relative cumulative photosynthesis for each spectral treatment following 2h of exposure just before being transferred to the benign recovery deck boxes (initial) and following 6h of recovery (final) ..... 131

Table 4.3: Experimentally determined recovery rates for the different spectral treatments averaged over all sample dates ..... 133

Table 4.4: Measured and modelled estimates of recovery rate constants for each experimental date ..... 134

## List of Figures

Figure 2.1: Lake Erie and the lake stations sampled throughout the summer of 1997 for time-series experiments . . . . . 26

Figure 2.2: Percent transmission of UVR wavelengths for the different 100% PAR spectral treatments . . . . . 31

Figure 2.3: Percent light transmission in the East (a), Central (b) and West (c) basins of L. Erie . . . . . 37

Figure 2.4: Temperature and *in vivo* chl *a* fluorescence profile from station 357 sampled June 4, 1997 . . . . . 39

Figure 2.5: Temperature and *in vivo* chl *a* fluorescence profiles from station 23 sampled July 29 (a) and July 1 (b) 1997 . . . . . 40

Figure 2.6: Instantaneous photosynthetic rates, cumulative photosynthesis and relative cumulative photosynthesis measured in all spectral treatments versus elapsed time in June (a, b, c) and July (d, e, f) . . . . . 43

Figure 2.7: Calculated $UVB_{inh.eff.}$ averaged over all dates and all treatments emphasising the non-linear nature of UVB-dependent inhibition over time . . . . . 50

Figure 2.8: Percent inhibition of photosynthesis as a function of weighted UVR (295-347 nm) using the Behrenfeld et al. (1993) best fit exponential function for the combined data set . . . . . 51

Figure 3.1: Conceptualized two compartmental model depicting active and inactive photosystem units with damage ($k_1$) and repair ($k_2$) rate constants regulating the flow between the two states . . . . . 72

Figure 3.2: Lake Erie and the lake stations sampled throughout the summers of 1997 and 1998 . . . . . 79

Figure 3.3: Percent transmission of UV wavelengths for the different 50% PAR spectral treatments . . . . . 82

Figure 3.4: Temperature and *in vivo* fluorescence water column profile station 961 sampled August 13, 1998 indicating relatively well mixed epilimnion typical of the stations sampled . . . . . 85

Figure 3.5: Irradiance (a, b) and cumulative exposure (d, e) worst and best model fits of the 1997 time series photosynthesis data using the *Phaeodactylum tricornutum* weighting function (Cullen et al. 1992) with residual plots (c, f) showing evidence of systematic lack of fit . . . . . 87

Figure 3.6: Repair kinetic model best and worst fits of the 1998 time series photosynthesis data using each respective biological weighting function derived . . . . . 92

Figure 3.7: Irradiance (E) and cumulative exposure (H) model performances vs estimated recovery rate constants (R model) for the 1998 data . . . . . 94

Figure 3.8: BWFs derived from PCA using the R kinetic model for all five 1998 experimental dates . . . . . 96

Figure 3.9: Relative weighting coefficients for each 1998 BWFs . . . . . 98

Figure 3.10: Irradiance (E) and cumulative exposure (H) model performances vs estimated recovery rate constants (R model) for the 1997 data . . . . . 102

Figure 3.11: Recovery rate constants vs epilimnion depth for the 1997 and 1998 data . . . 103

Figure 4.1: Organized circulation pattern, Langmuir circulation, used in the modelling of the

inhibition of integrated primary production ..... 122

Figure 4.2: UVB irradiance spectra under 'normal' (300 DU) and 'depleted' (240 DU) stratospheric ozone concentration ..... 126

Figure 4.3: Temporal change in relative cumulative photosynthesis for the various 2h pre-exposure spectral quality treatments (a) July 29/97 and (b) August 11/98 ... 130

Figure 4.4: Inhibition of integrated primary production predictions for typical summer stratification events in the (a) Eastern and (b) West basins for different mixing rates ..... 136

Figure 4.5: Basin-specific inhibition of integrated primary production predictions for (a) a 10m mixed layer, (b) complete mixing and (c) typical summer epilimnion depths for a water column with an average vertical displacement speed of $10m \cdot h^{-1}$ . 138

Figure 4.6: Solar radiation transmission properties (a) and inhibition of integrated primary production predictions (b) for the West basin (used mean depth of 7.6m) during a shallow (1m) 'temporary' thermocline event ..... 140

Figure 4.7: Sensitivity analysis of integrated photoinhibition predictions using two levels of recovery rate constants and overall UVR sensitivity under different mixing scenarios ..... 141

Figure 4.8: Comparison of the impact of low vs high recovery rate constants on primary production inhibition in a static water column ..... 143

# Chapter 1

## Introduction

## Primary Production

The productivity of any organism is related to the rate at which organic matter is synthesized. Net productivity is the balance between the amount of energy fixed into organic carbon and that which is lost to predatory (i.e. grazing) and non-predatory (e.g. respiration, death) losses (Wetzel 1983). In lentic and lotic systems, primary production is the productivity of all micro- and macro-algae, as well as higher plants, but here the discussion will be focussed on the free-floating microalgae (i.e. phytoplankton). Primary production by phytoplankton has long been a subject of research because of its importance as the foundation of many aquatic food webs and, more recently, because of its major role in global carbon cycling and, by implication, climate change (Falkowski and Raven 1997).

Primary production is a function of both phytoplankton production rates and standing crop, which are both 'regulated' in fundamentally different ways (Harris 1986). Production rates of phytoplankton are largely controlled by physical factors such as light, temperature and mixing depths (Tilzer 1991). Temperature exerts its influence by affecting enzymes involved in photosynthesis (Fee et al. 1987, Reynolds 1984) and metabolic activity (e.g. respiration; Tilzer 1991), whereas light intensity and mixing depths determine the amount of light reaching phytoplankton cells for photosynthesis (Reynolds 1989). The biomass yield (or standing crop), on the other hand, is controlled by a multitude of factors. The maximum achievable standing crop follows Liebig's law of the minimum, and is set by the availability of nutrients, which determines the maximum carrying capacity of a water body (Tilzer 1991). Generally, however, a variety of loss processes such as respiration, grazing and sedimentation will prevent this upper limit from being reached.

Seasonal patterns in primary production in the temperate zone are mainly driven by fluctuations in solar and kinetic energy. The former determines the light and, thereby, the heat inputs to an ecosystem, while the latter controls the mixing processes of the water column, that is, the heat distribution and its dissipation (Reynolds 1989). The variations in both these factors are important determinants of the physico-chemical properties of lakes and the amplitude of change in these properties is a function of latitude, higher latitudes experiencing greater ranges in variability (Beaver and Crisman 1991, Wetzel 1983).

In temperate lakes, thermal stratification is an important physical change which greatly influences primary production (Valiela 1984). It occurs when the temperature of lake surface waters increases at a greater rate than the heat can be distributed by mixing processes. This results in a relatively shallow well-mixed stratum of warm water below which lies the thermocline, a stratum of water where temperature changes rapidly with depth (typically $>1\,^{\circ}C \cdot m^{-1}$; Wetzel 1983). This physical change confers stability to the water column, implying that greater amounts of energy are required to break down this density barrier. In temperate latitudes, the process of stratification generally begins in late spring-early summer, transiently favouring primary production through increasing light availability (reduced mixing depth and increased solar insolation) and growth temperatures (Barnes and Hughes 1988, Valiela 1984). Conversely, in late summer-early fall, as water temperatures cool due to shorter days and possibly more frequent meteorological disturbances, the thermocline depth increases resulting in gradually deeper mixing depths until the whole water column has turned over (Valiela 1984). In the early stages of the break down of thermal stratification, primary production may be favoured due to nutrient inputs from deeper nutrient-rich waters (Barnes and Hughes 1988).

Although an accepted generality, this pattern will vary with lake trophic status (Lampert and Sommer 1997).

The seasonal fluctuations in mixing depths of lakes due to changes in heat inputs and the frequency and intensity of meteorological disturbances are also important influences on primary production (Reynolds 1989). The depth of mixing will largely determine the mean irradiance to which phytoplankton are exposed, thereby affecting primary production. If mixing depth is sufficiently great, respiratory losses should equal or exceed photosynthetic income when averaged over a 24 h period, and no net primary production should occur; this reasoning has been formalized (and criticized) as the critical depth concept (e.g. Smetacek and Passow 1990). Mixing depth becomes important in the context of seasonal changes in mixing and undoubtably influences production in temperate lakes when deeper mixing occurs in the spring and fall months. The seasonally alternating mixing and thermal stratification events also influence the cycles of nutrients essential in sustaining primary production (Valiela 1984). Well-mixed water columns have relatively high concentrations of nutrients in surface waters whereas under stratified conditions, nutrient depletion occurs due to constant uptake and relatively low regeneration and resuspension processes as well as reduced inputs from nutrient-rich deep waters.

Although the regularly alternating physico-chemical properties of temperate lakes are the main driving forces governing the recurring seasonal trends in primary production, biological factors such as grazing and species specific optimum growth conditions also contribute to seasonal fluctuations in rates of production and biomass levels (Reynolds 1984). The seasonal patterns of plankton has been described by the PEG-model which considers both

the physico-chemical and biological factors influencing phytoplankton standing crops and dominant species successions (Sommer 1989). This model relates phytoplankton biomass and species composition changes to water column temperatures and mixing dynamics, light and nutrient availability as well as grazing pressure. Generally, the observed seasonal patterns in phytoplankton succession can be coarsely related to seasonal shifts between energy-limiting (spring and fall) and nutrient-limiting (summer) conditions. These different limiting conditions influence species succession because species vary in their preferences for light and temperature, in their physiology and their nutrient uptake and nutrient saturation parameters (Reynolds 1984 and references therein).

## Light Availability

Primary production is inherently dependent on solar radiation to drive the photosynthetic conversion of inorganic carbon to organic substrates. Physiologically, phytoplankton will respond to light by adjusting, for example, their pigment content or their energy transfer efficiencies to reach maximum achievable growth within the given conditions. In light limited conditions, the rate of photosynthesis will be determined by the rate of photon absorption (rate limiting step; Falkowski and Raven 1997). Phytoplankton can deal with these low light conditions by either changing their number of functional photosynthetic units (i.e. photosystem II (PSII)) or altering the absorption cross section of PSII (Falkowski and Raven 1997). In natural communities, the efficiency with which phytoplankton will utilize any absorbed light will not only depend on their light-history, that is their acclimation state, but also on community size structure and taxonomic composition (Fahnenstiel et al. 1989 and references therein, Madariaga and Joint 1994).

In light saturated conditions, photon absorption by definition exceeds the rate at which electrons are transferred in the photosynthetic electron transport chain ($P_{etc}$), making electron transport, and the factors which limit it, the controlling factor for photosynthetic rate (Falkowski and Raven 1997). Maximum achievable photosynthesis is related to the number of functional photosynthetic units as well as the maximum rate at which electrons are transferred from water to carbon dioxide, that is the capacity of the photosynthetic unit to generate reducing power (Tilzer and Beese 1988). While light limited rates of photosynthesis are largely governed by the available light, carbon fixation, the ultimate goal of photosynthesis, is intrinsically temperature dependent because it is enzymatically controlled (Falkowski and Raven 1997, Jewson 1976). But light saturated rates will be related to light-history because some of the Calvin cycle enzymes are activated by intermediates or by the change in pH in the stroma which both occur during photosynthesis (Gallegos et al. 1983, Häder and Tevini 1987). Other factors such as nutrient availability (Senft 1978), phytoplankton community structure (Fahnenstiel et al. 1989 and references therein), phytoplankton size (Madariaga and Joint 1994) and zooplankton abundance (Makarewicz 1991) will also influence the rates of light saturated photosynthesis of phytoplankton communities.

Inhibition of photosynthesis by supersaturating light levels is not uncommon in aquatic systems and phytoplankton have evolved mechanisms to minimize and/or cope with the damaging effects of excess light. Photoinhibition is inherently dependent on light intensity (i.e. irradiance) and the duration of exposure to inhibiting radiation, and is manifested as a decrease in the light saturated rates of photosynthesis (Falkowski and Raven 1997). As mentioned above, maximum photosynthetic rates are related to the number of functional photosynthetic

units and the rate of electron flow through the $P_{etc}$. To maximize the rate of electron flow or to minimize the effects of unbalanced excitation energy distribution between PSI and PSII, one available coping mechanism involves the phosphorylation of the light harvesting complexes (LHC) (Häder and Tevini 1987). This rapid response to high light, regulated by the redox state of the plastoquinone (PQ) intermediates in the $P_{etc}$, favours a balance between photon absorption and electron transport (Falkowski and Raven 1997). Excess excitation energy can also be dissipated thermally, via photon absorption by accessory pigments (i.e. carotenoids) (Falkowski and Raven 1997). Additionally, carotenoids confer protection against photooxidation by reactive oxygen species (specifically singlet oxygen) which can be prevalent in high light conditions (Häder and Tevini 1987).

The above mentioned light climate conditions were discussed within the range of natural variability, however, anthropogenic disturbances have lead to changes in the spectral balance of solar radiation and concomitant detrimental effects on primary production have been observed.

## Ultraviolet Radiation in the Environment

Since the early 1900s man-made chemicals have been making their way into the natural environment in significant quantities. By the early 1970s, concern for the environmental repercussions of anthropogenic compounds in natural ecosystems was prevalent. In 1974 chlorofluorocarbons (CFCs) were linked to the catalytic destruction of stratospheric ozone ($O_3$) (Molina and Rowland 1974) and, in 1987, 27 countries signed the Montreal protocol committing themselves to reducing the production of $O_3$ destroying substances (U.S. EPA 1998). Today, 160 countries have joined this international effort to eliminate the use and

production of $O_3$ depleting chemicals. Despite these efforts, it is anticipated that $O_3$ destruction will continue well into the next century, not only because CFCs are rather persistent chemicals but also because increases in greenhouse gases will lead to reduced stratospheric temperatures accelerated rates of $O_3$ destruction (Whitehead et al. 2000 and references therein).

The global $O_3$ layer plays a vital ecological role as it strongly absorbs the ultraviolet B (UVB; 280-320 nm) portion of the solar spectrum (Lubin et al. 1989), protecting the earth from this high-energy, damaging, radiation (Kondratyev and Varotsos 1996). In the past two decades, intense research into the biological effects of $O_3$ depletion and the concomitant increase in UVB radiation has been focussed in the Antarctic (Helbling et al. 1992, Karentz et al. 1991a,b, Karentz and Spero 1995, Schofield et al. 1995, Smith et al. 1992, Weiler and Penhale 1994), where a prominent $O_3$ 'hole' ($26 \times 10^6$ km$^2$ in 1998; Meteorological Service of Canada 1999) develops every spring. However, decreasing levels of stratospheric $O_3$ have recently been reported in the northern mid-latitudes (Stolarski et al. 1992), where increased levels of UVB can be potentially devastating to these highly productive temperate regions (Lesser 1996).

The Laurentian Great Lakes (LGL) are the most important freshwater resources in North America, and in particular, Lake Erie sustains a high fish diversity and biomass (Bolsenga and Herdendorf 1993). Once pronounced 'dead', L. Erie has successfully recovered following the implementation of nutrient loading restrictions, particularly of phosphorus inputs (Dahl et al. 1995, Graham et al. 1996). Being part of the St-Lawrence Seaway, however, L. Erie has become vulnerable to the invasion of exotic species facilitated by the discharge of ship ballast waters. Of particular importance is the invasion of the zebra and quagga mussels

(*Dreissena* sp.) which coupled with the nutrient loading restrictions have lead, in recent years, to an increase in water clarity in L. Erie (Dahl et al. 1995, Graham et al. 1996). This change in water clarity may result in a concomitant increase in the depth to which biologically effective ultraviolet radiation (UVR) can penetrate in the water column, thereby, exacerbating the effects of increased UVB fluxes associated with $O_3$ depletion in this region. Despite the ecological and economical importance of the LGL, research into the biological consequences of enhanced UVB levels in these large lakes remains sparse (Gala and Giesy 1991, Smith et al. 1998 & 1999, Marwood et al. 2000, Wilhelm and Smith 2000).

UVB is strongly absorbed by humic substances which are more abundant in lakes than in oceans (Kirk 1994). As a result, UVB in most freshwater systems is rapidly attenuated in the first few meters of the water column (Scully and Lean 1994, Kirk 1994), whereas biologically effective UVB levels can penetrate up to 20-30 m in clear ocean waters such as the Southern Ocean (Smith et al. 1992, cf. Whitehead et al. 2000). However, the top few meters of many freshwater systems provide favourable growth conditions for many organisms (e.g. phytoplankton, zooplankton). Consequently, lacustrian ecosystems are vulnerable to enhanced levels of UVB (Williamson 1995). In aquatic ecosystems, all organisms can potentially be affected by enhanced levels of UVB. However, particular attention has been paid to phytoplankton at the base of the food chain, where changes in total production, nutritive value and/or taxonomic composition may have important repercussions at higher trophic levels. Moreover, these photosynthesizing organisms are important sinks for atmospheric carbon (Häder 1994) and an important concern is that decreased primary production due to enhanced UVB fluxes may exacerbate the global warming trends (Williamson 1995) and, by association,

intensify stratospheric $O_3$ destruction (Whitehead et al. 2000).

## Mechanisms of Action of UVR

### Changes in the Chemical Environment

Ultraviolet radiation can affect phytoplankton indirectly by altering their chemical environment. Free radical or excited molecular species production (e.g. $^1O_2$, ROO$^\cdot$, OH$^\cdot$), enhanced photochemical breakdown of dissolved organic matter (DOM), an important light-absorbing component of aquatic ecosystems (Scully and Lean 1994), and altered trace nutrient cycling (iron, manganese, copper, cobalt/vitamin $B_{12}$) are some of the environmental chemistry changes that can be induced by UVB and ultimately affect phytoplankton production (Mopper and Kieber 2000, Palenik et al. 1991). Free radicals in the water column may react with, and oxidize, cell membranes. The photochemical conversion of DOM may: 1) increase the penetration of UV radiation in the water and/or 2) stimulate the microbial food web (Vincent and Roy 1993), by converting refractory DOM into labile DOM available to bacteria. Furthermore, the photochemical dissolution of colloidal or chelated trace metal complexes may be beneficial, in the case of iron, or detrimental, in the case of copper, to the biota.

### Biological Effects

Biological effects directly induced by UVB can also occur and they are wide ranging. Decreased growth (Quesada et al. 1995) and photosynthetic rates (Villanfañe et al. 1995, Cullen and Lesser 1991), altered nutrient uptake capabilities (Döhler et al. 1987, Döhler 1994), and impaired orientation mechanisms, motility and swimming (Häder 1986, Häder 1994) are some of the detrimental effects UVB has been shown to induce in phytoplankton. A major role

of UVA in photoinhibition has also been shown and at times has been deemed more important than UVB as a photoinhibitor in freshwater (Bühlmann et al. 1987, Smith et al. 1998) and marine (Helbling et al. 1992, Neale et al. 1994, Smith et al. 1992) ecosystems.

The main intracellular targets of UVB radiation are the nucleic acids, DNA and RNA, which readily absorb the shorter UV wavelengths (260 nm maxima) due to the aromatic $\pi$-electron systems of their pyrimidine and purine bases (Tevini 1993, Karentz et al. 1991a). The induction of photoproducts in DNA (cyclobutane dimers, pyrimidine (6-4) pyrimidone adducts, photohydrates and DNA-protein cross-links), can cause mutations and reduce RNA transcription, with far reaching effects on cell survival (Karentz et al.1994, Vincent and Neale 2000). Cyclobutane dimers and pyrimidine (6-4) pyrimidone adducts are probably the most damaging nucleic acid alterations which affect cell survival (Karentz et al. 1994). While pyrimidine (6-4) pyrimidone adducts are produced at less than one tenth of cyclobutane dimers, they cannot be excised and repaired like cyclobutane dimers, and therefore are relatively more toxic, capable of producing long term damage and ultimately death (Vincent and Quesada 1994, Vincent and Neale 2000).

Additional molecular targets of UVB radiation are proteins and lipids. In proteins, it is the aromatic amino acids (phenylalanine, tyrosine and tryptophane) which are responsible for the absorption in the UV range of the spectrum (Häder and Tevini 1987, Karentz et al. 1991b). Consequently, disulfide groups of amino acids, important for their tertiary structure, can be directly split by UVR (short and longer ultraviolet wavelengths) or indirectly via the action of free radicals produced by UVR, thereby changing the structure and function of proteins (Häder and Tevini 1987, Palenik et al. 1991, Armstrong and Buchanan 1978). Two examples of UVB-

associated protein inactivation are the photomodifications of 1) an integral protein associated to photosystem II (PSII); and 2) the carbon-fixing enzyme, ribulose-1,5-bisphosphate carboxylase/oxygenase (Rubisco). In the PSII complex, the D1 herbicide binding protein seems to be a target of UVB radiation (Greenberg et al. 1989), its degradation being mediated by photosensitizers. The photomodification of Rubisco can occur via a cross-linking between a large and small subunit of the enzyme complex (Wilson et al. 1995). Damage to either of these proteins can affect photosynthesis either by limiting the supply of reducing power (i.e. ATP and NADPH generated by the photosynthetic electron transport chain) or by reducing maximum photosynthetic potential (i.e. constraining the capacity of the Calvin cycle).

Lipids are also susceptible to UVR toxicity, especially by the increased production of reactive oxygen species (namely $^1O_2$ and $OH^\cdot$), resulting in the oxidization of isolated or conjugated double bonds in the fatty acyl moieties of cellular lipids (Asada and Takahashi 1987, Vincent and Neale 2000). Direct absorbance of UVB by the double bonds of the fatty acids can produce lipohydroperoxides (LOOHs) via radicals in the presence of oxygen (Häder and Tevini 1987). Photosensitizers (often photosynthetic pigments) can lead to lipid peroxidation via two types of reactions 1) by directly reacting with the substrate thereby producing radicals (Type I); or 2) indirectly by exciting ground state triplet oxygen ($^3O_2$) to its singlet oxygen ($^1O_2$) excited state which can react with lipid substrates producing LOOHs (Type II) (Girotti 1985). Lipid peroxidation reactions can also be initiated by transition metals (e.g. iron and copper) by direct interaction with LOOHs or indirectly though the production of hydroxyl radicals ($OH^\cdot$) (Haber-Weiss cycle; Girotti 1985).

## Protection and Repair Mechanisms

### Protection

Phytoplankton have evolved mechanisms to deal with damaging UVR radiation, namely avoidance, screening, quenching and repair (Vincent and Roy 1993). Phytoplankton perceive light via photoreceptors and respond accordingly by moving to more favourable depths within the water column (Vernet 2000 and references therein). However, as of yet, no specific UVB photoreceptor has been described in phytoplankton, while green and UVA/blue light photoreceptors are well known (Vernet 2000, Rüdiger and López-Figueroa 1992). As such, algae can respond to increases in photosynthetically active radiation (PAR) and UVA, thereby concurrently reducing their exposure to UVB radiation, but are effectively unable to detect independent increases of UVB due to ozone depletion (Roy 2000). While avoidance mechanisms are the first line of defence against damaging UVB exposure, ozone depletion which results in disproportionate increases in UVB may result in unavoidable exposure.

Given that some exposure to UVR is inevitable, phytoplankton can alleviate the potential for damage by screening the inhibiting radiation before it damages the intracellular components. This involves the production of UVR (mainly long UVB and short UVA) absorbing compounds such as mycosporine-like amino acids (MAAs; shinorine, porphyra-334, mycosporine glycine-valine and palythine; Villafañe et al. 1995) which are induced by, and provide protection, albeit incomplete, from UVB and UVA radiation (Lesser 1996, Roy 2000 and references therein). Cellular concentration of MAAs, in particular mycosporine glycine-valine and palythine, have been shown to increase in Antarctic phytoplankton assemblages exposed to UVR, however, this acclimation response can require days to weeks (Villafañe et al.

1995, Roy 2000).

Light, both PAR and UVR, is also absorbed by the light harvesting pigments of the antennae of the two photosystems, which can produce toxic radicals and excited triplet state chlorophylls. These can be scavenged or quenched by pigments (carotenoids) and a variety of enzymes (e.g. superoxide dismutase (SOD) and ascorbate peroxidase (Asc)) to mitigate their destructive nature (Asada and Takahashi 1987, Vincent and Roy 1993). Carotenoids will function closely with chlorophylls converting their triplet excited state ($^3Chl^*$) to a singlet ground state ($^1Chl$), and scavenging $^1O_2$, converting it to its ground state $^3O_2$ (Asada and Takahashi 1987). Ultimately this absorbed energy is dissipated as heat. In the chloroplasts, superoxide ($O_2^-$) and hydrogen peroxide ($H_2O_2$) are produced and these species can be scavenged by SOD and Asc, respectively (Asada and Takahashi 1987, Lesser and Schick 1989, Miyake et al. 1991). Cellular concentrations of $H_2O_2$ and $O_2^-$ have been shown to increase following UVB exposure in the dinoflagellate *Prorocentrum micans* (Lesser 1996) and so has the specific activity of SOD in cultured and isolated symbiotic zooxanthellae (Lesser and Schick 1989).

*Repair*

Although some degree of tolerance, adaptation or protection from UVR can be achieved by the different mechanisms listed above, some damage will eventually occur and will need to be repaired. Repair processes related to DNA have been extensively studied (Vincent and Roy 1993) and this damage is mitigated by inducible cellular repair mechanisms: 1) excision repair; 2) photoenzymatic repair; 3) post-replication and 4) SOS repair (Tevini 1993). Excision repair, which is light independent, involves an endonuclease which recognizes the damaged site, an

exonuclease which removes the photoproduct, and a DNA polymerase and ligase which resynthesises de novo the correct DNA sequence and closes the gap, respectively. Photoenzymatic repair (PER), which is light dependent, involves a DNA photolyase which binds and, following the absorption of a photon of light (300-500nm), splits cyclobutane dimers into non-toxic monomers (Roy 2000). Post-replication repair and SOS repair involve closing a DNA sequence gap left during replication or removing false bases placed during replication, respectively. Cell survival is related to the number of photoproducts induced by UVB radiation and relies greatly on PER (Karentz et al. 1991a). However, since PER induction relies on UVA and visible light, which do not change with $O_3$ depletion, this repair mechanism may be unable to offset the increased rates of damage caused by enhanced UVB fluxes (Smith et al. 1992, Karentz et al. 1991a). Repair of genetic material is critical since, for example, damaged proteins are repaired by *de novo* synthesis which requires the transcription of nucleic acids (Whitehead et al. 2000). If this process is interrupted by damage to DNA and RNA, the cells will be essentially unable to repair damaged components and will ultimately die.

The survival fitness of phytoplankton exposed to damaging UVR will largely depend on their ability to establish an equilibrium between the rates at which they are being damaged and the rate at which they can repair that damage (Lesser et al 1994). The kinetics of these processes need to be elucidated to obtain a more complete picture of the overall effects of UVB in natural systems, and must be considered in the context of vertical mixing processes (Cullen and Lesser 1991, Lesser et al. 1994, Vernet 2000). In a mixed water column, phytoplankton cells will not remain at the surface for extended periods of time. Although the kinetics of UVR damage have been studied and are known to be rapid (<30 min) (Lesser et al. 1994), the

kinetics of repair are relatively unknown. Furthermore, it is as yet unclear how vertical mixing processes will alter the UV photoinhibitory response of phytoplankton.

### Biological Weighting Functions

Spectral weighting functions (SWFs) are functions that quantify the biological response of interest as a function of wavelength (Neale 2000, Coohill, 1997). Action spectra and biological weighting functions (BWFs) are two specific types of SWFs, but their derivation and applicability are very different (Neale 2000). Various action spectra based on different biological parameters of interest have been developed, such as the photoinhibition and DNA action spectra (Jones and Kok 1966, Setlow 1974). Although the functions derived from these action spectra differ, they commonly demonstrate that the shorter UVB wavelengths have a higher biological activity than the longer UVA wavelengths, mainly a consequence of the higher energy per photon content of the shorter wavelengths. However, action spectra are based on a biological response to monochromatic radiation, which is clearly not encountered in the natural environment. While the monochromatic approach is useful in isolating the mechanisms of action of the different UVR wavelengths, it lacks applicability in quantifying the effects of UVR in natural systems.

Ideally, a SWF will consider the interactions between the radiation that damages an organism and the longer wavelengths which induce repair processes (Cullen et al. 1992). This is achieved by the use of BWF, based on polychromatic exposures, whereby the response of interest integrates the presence of both the damaging and the beneficial wavelengths of solar radiation. BWFs quantifying the effects of UV radiation on photosynthesis have been developed for laboratory cultures (Cullen et al. 1992, Neale et al. 1998a) and marine

phytoplankton communities (Neale et al. 1998b,c) but, as of yet, no BWFs have been published for freshwater algal communities. BWFs are essential to quantify the effects of UVR on phytoplankton communities which experience great spectral variations in their radiation field due to mixing processes (Cullen and Neale, 1997). Used in conjunction with kinetic and mixing models, BWFs can be powerful tools in describing the effects of UVR on integrated primary production.

## Objectives

The aim of this work was to investigate the effects of UVR in L. Erie phytoplankton communities. The extent of inhibition by UVR on primary production was examined and evaluated on a phytoplankton size class basis. In order to appropriately quantify the effects in L. Erie, the kinetics of photoinhibition by damaging radiation were investigated and biological weighting functions specific to L. Erie phytoplankton were derived. Finally, to better characterise the UVR effects in L. Erie, a new broadly applicable kinetic model was used in conjunction with the derived BWFs to model the inhibition of integrated primary production in a mixed water column.

In chapter 2, the extent of UVB-associated inhibition of photosynthesis over time (8h) is investigated in L. Erie phytoplankton communities. The percent production in the large (>2 μm) and small (<2 μm) phytoplankton size fractions as well as the proportion of new dissolved organic carbon production is examined. Relationships between the observed response and various environmental variables or the taxonomic composition of the micro- and nanoplankton are explored. UVB is shown to be a significant factor for near-surface populations, but prediction of its effects to be elusive without further model development.

In chapter 3, a new model for the response of photosynthetic carbon fixation to UVR is formulated and tested against observations on natural communities in L. Erie. As part of the model development, new spectral weighting functions, the first for any freshwater phytoplankton, are determined. The new model is shown to make good predictions of UVR effects on photosynthesis, while previous models do not, and a strong role for recovery processes is indicated.

In chapter 4, the new model is used to calculate losses of daily production under mixing and water transparency scenarios that span the common range of conditions in L. Erie. The model's predictions of rates of recovery from photoinhibition are tested against direct measurements of recovery following varied spectral exposures, and it is shown that phytoplankton are generally able to recover within one photoperiod. The modelling leads to the first realistic estimates of photoinhibitory loss of primary production for the Great Lakes, or indeed any freshwater system.

# Chapter 2

## Effects of ultraviolet B radiation on rates and size distribution of primary production by Lake Erie phytoplankton

## Abstract

The impact of ultraviolet radiation (UVR) on phytoplankton primary production in 1 to 8h exposures to natural solar radiation was investigated in 10 experiments during the spring and summer of 1997 in Lake Erie. On average, only 1h of exposure was needed to produce half the UVB (297-320 nm)-dependent inhibition realized in 8 h exposures, indicating rapid kinetics of photoinhibition. UVB-dependent inhibition of cumulative photosynthesis averaged 36% (maximum 58%) in 8h simulated surface exposures. In the same exposures, conservative estimates of inhibition by total UVR (UVB plus part of UVA) averaged 48%, indicating an important role for UVA (320-400 nm) as well as UVB. The efficiency of UVB in producing photoinhibition varied among dates but could not be explained in any simple way by measures of phytoplankton light history, or dominant genera of phytoplankton. However, phosphorus (P) deficient mixed assemblages were more susceptible to UVB damage in short-term (1h) exposures, that is, UVB inhibition efficiency was higher for P-limited compared to P-replete algal communities. The impact of UVR on the particulate ($PO^{14}C$; < 2 and > 2 μm) and dissolved ($DO^{14}C$) organic carbon pools was investigated concurrently. The percent of total organic carbon ($TO^{14}C$) production in the dissolved pool (% $DO^{14}C$) was a function of the UVB exposure level with the harshest treatments (100% PAR and UVB) showing significantly higher % $DO^{14}C$ production. In the particulate pool, the proportion of the $TO^{14}C$ production in the particulate picoplankton fraction was significantly inhibited by both UVB and UVA while the production in the larger phytoplankton pool was relatively higher in the presence of UVB. Nutrient sufficiency or deficiency was not related to either the % $DO^{14}C$ or % $PO^{14}C$ in either phytoplankton size fraction. The apparent size-dependent UVR impacts and the relative

increases in algal DOC due to UVR stress may have important implications for the food web dynamics of L. Erie. Furthermore, basin-specific PAR and UVR transmission properties showed that the West basin of L. Erie is potentially more susceptible to UVR photoinhibition than either the East or Central basins. The proportion of the euphotic zone occupied by damaging UVR being 50 - 60% higher in this part of the lake.

## Introduction

In the past two decades, the depletion of the $O_3$ layer, particularly in the Antarctic region of the globe, has stimulated much research on the possible biological consequences of this phenomenon (e.g. Helbling et al. 1992, Karentz and Spero 1995, Neale et al. 1998b, Schofield et al. 1995, Smith et al. 1992, Weiler and Penhale 1994). Decreasing levels of stratospheric $O_3$ and increasing surface-incident ultraviolet B (UVB) flux have also been reported in the northern mid-latitudes (Stolarski et al. 1992, Kerr and McElroy 1993). UVB is strongly absorbed by humic substances which are more abundant in lakes than in oceans (Kirk 1994). As a result, this portion of the solar spectrum, in most fresh waters, is rapidly attenuated in the first few metres of the water column (Scully and Lean 1994, Kirk 1994), whereas UVB can penetrate up to 20-30 m in clear ocean waters such as the Southern Ocean (Smith et al. 1992). However, the relatively warm and well-illuminated shallow waters provide favourable growth conditions for many lacustrine organisms, especially phytoplankton. Consequently, lake ecosystems are also vulnerable to enhanced levels of UVB (Williamson 1995).

The Laurentian Great Lakes are among the many potentially UVB-susceptible freshwater ecosystems found in the north temperate zone. Lake Erie in particular sustains a high fish diversity and biomass (Bolsenga and Herdendorf 1993) and, in recent years, has experienced increased water clarity following the introduction of *Dreissena* spp. (zebra and quagga mussels) and nutrient loading restrictions (Charlton et al. 1993, Holland 1993, Dahl et al. 1995, Graham et al., 1996). L. Erie is the shallowest of the five Laurentian Great Lakes, and is separated into three distinct basins (East, Central and West) by Point Pelee and the Pennsylvania Ridge at the west and east ends of the Central basin, respectively (Mortimer

1987). The unique topography of this large lake has a strong influence on its physical and biological processes. For example, the shallow West basin (mean depth = 7.6 m) typically does not stratify in the summer months and experiences much more rapid seasonal changes in its heat storage than either the Central (mean depth = 18.6 m) or East (mean depth = 26 m) basins (Bartish et al. 1987). Additionally, distinct east-west nutrient, turbidity and water clarity gradients exist (e.g. Bartish 1987, Dahl et al. 1995). The increased water clarity associated with the invasion of zebra and quagga mussels may exacerbate the effects of enhanced incident UVB fluxes in L. Erie, but the responses are likely to be basin-specific because of their differing physical and optical characteristics.

Ultraviolet radiation (UVR) effects on phytoplankton have been extensively studied and it is generally accepted that UVR-sensitivity is species specific, this being a consequence of differing phenotypic (e.g. external morphology and cellular organelle arrangement) and genotypic (e.g. DNA base content and sequence; antioxidant synthesis and repair capabilities) characteristics (Karentz et al. 1991a, Bothwell et al. 1993). Of the phenotypic traits, cell size has been deemed important in the overall algal UVR-sensitivity, with smaller cells suffering more DNA photoproduct induction (Karentz et al. 1991a). The usual interpretation is that smaller cells have less internal protection of the genetic material conferred by strong UVR absorbers such as proteins and nucleic acids (Tevini 1993, Mitchell and Karentz 1993). Strong UVR absorption is also achieved by a class of so-called "sunscreens", the mycosporine-like amino acids (Roy 2000). However, the efficiency with which phytoplankton can utilize these compounds is constrained by both physical (i.e. size) and physiological (i.e. osmotic) limits (Garcia-Pichel 1994). In the literature, there is evidence both supporting and refuting the

hypothesis of UVR-dependent changes in the taxonomic composition of algal communities (Bothwell et al. 1993, Halac et al. 1997, Worrest et al. 1981) as well as size-specific effects of UVR (Boelen et al. 2000, Karentz et al. 1991a, Laurion and Vincent 1998). Whether these effects occur is important because changes in the size and species composition of these photosynthesizing organisms can impact the function of aquatic food webs and the global carbon budget (Häder 1994, Williamson 1995).

In addition to the obvious link between phytoplankton and higher trophic levels, algae are also intricately linked to lower trophic levels, namely bacteria and the microbial food web (Thingstad et al. 1997). Healthy phytoplankton partake in the extracellular release of dissolved organic carbon (DOC) (Bjørsen 1988) which, in turn, is taken up by the bacterioplankton to satisfy their carbon requirements (Lignell 1990). Not only is the production and the overall availability of this algal DOC subject to change by UVR exposure (Pausz and Herndl 1999), but, once in the aquatic environment, photomodification of this essential carbon pool can occur (Tranvik and Kokalj 1998).

In this chapter, photoinhibition in L. Erie phytoplankton communities exposed to UVR were measured during spring and summer, the seasons of greatest UVR exposure. The rate and extent of UVB-dependent photoinhibition was assessed and compared against several factors that may modify the susceptibility to UVR damage (e.g. nutrient status, light history, and phytoplankton community composition; e.g. Gala and Giesy 1991, Helbling et al. 1992, 1994, Lesser et al. 1994, Neale et al. 1998a,b, Villafañe et al. 1995). Furthermore, the differential effects of UVR on the particulate (< 2 μm and > 2 μm size fractions) versus the dissolved organic carbon pools were investigated.

# Materials and Methods

## Study Site

Sampling and field experiments were conducted at stations throughout L. Erie (42°N, 81°W). L. Erie (Fig. 2.1) has an area of 25 500 $km^2$ and is separated into three distinct basins distinguished by their bathymetry and differing trophic status and water clarity (Burns 1985, Dahl et al. 1995). The smaller West basin (mean depth ($Z_m$) = 7.6 m; 3 680 $km^2$) is mesotrophic and turbid, due to high nutrient and sediment inputs. The larger Central basin ($Z_m$ = 17.8 m; 15 390 $km^2$) receives less nutrient and sediment loading (largely from the West basin) and is oligotrophic. The East basin ($Z_m$ = 27.0 m; 6 150 $km^2$), is the deepest, clearest, and most oligotrophic of the three basins. The deeper East and Central basins normally stratify during the summer months, while the relatively shallow West basin typically remains unstratified.

## Experimental Design and Sampling Protocol

Experiments were conducted on the C.C.G.S. Limnos at various stations during five cruises from early May to late August 1997 (Table 2.1) under relatively clear sky conditions. The physical structure of each lake station was measured by conductivity, temperature and depth sensors (EBTT and Water Quality Profiler, SeaBird Electronics Inc., SBE-25 models). In addition, casts of a SeaBird SBE-19 equipped with a SeaTech fluorometer were conducted to characterise the *in vivo* chlorophyll *a* fluorescence profile of the water column. Incident solar radiation spectra were measured with a diode-array spectroradiometer (Oriel Corp. Stratford, CT) equipped with a collecting sphere, at 0.5 nm intervals from 295 to 700 nm every 30 minutes (Smith et al. 1999). In practice, little measurable radiation was found at the lower end

Figure 2.1: Lake Erie and the lake stations sampled throughout the summer of 1997 for time-series experiments

Labrador Sea
Gulf of St. Lawrence
Hudson Bay
CANADA
Pacific Ocean
43°
42°
79°
80°
81°
82°
81°
961
962
961
951
946

Table 2.1: Summary of limnological variables of the stations sampled for time-series experiments conducted on L. Erie between the months of May and August, 1997.

| Date | Station | Basin | Epilimnion Thickness (m) | Epilimnion Temperature (°C) | Chlorophyll a at 5 m ($\mu g \cdot L^{-1}$) | $K_{dPAR}$ ($m^{-1}$) | Mean PAR % of incident |
|---|---|---|---|---|---|---|---|
| 7/5 | 946 | C | 22 (iso.) | 6.0 | 1.5 | 0.43 | 10.6 |
| 3/6 | 946 | C | 22 (iso.) | 8.8 | 2.5 | 0.29 | 15.1 |
| 4/6 | 337 | W | 9 (iso.) | 13.2 | 9.8 | 1.61 | 6.9 |
| 5/6 | 961 | C | 19 (iso.) | 13.4 | 1.2 | 0.83[a] | 6.3 |
| 1/7 | 23 | E | 5 | 20.3 | 0.7 | 0.36 | 46.4 |
| 2/7 | 967 | W | 8 | 23.5 | 2.1 | 0.36 | 32.8 |
| 29/7 | 23 | E | 15 | 22.0 | 3.5 * | 0.24 | 27.0 |
| 30/7 | 953 | C | 12 | 22.2 | 1.4 | 0.32 | 25.5 |
| 31/7 | 962 | C | 11 | 23.7 | 2.0 | 0.36[a] | 24.8 |
| 27/8 | 337 | W | 9 (iso.) | 21.1 | 15.5 | 1.16 | 9.6 |

[a] Values of $K_{dPAR}$ derived from the following relationship: $K_{dPAR}$ = -0.026*Transmission−2.258, a relationship derived from measured $K_{dPAR}$ and transmission values from CTD casts.

*Note that on this date *in vivo* chl *a* fluorescence was not uniformly distributed within the mixed layer (*see* Fig. 2.5)

of the measured spectrum so UV-B in this study was quantified as the amount of radiation between 297 - 320 nm. The radiometer was calibrated with a lamp traceable to the National Bureau of Standards specifications and wavelength calibration was done with reference to known absorption lines in the incident solar spectrum. The same radiometer was used to measure the spectral transmission of the optical filters and incubation vessels used in the time series experiments.

Circumstances permitting (i.e. enough light), underwater penetration of photosynthetically active radiation (PAR) was measured at each sampled lake station using a LI-COR LI-1000 with an underwater cosine quantum sensor. The light attenuation coefficient was then determined and used to calculate the percent mean PAR within the mixed layer. Mean PAR was calculated as:

$$I_a = \frac{I_o}{-k_d Z_e}(e^{-k_d Z_e} - 1) \qquad (2.1)$$

where $I_o$ is the percent incident irradiance (100%), $k_d$ is the vertical light attenuation coefficient and $Z_e$ is the depth of the epilimnion. Mean PAR was reported as a percent of $I_o$.

Whole water samples for on-board experiments were taken early in the morning at 5 m depth (except July 1 when water sample taken from 3 m) with Niskin bottles so the incubations could begin by 1000 h (E.D.T). In these time series experiments, all reported photosynthetic rates are means of three replicate samples from independent incubation vessels. Lake water samples were inoculated with $^{14}$C-sodium bicarbonate (ICN Biomedicals; 2$\mu$Ci $\mu$L$^{-1}$) and dispensed into acid-washed quartz tubes (55 mL capacity) or polystyrene flasks (65 mL

capacity). The incubation vessels were then placed in ultraviolet-transmitting plexiglass deck-boxes fitted with different optical filters and sampled at pre-established time intervals. Quartz tubes were sampled following 0.5h, 1h, 2h, 4h, 6h and 8h of exposure, while polystyrene flasks were sampled after 1h, 3h and 8h.

At each sampling time and at time zero, a 5 mL subsample from each experimental vessel was acidified with 100 µL of 6 N HCl, and after 24 h fixed with 15 mL of EcoLume™ scintillation cocktail (ICN Pharmaceuticals). Total activity (200 µL) samples were also taken to verify the isotope additions. At the end of the incubation period, an additional 5 mL sample from each treatment was taken and size fractioned, by overlapping different pore sized filters, into > 2 µm (2 µm membrane filter, Nucleopore), < 2 µm (glass fibre, GF/F) and dissolved organic carbon (collected filtrate) fractions to assess the relative distribution of the carbon tracer. The filtrate sample was acidified and fixed as above, while each filter was also acidified with 100 µL of 6 N HCl and after 24 h fixed with 5 mL of EcoLume™ scintillation cocktail (ICN Pharmaceuticals). Photosynthetic carbon assimilation was calculated using dissolved inorganic carbon concentrations measured on filtered (glass fibre, GF/F) lake water from each station. Initial total chlorophyll *a* concentration was measured by fluorometry (e.g. Smith et al. 1999) and phytoplankton community composition by microscopic examination of samples preserved with Lugol's iodine.

The optical filters were window screen (ca. 50% transmission at all wavelengths) and Mylar-D which selectively removes UVB. Different combinations of these filters with the two different types of experimental vessels yielded a total of eight treatments with two levels of irradiance (100% and 50% PAR) and four (100%, 50%, 30% and 15% UVB exposure levels)

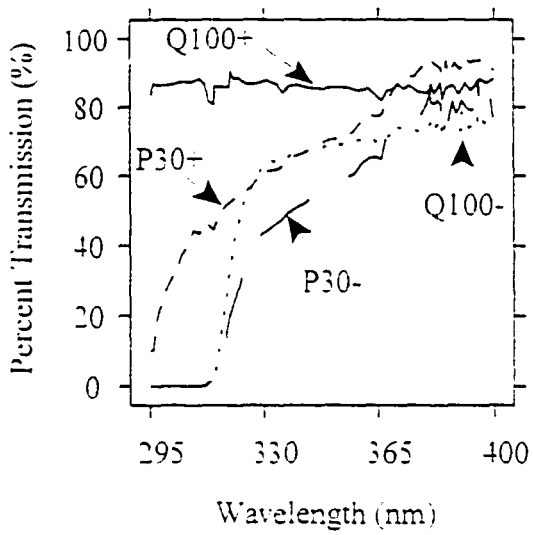



Figure 2.2: Percent transmission of UVR wavelengths for the different 100% PAR spectral treatments. Q100+ and Q100- denote quartz tube transmission spectra with and without Mylar-D; P30+ and P30- denote polystyrene flask transmission spectra with and without Mylar-D.

Table 2.2: Percent photosynthetically active radiation (PAR), ultraviolet A (UVA) and ultraviolet B (UVB) in the different spectral treatments of the time series experiments.

| Treatment | % PAR | % UVA | % UVB |
|---|---|---|---|
| Q100+ | 100 | 100 | 100 |
| Q100- | 100 | 100 | 0 |
| Q50+ | 50 | 50 | 50 |
| Q50- | 50 | 50 | 0 |
| P30+ | 100 | 50 | 30 |
| P30- | 100 | 50 | 0 |
| P15+ | 50 | 25 | 15 |
| P15- | 50 | 25 | 0 |

Note: Q denotes quartz tube; P denotes polystyrene flask

different spectral qualities (Fig. 2.2; Table 2.2). All of the experimental treatments conducted in this study included at least a portion of the UVA waveband and the main emphasis is on comparisons between UVB-exposed and UVB-excluded (Mylar) treatments. However, comparisons between quartz and polystyrene vessels provided an indication of the effect of partial removal of UVA as well.

Measures of response to UVR and PAR

The sensitivity of the different algal assemblages to UVB was assessed using a UVB inhibition efficiency index:

$$UVB_{inh.eff.} = \frac{1 - \frac{PS_{Q50-}}{PS_{Q50-}}}{UVB_{dose}} \qquad (2.2)$$

where $PS_{Q50-}$ and $PS_{Q50-}$ are cumulative photosynthesis in the quartz tube 50% PAR full spectrum and Mylar-D treatments, respectively, and $UVB_{dose}$ is the unweighted cumulative UVB exposure. The unweighted UVB exposure was used because the spectral quality within these treatments did not vary appreciably between sampling dates, and the unweighted UVB exposure showed a good linear relationship with the weighted (*Phaeodactylum tricornutum* BWF; Cullen et al. 1992) exposure. Although only the 50% irradiance treatments were statistically analysed for any relationships with nutrient and light status indicators, $UVB_{inh.eff.}$ values were also calculated for the other three treatments and they did not significantly differ between treatments. However, only the 50% quartz treatments were used for UVB-sensitivity analysis to minimize any masking effects that the relatively large flux of UVA and/or PAR

might have in the 100% PAR treatments.

A light gradient incubator was additionally used at each station to assess light adaptation and the contribution of PAR to photoinhibition (Smith and Maly 1993). Nine to eighteen subsamples of 5 mL each were incubated for 1 h, with photosynthetic carbon assimilation estimated by the acidification method as described above. Light was from a quartz halogen lamp (PAR only), ranging from 0.4 to ca.2000 $\mu E \cdot m^{-2} \cdot s^{-1}$. The photosynthetic light response was fitted to the model of Platt et al. (1980):

$$P^B = P_s^B \cdot (1 - e^{-\alpha^B I / P_s^B}) \cdot e^{-\beta^B I / P_s^B} \qquad (2.3)$$

where $P^B_s$ is the maximum rate of photosynthesis attainable in the absence of photoinhibition, $\alpha^B$ is the initial slope of the response (a measure of light utilization efficiency), and $\beta^B$ is the photoinhibition parameter. There was in fact no photoinhibition in any of the experiments ($\beta^B = 0$) so the model was re-fitted without the photoinhibition term to estimate the actual light-saturated rate of photosynthesis ($P^B_m$) and the ratio of $P^B_m : \alpha^B$, the photoadaptation parameter or $I_k$.

## Nutrient Status

Phosphorus (P) deficiency was evaluated by a total of five indices, the atomic ratio of particulate carbon to phosphorus (C:P), alkaline phosphatase activity (APA), P debt assays, phosphorus turnover times (using $^{33}P$) and the atomic ratio of particulate nitrogen to phosphorus (N:P). Nitrogen (N) deficiency was evaluated by two indices, the particulate carbon to nitrogen (C:N) atomic ratio and N debt assays (Guildford et al. 1994). Values suggested by

Healey and Hendzel (1979), based on culture work with freshwater species, were used to indicate the presence of nutrient deficiency.

## Statistical Analysis

Analysis of variance was used to investigate the dependence of UVB sensitivity on environmental parameters. ANOVAs were also used to test for effects of light and nutrient status as well as effects of UVR on dissolved organic carbon production. The size-specific particulate organic carbon production rates violated the normality assumption for ANOVAs and could not be appropriately transformed. These data were analysed by nonparametric ranking analysis, to test for effects of UVR or other environmental variables on the size distribution of production. Due to the large spatial variability in biological and physicochemical characteristics in L. Erie, both the parametric and non-parametric analyses treated each station as a block, thereby removing the variability due to location. *A posteriori* planned, pairwise, comparisons were made using the post-hoc Tukey test to compare UVB exposure level effects (four pairwise comparisons), overall UVB effect, UVA effect and nutrient status effects.

# Results

## Limnological Conditions

A total of 134 temperature profiles revealed the variability in establishment and depth of seasonal thermoclines over the sampling period and among basins. Seasonal thermoclines were not observed at any station in May, and increased in frequency and mean depth from June to August (mean epilimnion depth ca. 15 m). Water clarity was spatially heterogenous, with a distinct east-west gradient in PAR attenuation. Median values of the diffuse vertical attenuation coefficient for PAR (Fig. 2.3) showed highest penetration in the East Basin, with a median seasonal euphotic depth of 18.1 m. By comparison, the Central and West basins had median seasonal euphotic depths of 14.4 and 7.3 m, respectively.

The average seasonal thermocline depth was also basin-specific, with maximum values occurring in the deeper East Basin (median 15.0 = 5.3 m). While the East and Central basin stations typically stratified in the warm summer months (97.5 and 88.1 % of the surveyed stations, respectively) the West basin stations did not develop thermoclines as frequently (48.1 % of the surveyed stations). Additionally, shallow 'temporary' thermoclines, defined as a slight change in temperature (ca. 0.5-1°C·m$^{-1}$) with depth, typically occurring in the top two meters of the water column, were also recorded in ca. 30% of all stations for which both temperature and *in vivo* fluorescence profiles (a total of 37 stations) were available. These so-defined 'temporary' thermoclines were differentiated from seasonal thermoclines which were typically deeper (10 - 20 m) and exhibited sharper changes in temperature with depth (ca. 2-3°C·m$^{-1}$). In 1997, 'temporary' thermoclines were noted more frequently in early June

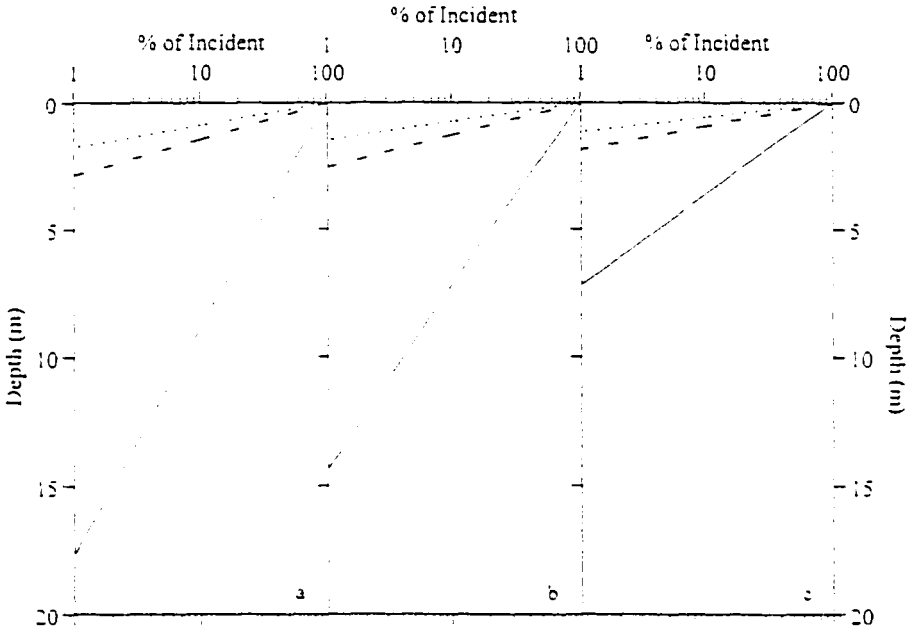



Figure 2.3: Percent light transmission in the East (a), Central (b) and West (c) basins of L. Erie. Values calculated from median broadband diffuse attenuation coefficients for PAR (this study), UVA and UVB (Smith et al. 1999). Solid lines: PAR; dashed lines: UVA; dotted line: UVB.

compared to July and August, and predominantly occurred in the West basin. Vertical profiles usually showed lower *in vivo* chl *a* fluorescence above these 'temporary' thermal boundaries than below (e.g. Fig. 2.4).

The limnological conditions for each station at which experiments were done are listed in Table 2.1. Seasonal thermoclines were not established at any of the experimental stations in May, June and August whereas in July all showed signs of thermal stratification. With one exception, the water samples collected for each experiment were representative of the mixed layer, as evidenced by the vertically uniform *in vivo* chl *a* fluorescence and temperature distributions. The epilimnion of the East Basin station 23, sampled in late July at 1045h, was not uniformly mixed (Fig. 2.5b). This station was also sampled on July 1 and on both these occasions, subsurface chl *a* fluorescence maxima were observed near the seasonal thermocline. Although uniform mixing was evident within the epilimnion on July 1, the calmer waters in late July were associated with a depth dependent *in vivo* chl *a* fluorescence distribution within the epilimnion (Fig. 2.5). Subsurface chl *a* maxima were also noted at stations 953 and 962 sampled in July, at 11 and 14 m (top of seasonal thermocline) depths, respectively. Light availability, as indicated by mean PAR (Table 2.1), attained its maximum in the shallow surface mixed layer on July 1 and minimal values under unstratified conditions at deep stations (e.g. June 5) and in the relatively turbid West Basin (e.g. Aug. 27).

### Phytoplankton Characteristics

Nutrient status of the whole water samples was assessed with multiple indicators (*see* Materials and Methods). Reported here are the numerical values for the carbon to phosphorus and carbon to nitrogen atomic ratios but an overall assignment of nitrogen or phosphorus

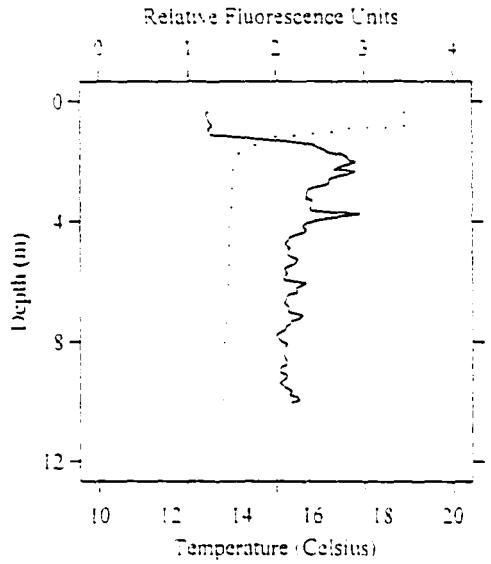



Figure 2.4: Temperature and *in vivo* chl *a* fluorescence profile from station 357 sampled June 4, 1997. Note shallow (1 m) 'temporary' thermocline and corresponding depression in *in vivo* chl *a* fluorescence. Solid line: relative fluorescence units; dashed line: temperature (°C).

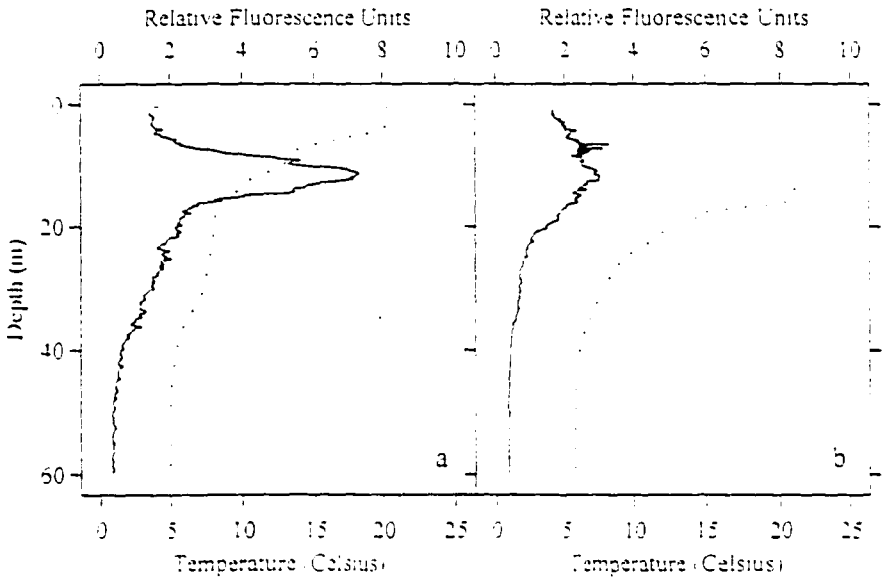



Figure 2.5: Temperature and *in vivo* chl *a* fluorescence profiles from station 23 sampled July 29 (a) and July 1 (b) 1997. Panel a: Subsurface chl *a* maxima with uniform chl *a* distribution within the thermal mixed layer (5 m). Panel b: Subsurface chl *a* maxima with incomplete mixing of the epilimnion (15 m) evidenced by the depth dependent change in fluorescence. Solid line: relative fluorescence units; dashed line: temperature (°C).

deficiency based on all the nutrient status indicators is given (Table 2.3). Nitrogen and/or phosphorus deficiency occurred at every experimental station except the West Basin station 337 sampled on June 4 and Aug. 27. The severity of deficiency was not extreme at any station, however.

The photosynthesis-irradiance curves from the light gradient incubator allowed estimates of the maximum photosynthetic rates ($P^B_m$), the initial slope ($\alpha^B$) and the light saturation parameter ($I_k$) (Table 2.3), and thus an assessment of the photoadaptive state of the phytoplankton. Low $I_k$ (<100 $\mu E \cdot m^{-2} \cdot s^{-1}$) values were observed on three experimental dates (June 3, June 4 and July 29), suggesting that the phytoplankton were adapted to relatively low light conditions. One station (Aug. 27) suggested a more high-light adapted state, while other stations were intermediate (Table 2.3).

The dominant genera of nano- and microphytoplankton varied between experimental dates but diatoms were important throughout, frequently dominating or co-dominating the mixed assemblages. Small flagellates of the *Ochromonas* (Chyrsophyceae) and *Cryptomonas* (Cryptophyta) genera were also commonly important. Picoplankton were not enumerated, but the size-fractionated primary production rates (below) indicated a substantial presence of photosynthetically-active picoplankton.

### Time Course and Extent of UVB Inhibition

Rates of photosynthesis at the outset of the incubations varied among experiments and frequently decreased to relatively low levels within the first two hours of exposure in both UVB exposed and shielded treatments (Fig. 2.6a,d). Cumulative photosynthetic rates normalized to uninhibited, light-saturated rates showed that the rate of decrease of relative

Table 2.3: Dominant nano- and microphytoplankton genera, photosynthetic parameters, nutrient status and $UVB_{inh\ eff}$ for the different stations sampled in L. Erie. Values for the maximum photosynthetic rates ($P^b_m$; μg C·μg Chl $a^{-1}$·$h^{-1}$) and the initial slope ($\alpha^b$; μg C·$m^2$·μg Chl $a^{-1}$·$E^{-1}$) represent the fitted values ± the asymptotic standard error of the estimate. The light saturation parameter ($I_k$; μE·$m^{-2}$·$s^{-1}$) values were calculated as $P^b_m$:$\alpha^b$ and are reported here as indicators of light adaptation status. Nutrient status for the whole water sample was assessed using all nutrient deficiency indicators (*see* Materials and Methods), however, only the elemental ratios are reported here. $UVB_{inh\ eff}$ reported in this table was calculated using the 50% PAR quartz tube treatments.

| Date | Station | Basin | Dominant Genera of Nano- and Micro-phytoplankton | $P^b_m$ | $\alpha^B$ | $I_k$ | Nutrient Deficiency Status | | Elemental Ratios | | $UVB_{inh\ eff}$ | |
|---|---|---|---|---|---|---|---|---|---|---|---|---|
| | | | | | | | P | N | C:P[a] | C:N[b] | 1h | 8h |
| 7/5 | 946 | C | *Aulacoseira* | 4.62 ± 0.20 | 7.22 ± 0.83 | 177.7 | N | Y | 124 | 9.2 | 12.83 | 1.18 |
| 3/6 | 946 | C | *Stephanodiscus* | 2.86 ± 0.13 | 13.06 ± 1.94 | 60.9 | Y | N | 194 | 9.1 | 3.96 | 0.32 |
| 4/6 | 337 | W | *Diatoma/Aulacoseira* | 5.68 ± 0.26 | 18.06 ± 2.78 | 87.4 | N | N | 67 | 8 | 1.35 | 1.07 |
| 5/6 | 961 | C | *Dinobryon/Aulacoseira* | n.a. | n.a. | n.a. | N | Y | 119 | 7.7 | 4.01 | 0.60 |
| 1/7 | 23 | E | *Dinobryon* | 3.93 ± 0.18 | 8.89 ± 1.11 | 122.8 | N | Y | 145 | 9.4 | 2.47 | 0.59 |
| 2/7 | 967 | W | *Ochromonas/Aulacoseira* | 3.66 ± 0.25 | 8.06 ± 1.67 | 126.2 | N | Y | 115 | 7.3 | 2.04 | 2.59 |
| 29/7 | 23 | E | *Anabaena/Cryptomonas* | 4.65 ± 0.30 | 14.72 ± 2.22 | 87.7 | Y | N | 118 | 7.6 | 6.88 | 1.22 |
| 30/7 | 953 | C | *Dinobryon/Fragilaria* | 4.92 ± 0.33 | 10.56 ± 2.22 | 129.5 | Y | Y | 103 | 8.6 | 7.36 | 1.85 |
| 31/7 | 962 | C | *Fragilaria/Ochromonas* | 8.39 ± 0.46 | 21.11 ± 3.61 | 110.4 | Y | Y | 106 | 8.3 | 3.96 | 0.20 |
| 27/8 | 337 | W | *Aulacoseira/Cryptomonas* | 5.13 ± 0.17 | 5.27 ± 0.28 | 270.0 | N | N | 115 | 6.5 | -0.98 | 0.13 |

[a]Particulate C:P atomic ratio, < 129 = no P deficiency, 129 - 258 = moderate P deficiency, > 258 = extreme P deficiency.
[b]Particulate C:N atomic ratio, < 8.3 = no N defic00iency, 8.3 - 14.6 = moderate N deficiency, > 14.6 = extreme N deficiency.

Figure 2.6: Instantaneous photosynthetic rates, cumulative photosynthesis and relative cumulative photosynthesis measured in all spectral treatments versus elapsed time in June (a, b, c) and July (d, e, f). Interval photosynthetic rates were calculated as labelled inorganic carbon incorporated within the specified time interval. Cumulative photosynthesis ($PS_{cum}$) was calculated as total incorporated carbon over the exposure period. Relative cumulative photosynthesis was calculated as $PS_{cum}:PS_{opt}$ which is the realized cumulative photosynthesis in each treatment ($PS_{cum}$) normalized to the cumulative photosynthesis in the absence of photoinhibition ($PS_{opt}$) based on an extrapolated 1h optimum rate. Panels a, b and c: interval photosynthetic rates, cumulative photosynthesis and relative cumulative photosynthesis, respectively, observed on June 4, 1997 station 337. Panel d, e and f: interval photosynthetic rates, cumulative photosynthesis and relative cumulative photosynthesis, respectively, observed on July 30, 1997 station 953. Error bars represent 2 SE. Legend: ● = 100% PAR, UVA and UVB; ○ = 100% PAR and UVA without UVB; ■ = 100% PAR, 50% UVA and 30% UV-B; □ = 100% PAR, 50% UVA without UV-B; ▲ = 50% PAR, UVA and UVB; Δ= 50% PAR, UVA without UVB; ★ = 50% PAR, 25% UVA and 15% UV-B; ☆ = 50% PAR, 25% UVA without UV-B.

Interval Photosynthetic Rates (gC•gChl$a$•h$^{-1}$)
Cumulative Photosynthesis Over Interval (gC•gChl$a^{-1}$)
Exposure Time (h)
Exposure Time (h)
Relative Cumulative Photosynthesis
a
b
c
d
e
f

photosynthesis was notably reduced in all treatments after the first two to three hours of exposure, i.e. the rate of photoinhibition was not constant over time (Fig. 2.6c,f). The harshest treatments (100% PAR, high UVA, UVB exposure) consistently resulted in the greatest suppression of photosynthesis. At comparable PAR exposure levels, the 30 and 15% UVB exposure level treatments usually demonstrated less photoinhibition than the corresponding 100 and 50% UVB treatments (Fig. 2.6), reflective of the milder UVR exposure encountered in the polystyrene flasks (30 and 15% UVB) (Fig. 2.2).

When phytoplankton were shielded from UVB radiation with Mylar-D, higher rates of photosynthesis were generally achieved, although at times differences were small (Fig. 2.6a,b,d,e). On average, the most severe exposures to UVB (100%) diminished cumulative photosynthesis by 16.4% in short-term incubations (1h), but the inhibition could be as high as 33.0% (e.g. July 29; station 23 East basin). After 8h of incubation, such exposures to UVB resulted in 36.3% less cumulative photosynthesis on average, and as much as 57.7% less (e.g. July 29). Rapid kinetics of UVB photoinhibition were reflected in all treatments (Fig. 2.6c,f), particularly, in 100% UVB exposure treatment, where ca. 50% of the UVB-dependent inhibition of cumulative photosynthesis was attained within the first hour of exposure (Table 2.4). The harshest UVB treatment yielded the greatest inhibition in both short and long incubations, and below 50% exposure the effects of UVB were not significant on average.

While an ideal UVA optical filter was not available, some inference of the inhibition potential of UVA can be made by comparing the UVB-shielded quartz and polystyrene treatments because the polystyrene removes approximately 50% of the UVA (predominantly shorter wavelengths, Fig. 2.2) while quartz has virtually 100% transmission; both are

Table 2.4: Average percent UVB-dependent inhibition of cumulative photosynthesis (PS) found following 1h and 8h of exposure to different spectral treatments and the 1h and 8h $UVB_{inh\ eff}$ values for the different UVB exposure levels. Percent UVB inhibition was calculated as $100 \cdot (PS_{UVBshielded} - PS_{UVBexposed})/PS_{UVBshielded}$ within the different treatments. Averages ± 1 SE; subscripts are the number of samples used in the average computation. Bold values are significantly ($\alpha = 0.05$) different from zero.

| UVB Exposure | PAR exposure | 1h | | 8h | |
|---|---|---|---|---|---|
| | | % UV-B inhibition | $UVB_{inh\ eff}$ | % UV-B inhibition | $UVB_{inh\ eff}$ |
| 100 | 100 | **16.4 ± 4.3**$_{10}$ | 5.1 ± 1.9$_{10}$ | **36.3 ± 6.1**$_{10}$ | 1.6 ± 0.4$_{10}$ |
| 50 | 50 | **8.7 ± 2.1**$_{10}$ | 4.4 ± 1.2$_{10}$ | **15.5 ± 3.8**$_{10}$ | 1.0 ± 0.3$_{10}$ |
| 30 | 100 | -4.5 ± 4.6$_{6}$ | -2.7 ± 2.7$_{6}$ | -0.5 ± 7.4$_{8}$ | -1.3 ± 1.1$_{8}$ |
| 15 | 50 | 5.1 ± 2.8$_{6}$ | 4.3 ± 4.4$_{6}$ | 14.2 ± 7.8$_{8}$ | 2.1 ± 1.3$_{8}$ |

essentially 100% transparent to PAR (Table 2.5). Following 1h of exposure, the higher UVA treatments averaged 21.0% lower cumulative photosynthesis than the lower UVA treatments. However, the kinetics of UVA inhibition so-defined showed a different pattern than the kinetics of UVB inhibition. The effects of UVA on cumulative photosynthesis did not, on average, increase with longer exposures and may even have diminished by 8h. Nevertheless, the 8h exposure period could result in as much as 43.1% (May 7, station 946), but on average 12.4%, lower cumulative photosynthesis in the high than the low UVA treatments (Table 2.5). The apparent combined effect of UVB and part of the UVA, so defined, was an average loss of 38.0% of cumulative photosynthesis in 1h exposures and 48.7% in 8h exposures under simulated surface conditions (i.e. 100% UVB exposure).

The contribution of PAR to photoinhibition in the short-term was assessed by reference to the photosynthesis-irradiance response of phytoplankton in the light gradient incubator (PAR only). There was no statistically significant evidence for PAR-dependent inhibition. The maximum levels of PAR in the incubator were comparable to the maximum solar PAR levels observed. Although the spectral quality differed between the incubator lamp and the natural solar radiation, it appeared unlikely that PAR would cause appreciable inhibition on the 1h time scale. The potential inhibition by PAR in longer term (8h) exposures could not be investigated with this experimental design.

### Inhibition Efficiency of UVB

Efficiency of inhibition by UVB ($UVB_{inh.eff.}$) was variable between lake stations and sample dates but spatial and temporal patterns were difficult to discern with our opportunistic sampling scheme. ANOVA showed that the $UVB_{inh.eff.}$ index did not vary significantly with

Table 2.5: Average percent partial UVA-dependent inhibition of cumulative photosynthesis (PS) found following 1h and 8h exposure to different spectral treatments. Partial percent UVA-dependent inhibition was calculated using UVB-shielded treatments only and comparing 100 vs 30 or 50 vs 15 in the following manner $100 \cdot (PS_{PARpolystyrene} - PS_{PARquartz}) / PS_{PARpolystyrene}$. Averages ± 1 SE; subscripts are the number of samples used in the average computation. Bold values are significantly ($\alpha = 0.05$) different from zero.

| PAR Exposure | UVA Exposure | | Partial % UVA inhibition | |
|---|---|---|---|---|
| | Quartz | Polystyrene | 1h | 8h |
| 100 | 100 | 50 | **$21.6 \pm 6.5_8$** | $12.4 \pm 7.7_8$ |
| 50 | 50 | 25 | **$20.3 \pm 5.7_8$** | $10.8 \pm 7.2_8$ |

UVB exposure level, but it did vary significantly with time (Fig. 2.7; $p < 0.00001$, $r^2 = 0.243$). The higher $UVB_{inh.eff.}$ values for the short versus long exposures underscore the rapid kinetics of UVB-dependent inhibition as well as the non-linear nature of the response to UVB. This non-linearity was further emphasized when attempts were made to describe the inhibition of cumulative photosynthesis as a linear function of the cumulative weighted UVB and short UVA (297 - 347 nm) exposure (Fig. 2.8), as others have done before. A linear regression through the combined data yielded a highly significant relationship ($p < 0.00001$) but the amount of variance explained was low ($r^2 = 0.126$). Analysis of individual dates revealed non-significant relationships in three experiments (range of p values < 0.000001 - 0.565) and considerable variation in the slope (i.e. sensitivity). Thus, there did not appear to be a consistent linear response among the communities encountered here.

Because of the rapid nature of the kinetics of UVB-dependent photoinhibition, it was assumed that any difference in sensitivity to UVB would more likely be reflected in the 1h vs the 8h $UVB_{inh.eff}$ index. Attempts were therefore made to identify any relationships between the 1h index of UVB sensitivity and species composition, nutrient status and/or light history. With this relatively small data set, only simple and strong effects would be identifiable and little success was achieved in finding them. Community composition was not an obviously decisive factor, since the same genera (e.g. Dinobryon) or higher groups (e.g. diatoms) could be dominant in both relatively sensitive and relatively tolerant assemblages (Table 2.3). ANOVAs of particulate C:P and C:N ratios (Table 2.3) and visual inspection of scatter plots of APA, P debt and N debt (not shown) failed to indicate any simple or statistically-significant relationships between these nitrogen or phosphorus deficiency indicators and the UVB

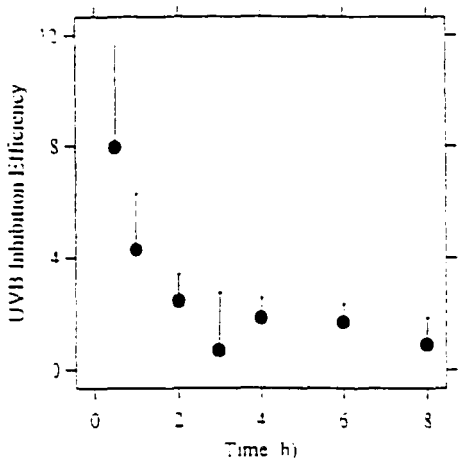



Figure 2.7: Calculated $UVB_{inh\,eff}$ averaged over all dates and all treatments emphasising the non-linear nature of UVB-dependent inhibition over time. Error bars represent 1 SD.

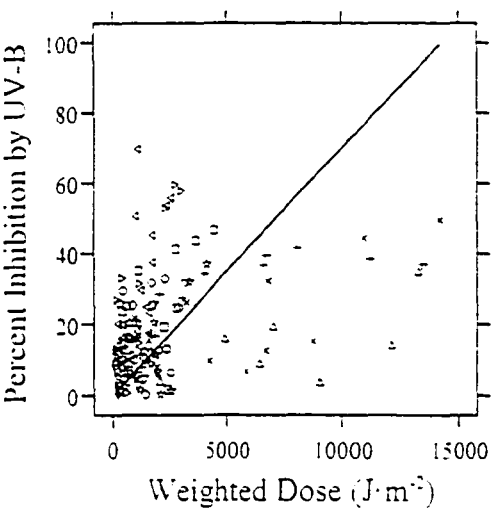



Figure 2.8: Percent inhibition of photosynthesis as a function of weighted UVR (295-347 nm) using the Behrenfeld et al. (1993) best fit exponential function for the combined data set. All time intervals for the different treatments for all the experiments are plotted. The line is the Behrenfeld et al. (1993) equation $Pc=0.007*Q_{exp}$, where Pc is the percent inhibition due to UVB and the $Q_{exp}$ is the weighted exposure differences between UVB exposed and shielded treatments. Legend: ○ = May 7; x = June 3; + = June 4; △ = June 5; ▽ = July 1; ◁ = July 2; ▷ = July 29; □ = July 30; ◇ = July 31; ☆ = August 27.

sensitivity of the phytoplankton. While no relationships were established between specific indicators of phosphorus deficiency and UVB sensitivity, algal assemblages assessed overall as phosphorus deficient had higher 1h $UVB_{inh\ eff}$ indices than those deemed phosphorus sufficient (ANOVA $p < 0.05$; $r^2 = 0.580$). This relationship was not present with the 8h $UVB_{inh\ eff}$ values. Further inspection of scatter plots failed to indicate any relationships between sensitivity and either photoadaptive state ($I_k$) or light history (mean PAR). The environmental influences examined may well have contributed to the observed variation in sensitivity, but with the possible exception of phosphorus limitation, an over-riding control by any one factor failed to be demonstrated.

*UVB Effects on Particulate and Dissolved Organic Carbon Production*

The distribution of $TO^{14}C$ between particulate ($PO^{14}C$) and dissolved organic ($DO^{14}C$) carbon pools after 8 h of incubation differed between UVB exposed and shielded treatments, but the effects were significant ($p < 0.0001$; $r^2 = 0.940$) only at the highest (100% PAR and UVB) and lowest exposures (50% PAR and 15% UVB) (Table 2.6). At these exposure levels, the presence of UVB significantly increased the percent of label in the DOC, with greatest effect in the harsher (100%) treatment. Among UVB exposed treatments, the 100% UVB exposures demonstrated significantly ($p < 0.00001$) higher % $DO^{14}C$ than all other UVB exposed samples. Among UVB shielded treatments, the 100% PAR and UVA exposure displayed significantly higher ($p < 0.00001$) % $DO^{14}C$ than all other treatments except the 100% PAR and 50% UVA treatment ($p > 0.30$).

Nonparametric ranking analysis of the size fractioned $PO^{14}C$ revealed that % $TO^{14}C$ production in the picoplankton was significantly ($p < 0.00001$; $r^2 = 0.957$) lower in UVB-

Table 2.6: Average percent of total organic production (% TO$^{14}$C) of eight experiments (May 7 and July 1 not included in analysis) in the different carbon pools for each treatment. The particulate pool is split according to the large nano- and microphytoplankton (> 2 μm) and the small picoplankton (< 2 μm). Each value is the mean of all replicates over the eight experiments ± 1 SE, the subscripts denote the number of samples used in the average computation.

| | UVB Treatment label | | | |
|---|---|---|---|---|
| | 100 | 50 | 30 | 15 |
| Dissolved | | | | |
| with UVB | $14.9 \pm 0.9_{21}$ | $8.2 \pm 0.4_{21}$ | $9.6 \pm 0.8_{21}$ | $8.3 \pm 0.7_{17}$ |
| without UVB | $10.9 \pm 0.5_{21}$ | $7.6 \pm 0.5_{21}$ | $10.1 \pm 0.7_{20}$ | $7.4 \pm 0.6_{21}$ |
| Particulate | | | | |
| > 2 μm | | | | |
| with UVB | $60.0 \pm 3.6_{18}$ | $54.7 \pm 4.5_{19}$ | $57.8 \pm 3.3_{21}$ | $55.3 \pm 3.6_{18}$ |
| without UVB | $56.3 \pm 3.7_{21}$ | $55.4 \pm 4.0_{20}$ | $54.0 \pm 3.6_{20}$ | $52.3 \pm 4.0_{21}$ |
| < 2 μm | | | | |
| with UVB | $25.2 \pm 3.0_{20}$ | $37.4 \pm 4.6_{18}$ | $32.7 \pm 3.3_{21}$ | $33.4 \pm 3.2_{19}$ |
| without UVB | $32.8 \pm 3.5_{21}$ | $37.1 \pm 3.7_{20}$ | $35.9 \pm 3.7_{20}$ | $40.4 \pm 3.9_{21}$ |

exposed than UVB-shielded treatments. The effect was again significant only at the highest (100% PAR and UVB) and lowest (50% PAR and 15% UVB) exposures (Table 2.6). The effects of UVB on the percent TO$^{14}$C production in the larger phytoplankton size fraction were smaller and significant only in the 100% PAR exposures. The harshest treatments showed a borderline significant increase with UVB exposure ($p = 0.051$) and the 30% UVB treatment showed significantly ($p < 0.01$) higher production in the UVB-exposed relative to the UVB-protected treatments (Table 2.6).

Comparing among UVB exposed treatments only, the exposure level had a pronounced effect on the share of total production in picoplankton, with the picoplankton share significantly ($p<0.00001$) depressed in the harshest exposure compared to others. The share in larger plankton was, by contrast, higher ($p<0.01$) in the harshest exposure. These effects of exposure level will reflect the variation of PAR and UVA, as well as UVB, among treatments. They indicate significant, but moderate-sized, average effects of total photoinhibitory stress on the disposition of recently-fixed carbon among size classes and dissolved vs particulate phases.

Nonparametric ranking analysis did not reveal any nutrient deficiency effects on the relative proportion of dissolved vs particulate production, or the size distribution of the particulate production.

### Expected UVB Impacts in L. Erie

Using basin-specific median UVA and UVB broadband attenuation coefficients from a parallel study (Smith et al. 1999), the water column depths simulated by the four UVB exposure levels and the proportion of the photic zone (measured in this study) that these represent were approximated for each basin (Table 2.7). While the East and Central basins

Table 2.7: Water column depths represented by each UVB exposure level treatment, calculated using basin specific median PAR, UVA and UVB broadband attenuation coefficients. Values in parentheses represent the proportion (in %) of the euphotic zone each depth represents.

| | Representative Depth (m) | | | | | |
|---|---|---|---|---|---|---|
| | East Basin | | Central Basin | | West Basin | |
| % UVB Exposure | | | | | | |
| 50 | 0.3 | (1.5) | 0.3 | (1.9) | 0.2 | (3.1) |
| 30 | 0.5 | (2.6) | 0.5 | (3.3) | 0.4 | (5.3) |
| 15 | 0.7 | (4.0) | 0.7 | (5.2) | 0.6 | (8.4) |
| UVB 1% depth | 1.8 | (9.8) | 1.8 | (12.5) | 1.5 | (20.3) |
| UVA 1% depth | 2.9 | (15.9) | 3.4 | (23.5) | 2.4 | (32.6) |
| PAR 1% depth | 18.1 | | 14.4 | | 7.3 | |

seem to have similar light transmission characteristics, the West basin has distinctly stronger attenuation. In all basins, the depth of 50% UVB penetration (the lower limit for demonstrable, significant UVB effects in this study) was only a small part of the total photic zone. A greater proportion of the photic zone is potentially influenced by UVR in the West than the other basins, with the share of photic zone occupied by the 1% UVB depth twice that of the East basin.

# Discussion

The effects of UVB on planktonic primary production have to date been studied largely in relatively clear oceanic waters, particularly those of the Southern Ocean (e.g. Cullen et al. 1992, Neale et al. 1998b,c, Smith et al. 1992) where the Antarctic ozone hole is such a prominent feature. L. Erie, by contrast, is a moderately turbid system even by freshwater standards. Its phytoplankton might, therefore, be expected to display acclimation to relatively low exposures, and to be correspondingly vulnerable to UVB damage (e.g. Helbling et al. 1994, Neale et al. 1998b). Evidence of adverse effects of UVB on short-term primary production in L. Erie were found. Inhibition of photosynthetic carbon assimilation by UVB was rapid and often extensive, consistent with fluorescence-based assays of photosynthetic competence in L. Erie phytoplankton (Marwood et al. 2000). Although variable, however, the degree of UVB-dependent inhibition under simulated near-surface conditions was within the range found in other studies of both marine and freshwater phytoplankton (e.g. Behrenfeld et al. 1993, Furgal and Smith 1997, Helbling et al. 1992, 1994, Neale et al. 1998b, Villafañe et al. 1995).

The sensitivity of algae to UVR is moderated by mechanisms that help the organisms to avoid effective exposure (e.g. screening compounds) as well as mechanisms that promote repair (e.g. DNA photolyase activity). Both aspects (avoidance and repair) are influenced by the interactive effects of radiation of differing wavelengths. Only with an appropriate model for the spectral and kinetic responses of the processes of interest (e.g. photosynthesis) can the sensitivity of different algal communities to any particular waveband (e.g. UVB) be accurately compared or integrated over meaningful depth and time scales (Smith and Cullen 1995, Cullen

and Neale 1997). Such models have been validated for only a few types of phytoplankton communities, however (Neale et al. 1998b,c, Smith et al. 1998). As an initial descriptive approach, variations in sensitivity were analysed with a simple index ($UVB_{inh\ eff}$) that entertains a linear exposure-response relationship regardless of the time scale of observation. Such an approach has been used, implicitly or explicitly, by other researchers (e.g. Behrenfeld et al. 1993, Boucher and Prézelin 1996, Gala and Giesy 1991, Helbling et al. 1994) and gives an intuitively obvious, if flawed, index. Concentrating on relatively short-term (1 h) $UVB_{inh\ eff}$ values should minimize the confounding effects of photoinhibition and/or remediation of UVB damage by longer wavelengths (Prézelin et al. 1994).

Although over a 10-fold range in the 1h $UVB_{inh\ eff}$ was observed among experiments, the variation in sensitivity could not be related to the species composition. Taxonomic composition should be important because the repair of UVB induced DNA photoproducts and photosystem reaction center damage is taxon-specific (Karentz et al. 1991a, Xiong et al. 1997), as is the induction and effectiveness of screening compounds (e.g. Hannach and Sigleo 1998, Neale et al. 1998a). Using a $UVB_{inh\ eff}$ index similar to the one used in this study, Gala and Giesy (1991) reported apparently characteristic differences between diatom/chrysophycean and cyanobacterial assemblages in L. Michigan, and suggested that pigment composition might be responsible. During this L. Erie study, however, communities were rather consistently dominated (among the nano- and microphytoplankton) by diatoms and chrysophyceans, which may have limited the scope for detecting broad taxonomic influences. Unquantified variations among the picoplankton may have further impeded detection of taxonomic influences.

In addition to intrinsic, taxonomically-related, characteristics, algal sensitivity to UVR

can also depend on environmental modifying factors such as water clarity, mixing depth and mixing rates (e.g. Helbling et al. 1992, Neale et al. 1998b), light history (e.g. Villafañe et al. 1995) and/or nutrient availability (e.g. Lesser et al. 1994). The measures of light climate and photoadaptive state in this study failed to reveal any relationships with the $UVB_{inh\ eff}$ for L. Erie phytoplankton, however. Evidence for the importance of light history and/or photoadaptive state in natural plankton communities has been derived mainly from comparisons of samples from very different ocean regions or depths (e.g. Helbling et al. 1992) or among different samples of polar phytoplankton, all at very low temperature (e.g. Neale et al. 1998b). The present study, involving only surface mixed layer samples from one temperate lake, may not have encountered sufficient variation in photoadaptive state to reveal the effects against the background of other influences.

It was observed that the 1h $UVB_{inh\ eff}$ sensitivity index was higher under conditions of P deficiency. Phosphorus is an essential macronutrient found in DNA, RNA and lipid- (e.g. phospholipid membranes) and ester-phosphorus (e.g. ATP) fractions (Morris 1980). Exposure to UVB can lead to the photooxidation of membrane lipids (Chamberlain and Moss 1987, Hessen et al. 1997, Kramer et al. 1991), a process likely initiated by active oxygen species (e.g. singlet oxygen and perhydroxyl radicals) which are particularly potent to chloroplast membranes characterised by high polyunsaturated fatty acid contents (Mishra and Singhal 1992). The resynthesis of these and other damaged cellular components (e.g. proteins) not only require the building blocks but also energy in the form of ATP. Phosphorus limitation in algae may thus constrain their ability to resynthesise critical cellular components. These results are, to our knowledge, the first evidence of any effect of nutrient status on UVB sensitivity in nature.

The modifying effect of P deficiency was not evident in long (8 h) exposures, suggesting that the cumulative damage may have overwhelmed differences in repair or recovery ability.

Although a linear exposure-response model was adopted to characterize UVB sensitivity on the short-term (1h), the average seven-fold (maximum 20-fold) higher 1 h $UVB_{inh\ eff}$ compared to the 8 h $UVB_{inh\ eff}$ indicated serious problems with the model on longer time scales. This was emphasised by the lack of fit of the Behrenfeld et al. (1993) linear dose-response relationship. The continuous-labelling protocol used in this study for assaying primary production is potentially subject to confounding effects from diel variations of photosynthetic capacity (Boucher and Prézelin 1996a) and intracellular tracer equilibration processes (Smith and Platt 1984). The protocol is nonetheless similar to methods employed successfully by others (e.g. Behrenfeld et al. 1993, Smith et al. 1998) and is probably not the principal source of the large, apparent, temporal variation in sensitivity. The apparent rapidity of UVB photoinhibition means that relatively brief exposures to UVB in surface waters, such as would occur under strong mixing conditions, can be damaging to primary production (Marwood et al. 2000, Neale et al. 1998c, Prézelin et al. 1994, Smith and Cullen 1995).

Longer UVA wavelengths are important in the mitigation of UVB damage, but UVA is also largely responsible for inhibiting primary production (Figueroa et al. 1997, Helbling et al. 1992, Kim and Watanabe 1993, Smith et al. 1998). Although the effect of only a portion of the full UVA waveband was measured, it contributed substantially to photoinhibition in L. Erie. There was also evidence that UVA inhibition kinetics differed from those of UVB, with an even more rapidly diminishing effect in longer incubations. Differences in damage and recovery kinetics between UVB and UVA have recently been described and related to

acclimatory processes and/or thresholds for inhibition (Figueroa et al. 1997, Hermann et al. 1997, Prézelin and Boucher 1994). Such findings emphasize the need for more realistic models that explicitly account for the interaction among different wavelengths, i.e. a biological weighting function, and the kinetics of the processes involved.

The impacts UVR can have on phytoplankton are not limited to decreases in primary production. Shifts in phytoplankton species composition have been reported following UVR exposures (Mostajir et al. 1999, Wänberg et al. 1996, Worrest et al. 1981), as have changes in the chemical composition of algae (Wang and Chai 1994, Goes et al. 1994). These shifts can lead to changes in the size distribution and nutritive value of phytoplankton which may have implications for higher trophic levels. Although these possible effects in L. Erie were not studied, the effects of UVR on the relative distribution of recently-fixed carbon between the particulate and dissolved pools were investigated. Extracellular release of photosynthetic products is a common feature of healthy phytoplankton (Bjørsen 1988), and it is well established that bacteria readily take up these compounds as carbon substrates (Ligneil 1990, Norrman et al. 1995). While UVR can have direct negative impacts on bacteria by inhibiting their growth (Karentz et al. 1994 and references therein, Wilhelm and Smith 2000), UVR can also enhance bacterial production by photomodifying the more refractory DOC in the water column thereby rendering it more bioavailable (Lindell et al. 1995). Enhanced production of algal DOC due to UVR is another possibility, whereby the stimulation of microbes could result in more carbon being shunted into the microbial loop, increasing the length of the aquatic food chain and reducing the potential production at higher trophic levels.

In L. Erie, the percent of $TO^{14}C$ in the dissolved organic carbon pool (% $DO^{14}C$) was

dependent on the severity of the exposure, with the harshest treatment showing the highest proportion of organic carbon in the dissolved fraction. The mechanism of extracellular release of photosynthetic products has been argued as both a passive (Bjørsen 1988) and an active process (Lignell 1990). Under the passive theory, an increase in membrane permeability due to UVR photooxidation of membrane lipids, can lead to increased "leakage" of algal cells (cf. Chamberlain and Moss 1987). However, whether UVR can directly or indirectly stimulate the active external transport of algal DOC is unknown. High light encountered in surface waters has been linked to increased production of extracellular release products (Mague et al. 1980), a possible consequence of increased photorespiration (Williams 1990). While other studies have reported no effects of UVR on the relative proportion of organic carbon in the particulate versus the dissolved pools (e.g. Pausz and Herndl 1999), the results of this study are in agreement with data from L. Erie in 1995 (R.E.H. Smith, unpub.) which indicated even larger UVR-dependent stimulation of %$DO^{14}C$ than found here. The observed accumulation of $DO^{14}C$ will reflect a balance between release from phytoplankton and utilization by heterotrophic microorganisms, so disparities between studies may have various explanations. At least in L. Erie, however, UVR, and specifically UVB, exposure appears to have a net positive effect on $DO^{14}C$ accumulation.

Of the two plankton size fractions investigated here, inhibitory effects of both UVB and UVA on carbon incorporation occurred in the picoplankton while the larger phytoplankton size fraction seemed to be relatively less affected by exposure to these wavebands. Various mycosporine-like amino acids (MAAs) have been identified in phytoplankton assemblages, which confer protection from both UVB and UVA radiation (Roy 2000, Sinha et al. 1998). The

ability to synthesize these types of compounds is taxon-specific (Xiong et al. 1997), and their photoprotective efficiency is size-specific with theoretical size limits of < 1 μm (Garcia-Pichel 1994). The < 2 μm L. Erie phytoplankton may not make effective use of UVR-absorbing pigments, a possible explanation for their higher sensitivity to the UVR portion of the solar spectrum. In addition to being absorbed by pigments, UVR is also strongly absorbed by proteins and free amino acids (Tevini 1993). The concentration of these molecules and the cell size of unicellular algae have been argued as UVR sensitivity influencing factors, cells with high surface area to volume ratios typically demonstrating more UVR damage per unit of DNA (Karentz et al. 1991a). While larger cells may not necessarily have more UVR damage mitigating abilities, their mere size may afford them more nuclear protection (i.e. DNA protection), thereby reducing their susceptibility to UVR damage. While these size specific UVR effects were small, they may not be negligible as picoplankton biomass, on average, approximates that of the combined nano- and microphytoplankton biomass in the Laurentian Great Lakes (Fahnenstiel et al. 1998).

In L. Erie, UVR is rapidly attenuated in the water column, with lake wide median 1% depths of integrated UVB and UVA of 1.5 and 2.5 m (Smith et al. 1999). Significant UVB effects on $TO^{14}C$ were limited to the harshest treatments, therefore, substantial effects will presumably be constrained to a relatively small part of the photic zone and the extent of depth integrated damage be limited. However, UVR transmission is not uniform among basins with UVR penetration increasing from west to east. Although the absolute differences in 1% UVR depths are small, they are more important if compared against the corresponding differences of PAR penetration. The West Basin, as the most turbid, might be expected to be less vulnerable

than the other basins, yet the 1% UVB photic depth represents a greater part of the photic zone (ca. 20%) in the West than in the other basins. The 50% UVB depth, the limit of demonstrable average effects in this study, also occupies a larger share of the photic zone in the West basin than elsewhere.

While, on average, cells will not reside in these high UVR (>50% surface incident) surface waters for extended periods of time, during calmer periods the establishment of shallow 'temporary' thermoclines can constrain organisms to the top meters of the water column. In 1997, the West basin developed these 'temporary' thermoclines more frequently. Considering that the median UVB photic zone was ca. 1.1 m in this part of the lake and the median 'temporary' thermocline depth was 0.5 m, important losses of integrated primary production and other effects are possible under some circumstances if it is taken into account that the bulk of the production in the West basin occurs in the top five meters of the water column.

Special circumstances (e.g. temporary thermoclines) notwithstanding, these results suggest minimal impact of UVB, at present levels, on short-term primary production rates in L. Erie. Longer-term effects, including alterations in form or quality of production, could be more substantial but cannot be evaluated with data to hand. Moreover, evidence that UVA is a more effective inhibitor of primary production in nature than is UVB was noted as others have observed (e.g. Bühlmann et al. 1987, Figueroa et al. 1997). Inasmuch as human influence on water clarity can alter UVR exposure substantially (e.g. Schindler et al. 1996, Yan et al. 1996), further study to elucidate the photoinhibitory action of the entire UVR spectrum is necessary.

# Chapter 3

## Models for UVR-dependent photoinhibition of Lake Erie phytoplankton

## Abstract

A model for UVR- and PAR-dependent photoinhibition, with explicit damage and recovery processes (the R model), was formulated and calibrated against observations of photosynthesis by L. Erie phytoplankton in the summer of 1998. The observations encompassed exposures to natural sunlight on time scales from 0.5 to 4 h, and with 7 different spectral treatments. The model explained 76-93% of the variation in photosynthetic rates, and indicated active recovery processes at 4 of the 5 experimental stations. UVR-dependent photoinhibition could not be satisfactorily and consistently explained by simpler models that assumed either a lack of recovery processes (H model) or an instantaneous equilibrium between damage and recovery (E model). Biological weighting functions (BWF), the first for freshwater phytoplankton communities, were derived to quantify the spectral dependence of photoinhibitory power. The BWFs had substantial commonality of shape through the UVR, with a steep decrease from 300 to 320 nm, but considerable differences from BWFs for other communities and/or biological systems. The R model, with a representative BWF from the calibration year, was applied to similar photosynthesis data from the previous year (1997) to determine how robust the model, and the central tendency of BWF shape, might be. Unlike the simpler models, the R model provided a highly significant fit to all 10 of the 1997 experiments, although the average percent explained variation (47%) was lower than in 1998. The R model was again superior to the simpler alternatives, and again indicated active recovery processes at most of the stations examined. The results indicated that variations in both spectral sensitivity (as expressed by the BWF) and recovery rates are important determinants of phytoplankton response to UVR.

## Introduction

Much research in aquatic ecology has been directed in recent years towards elucidating the repercussions of reduced stratospheric ozone and the associated increases in surface-incident ultraviolet radiation (UVR). Primary production has often been the biological process of choice to assess the impacts of UVR because it reflects a variety of physiological and ecological mechanisms, is measurable on phytoplankton communities and is an important and vulnerable process, ultimately influencing the productivity of higher trophic levels. Elucidating the effects of UVR has not been easy, partly because UVR is part of a continuous solar radiation spectrum that acts both beneficially and detrimentally on photosynthesizing organisms. Solar radiation drives the photosynthetic conversion of inorganic carbon to organic substrates, yet excessive visible light, as well as UVR, can inhibit photosynthesis (Cullen an Lesser 1991, Villafañe et al. 1995), damage intracellular components such as DNA (Karentz et al. 1991a, Prézelin et al. 1994) and inactivate certain key photosynthetic proteins (Greenberg et al. 1989, Wilson et al. 1995).

Phytoplankton have evolved a variety of mechanisms to prevent or counteract the damage from UVR and excessive light, such as DNA photoreactivation, synthesis of photoprotective pigments and dark repair processes (Karentz 1999, Roy 2000). While the timescales of photoinhibition vary on the order of minutes to hours, some photoprotection measures occur within seconds or minutes (e.g. energy dissipation via fluorescence, state transitions or non-radiative decay) and others occur on the order of hours to days (e.g. synthesis of protective pigments or chemical quenchers) (Ferris and Christian 1991, Villafañe et al. 1995). The kinetics of these processes are important when the timescales of vertical water

column mixing, and thus radiation exposure, are taken into account, and are influenced by factors such as nutrient availability and species composition. Nutrient limitation may increase algal photosensitivity to UVR by constraining the resynthesis of damaged proteins (Lesser et al. 1994), while the capacity for repair and the synthesis of protective pigments is known to be species specific (Karentz et al. 1991a,b, Xiong et al. 1997). Finite, but variable, kinetics of both photodamage and recovery processes in phytoplankton communities can therefore be anticipated.

Photoinhibition by UVR is wavelength-specific due to the variation of photon energies and intracellular targets of action across the UV waveband. Action spectra, which are derived through near-monochromatic exposures, are useful for identifying sites and mechanisms of photoinhibition in the target organisms but polychromatic exposures are more realistic when the ultimate goal is to investigate the impact of UVR in natural systems (Coohill 1997). The value of the polychromatic approach is rooted in the fact that the longer ultraviolet A (UVA) and short visible wavelengths play an active role in photoenzymatic repair (Mitchell and Karentz 1993, Roy 2000) which may be important in mitigating the impacts of the shorter ultraviolet B (UVB) wavelengths. However, UVA and visible light can also be inhibitory (e.g. Herrmann et al. 1997) and may reinforce some of the indirect modes of UVB impact, such as damage from reactive oxygen species (Vincent and Neale 2000). The final impact on the target organisms therefore reflects interactions among different parts of the incident spectrum, and is best reflected in a biological weighting function (BWF) derived from realistic polychromatic exposures (Neale 2000). For field studies, BWFs are now the tool of choice for describing the biological response to UVR. They are notably important when estimating primary production

in a mixed system, where phytoplankton cells experience large variations in intensities and spectral composition of UVR and photosynthetically active radiation (e.g. Cullen et al. 1992, Neale et al. 1998b). There are as yet no published BWFs for freshwater phytoplankton, and very limited information on the appropriate kinetic models for UVR-dependent photoinhibition (Smith et al. 1998).

Radiation weighted with a BWF can be used in conjunction with kinetic models to predict algal photoinhibition. Although some models have proposed that photoinhibition is a simple, linear, function of cumulative UVB dose (Behrenfeld et al. 1993, Boucher and Prézelin 1996), there is in fact no mechanistic basis for expecting such relationships, and every reason to expect non-linear functions instead (Cullen and Neale 1997). Starting with a simple two-compartment model for conversion between inhibited and non-inhibited states, non-linear predictive equations can be derived by assuming certain limiting conditions (Neale 2000). In one limiting case, it has been assumed that a rapid equilibrium is established between damage and repair processes (irradiance-dependent model, Cullen et al. 1992). Alternatively, it can be assumed that repair is essentially inactive and that photoinhibition is a function of cumulative exposure (cumulative exposure model, Neale et al. 1998b).

Both limiting cases of the two compartment model have had success in describing UVR-dependent photoinhibition in different applications (Neale et al. 1998b, Cullen et al. 1992, Lesser et al. 1994). The irradiance-dependent model has correctly described photoinhibition of algae fully acclimated to the prevailing UVR regime, as best seen in studies of laboratory cultures (Cullen et al. 1992, Lesser et al. 1994). The cumulative exposure model, on the other hand, has successfully described the response of natural communities, particularly

those encountered under conditions of deep vertical mixing (and presumably low average light exposure) and/or low temperatures (Neale et al. 1998b, Smith et al. 1998). Neither model has been successful in application to all situations.

The Southern Ocean has attracted more attention from UVR researchers than any other single system, because of the extreme situation presented by the Antarctic stratospheric ozone hole. Even there, however, it is only recently that suitable kinetic models and BWFs have been developed and applied to produce realistic estimates of UVR-dependent photoinhibition (Cullen et al. 1992, Neale et al. 1998b,c). One study to date has attempted similar estimates for freshwaters (L. Ontario, Smith et al. 1998) but it had to depend on BWFs derived elsewhere and on very limited information about spectral penetration. Especially for the larger systems, in which mixing is very important, current estimates of UVR impact on primary production in freshwaters cannot be considered realistic or reliable indicators of the vertically and temporally integrated effect.

This chapter is comprised of essentially two series of experiments. As a first venture, the kinetics of UVR-dependent photoinhibition in Lake Erie phytoplankton were investigated in 1997. Using the available tools in the literature, i.e. published biological weighting functions (e.g. *Phaeodactylum tricornutum* BWF) and the irradiance-dependent and cumulative exposure kinetic models, attempts were made to describe the photoinhibitory response and the results show that neither model was acceptable. BWFs specific to L. Erie phytoplankton were therefore derived and a more appropriate kinetic model that would incorporate a finite repair term, thereby eliminating the need for *a priori* assumptions about recovery rates, was developed.

## Materials and methods

### Theory

Fundamentally, photosynthetic rates are proportional to the amount of photosynthetically available light (PAR). This basic relationship can be modified through photoinhibition from excessive PAR and/or the more photoreactive ultraviolet radiation (UVR). Theoretically, photosynthesis in the presence of inhibiting radiation will reflect both damage and repair kinetics, which vary with exposure (UVR and PAR) and intrinsic physiological capabilities. The relationship between photosynthesis and the damage and repair rate constants can most simply be represented as:

$$\frac{dP_{(t)}}{dt} = -k_1 E^{*}_{inh} P_{(t)} + k_2(1 - P_{(t)}) \qquad (3.1)$$

where the $k_1$ and $k_2$ are the damage and recovery rate constants, $E^{*}_{inh}$ is the biologically weighted irradiance and $P_{(t)}$ is the photosynthetic rate at time t. This mathematical expression represents a two compartment model with damage and repair rate constants describing the rate of transitions between functional and damaged states (Fig. 3.1). Eq. 3.1 can be further generalized if a term for the effect of limitation by sub-saturating PAR is added:

$$\frac{dP_{(t)}}{dt} = -k_1 E^{*}_{inh} P_s(1 - e^{-\alpha I / P_s}) + k_2(1 - P_s(1 - e^{-\alpha I / P_s})) \qquad (3.2)$$

where $P_s$ is the uninhibited, light saturated, photosynthesis, $\alpha$ is the initial slope of the photosynthesis-irradiance relationship, and I represents PAR. The first term on the right hand

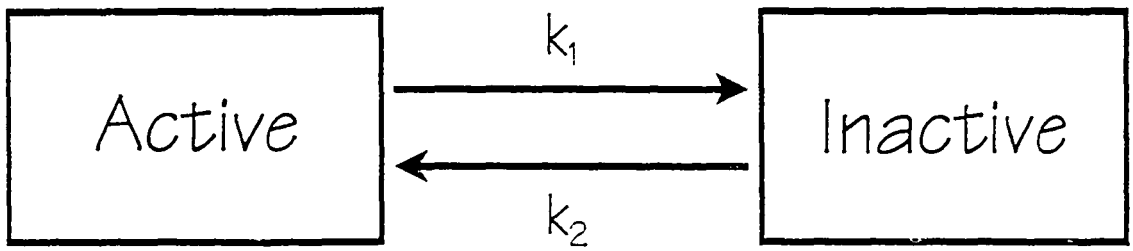



Figure 3.1: Conceptualized two compartmental model depicting active and inactive photosystem units with damage ($k_1$) and repair ($k_2$) rate constants regulating the flow between the two states.

side of Eq. 3.1 describes the damage kinetics, that is the rate at which active components are being inactivated, and it depends on the amount of incoming inhibiting radiation. Conversely, the second term describes the recovery kinetics, that is the rate at which the inactivated components are being reactivated by various physiological mechanisms.

Limiting cases of this two compartment model have been described in the literature. The irradiance-dependent (E) model assumes that the rate of change of photosynthesis over time, relative to the rate obtaining in the absence of photoinhibition, is zero (i.e. $dP'_{,}/dt = 0$) because the damage and recovery constants are large, and lead to a near-instantaneous equilibrium (Cullen et al. 1992). The cumulative exposure (H) model, on the other hand, assumes that repair is inactive (i.e. $k_2 = 0$), and that the kinetics of photoinhibition are simply a function of total exposure. These two kinetic models were tested for their ability to explain the results observed in 1997. The radiation reaching the samples was weighted with the published BWF (i.e. spectrum of effectiveness coefficient ($\epsilon_{(\lambda)}$) for $\lambda$=295 to 400 nm) measured by Cullen et al. (1992) for the marine diatom *Phaeodactylum tricornutum*. In 1997, PAR could not be shown to contribute to photoinhibition, a finding similar to that of Cullen et al. (1992) and Neale et al. (1998b), so only the UVR wavebands were included in calculating biologically-effective exposures. With relatively few spectral treatments in the 1997 experimental protocol, it was not possible to derive BWFs through the UVR.

The irradiance-dependent, E, model expresses the realized rate of photosynthesis in a given treatment ($P^B$) relative to the rate in the absence of photoinhibition ($P^B_{opt}$) as:

$$\frac{P^B}{P^B_{opt}} = \frac{1}{1 + E^*_{inh}} \qquad (3.3a)$$

where

$$E^{*}_{inh} = \sum_{\lambda=280nm}^{400nm} \varepsilon(\lambda) \cdot E(\lambda) \cdot \Delta\lambda \qquad (3.3b)$$

The irradiance model makes predictions about instantaneous photosynthetic rates and their response to instantaneous irradiance. The instantaneous photosynthetic rates were approximated in the present case by calculating the average rates over successive incubation intervals.

The cumulative exposure, H, model, has the form:

$$\frac{P^{B}_{avg}}{P^{B}_{opt}} = \frac{1 - e^{-H^{*}_{inh}}}{H^{*}_{inh}} \qquad (3.4a)$$

where

$$H^{*}_{inh} = \int_{0}^{t} \left[ \sum_{\lambda=280nm}^{400nm} \varepsilon_{H}(\lambda) \cdot E(\lambda) \cdot \Delta\lambda \right] dt \qquad (3.4b)$$

The model assumes no repair, so the degree of inhibition is proportional to cumulative exposure. Unlike the E model, the H exposure model makes predictions about cumulative photosynthesis, which was more directly observable from the experimental measurements in this study.

For both E and H models, $P^{B}_{opt}$ was estimated in practice as the rate of maximum photosynthesis observed over the first hour of exposure under saturating PAR, which prevailed

in all treatments, with minimal UVR exposure.

The pioneers of these models were entirely aware of their limitations and while they expected that the use of these models may be justified at times, they also knew that if repair was significant, yet steady state was not attained, the simplified models would not be applicable (Neale 2000). In such cases, a more generally applicable model is obtained by integrating Eq. 3.1 as a function of time:

$$\frac{P'_{avg}}{P_{pot}} = \frac{(1 - \frac{k_2}{k_1 E^*_{inh} + k_2})(1 - e^{-(k_1 E^*_{inh} + k_2)T})}{(k_1 E^*_{inh} + k_2)T} + \frac{k_2}{k_1 E^*_{inh} + k_2} \qquad (3.7a)$$

where

$$E^*_{inh} = \sum_{\lambda=297}^{400} \varepsilon(\lambda) \cdot E(\lambda) \cdot \Delta\lambda \qquad (3.7b)$$

and $P'_{avg}/P_{pot}$ (dimensionless) is cumulative photosynthesis relative to a potential cumulative photosynthesis in the absence of photoinhibition. For convenience, the more general model may be termed the R (for repair) model and in contrast to the simpler versions (E and H models), the R model yields separate estimates of the damage and recovery rate constants.

## Statistical Analysis

In practice the irradiance model was fitted by non-linear regression as:

$$\frac{P^B}{P^B_{opt}} = \frac{1}{1 + a \cdot E^*_{UVR}} \qquad (3.5)$$

where $E^{\bullet}_{UVR}$ is UVR irradiance weighted ($W \cdot m^{-2}$) by the *P. tricornutum* BWF normalized to $\varepsilon_{(300)}$. The coefficient *a* allows for variations in overall sensitivity of the phytoplankton while assuming that the shape of the BWF is appropriate. If the L. Erie phytoplankton obeyed the weighting function and irradiance model perfectly, the coefficient *a* would equal $\varepsilon_{(300)}$ for the *P. tricornutum* BWF and have inverse irradiance units ($(W \cdot m^{-2})^{-1}$).

The cumulative exposure model was fitted as:

$$\frac{P^{B}_{avg}}{P^{B}_{pot}} = \frac{1 - e^{-a \cdot T \cdot E^{\bullet}_{UVR}}}{a \cdot T \cdot E^{\bullet}_{UVR}} \tag{3.6}$$

where $E^{\bullet}_{UVR}$ is UVR irradiance weighted as above, but averaged over the exposure period T, and the coefficient *a* allows, again, for variations in overall UVR sensitivity.

In practice, the R model was fitted to observations of $P'_{avg}/P_{pot}$ and weighted relative irradiances as:

$$\frac{P'_{avg}}{P_{pot}} = \frac{(1 - \frac{k_2}{A + k_2})(1 - e^{-(A - k_2)T})}{(A + k_2)T} + \frac{k_2}{A + k_2} \tag{3.8a}$$

where A was

$$A = k_1'(E^{\bullet}_{UV} + bE_{PAR}) \tag{3.8b}$$

where $k_1'$ ($s^{-1}$) is an estimated parameter fitted by non-linear regression, b is the PAR effectiveness coefficient ($(W \cdot m^{-2})^{-1}$) estimated from the derived biological weighting function

(see section below, *Biological Weighting Functions*), $E_{PAR}$ is the unweighted PAR irradiance ($W \cdot m^{-2}$), $E^{\bullet}_{UVR}$ is the average relative weighted UVR (dimensionless; weighted by the absolute $\varepsilon_{R(\lambda_i)}$) and T is the exposure time. For each photosynthetic rate measured in the different spectral treatments throughout the exposure period, different values of $E_{PAR}$, $E^{\bullet}_{UVR}$ and T were used.

## Biological Weighting Functions

Biological weighting functions (BWF) were statistically estimated for each 1998 sample date following the method described by Cullen and Neale (1997). UVR spectral irradiances, at 2 nm wavelength intervals, were normalized to $E_{PAR}$ ($W \cdot m^{-2}$) and principal components analysis (PCA) was performed to derive principal components (PCs), representative of the original spectral shape of the various spectral treatments. Coefficients of influence ($m_k$; $(W \cdot m^{-2})^{-1}$) for each PC were then estimated by non-linear regression using the R model (Eq. 3.8a). Irradiance was expressed as a function of component scores ($c_{i,k}$; dimensionless) for each treatment:

$$A = E_{PAR_i}\left(m_0 - \sum_{k=1}^{i} m_k c_{i,k}\right) \qquad (3.9)$$

where $m_0$ is the coefficient of influence for the mean spectrum – PAR and $m_k$ are the coefficients of influence for the PCs. In Eq. 3.9, $k_i'$ is embodied in the coefficients of influence ($m_k$). The biological effectiveness coefficients ($\varepsilon_R(\lambda)$) at each wavelength were then calculated as:

$$\varepsilon_R(\lambda) = \frac{\sum_{k=1}^{z} m_k w_k(\lambda)}{SD\left[E_N(\lambda)\right]} \qquad (3.10)$$

where $w_k$ are the component weightings and $E_N$ is the normalized UVR spectral irradiance. The number of PCs needed to derive the different BWFs, $z$, was determined by partial $F$-test and the standard error of the effectiveness coefficients at each wavelength was calculated using error propagation (Cullen and Neale 1997). All statistical analyses were performed with Systat (ver. 7.0, SPSS Inc.).

## Study Site

Sampling and field experiments were conducted at stations in all three of the Lake Erie basins (East, Central and West, Fig. 3.2) under relatively clear skies. Experiments were conducted with samples from ten stations in 1997, between the months of May and August, but the radiation exposure design did not permit derivation of BWFs. The more elaborate design used at five stations in June, July and August of 1998 did permit derivation of BWFs and thorough testing of the R model. The rather distinct spatial gradients, from relatively shallow, turbid and mesotrophic waters at the western end of the lake to comparatively deep, clear and oligotrophic waters at the eastern end, likely resulted in inter-basin differences of algal biomass, taxonomic composition and possibly physiological status (e.g. light adaptation, nutrient limitation). However, the goal of this study was not to investigate the inter-basin differences but rather to investigate the kinetics of UVR-dependent inhibition in L. Erie

Figure 3.2: Lake Erie and the lake stations sampled throughout the summers of 1997 and 1998.

CANADA
Pacific Ocean
79°
80°
81°
82°
83°
43°
42°
.932
.945
.946
.951
.961
.962

phytoplankton and to develop a photoinhibition model (the R model) that would be applicable to various environments. The spatial heterogeneity of L. Erie was, therefore, an advantage to this study.

## Experimental Procedures

The experimental protocol was similar to that described in Chapter 2 for the 1997 experiments with the following modifications for 1998. In addition to the optical filters used in 1997 (i.e. window screen and Mylar-D), a Hoya glass UV34 filter with 50% transmission at 340 nm and a UVR opaque plexiglass filter (UF3 acrylic; Cadillac Plastics, London, Ont.) were used. In 1998, quartz tubes were used as the incubation vessels in all treatments, but polystyrene sleeves were made which allowed for an additional spectral treatment, providing 50% transmission at 365 nm. Furthermore, supplemental UVB lamps (Southern N.E. Ultraviolet Co., Brantford, CT, U.S.A. #RPR-3000) were used to provide an enhanced UVB treatment (approximately 30% enhancement). The combinations of these filters and supplemental lights yielded a total of ten treatments with two levels of irradiance (100% and 50% PAR) and seven different spectral quality treatments (Fig. 3.3).

The 1998 experiments involved a total of 4 hours exposure, with sampling at 0.5h, 1h, 2h and 4h. Only total organic carbon fixation was measured, with no size fractionation. As in 1997 (Chapter 2), the photosynthetic parameters ($P^{B}_{m}$ and $\alpha^{B}$) were estimated with a light gradient incubator (PAR only) using the model of Platt et al. (1980). At no time was photoinhibition a significant contributor to the photosynthesis vs light relationship in these short (1h) incubations. The Platt et al. (1980) model was therefore fitted without the photoinhibition term (*see* Chapter 2).

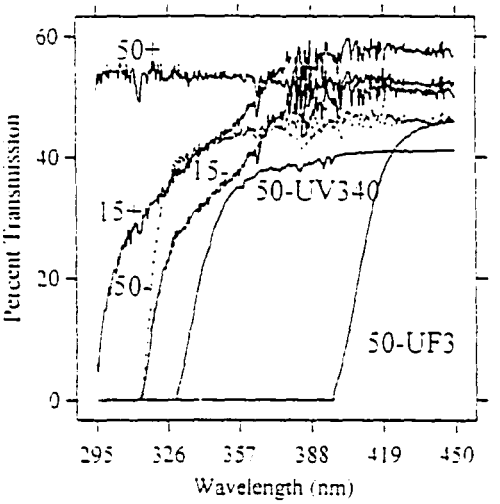



Figure 3.3: Percent transmission of UV wavelengths for the different 50% PAR spectral treatments. Legend: 50+ and 50-, treatments with and without UVB (Mylar-D); 15+ and 15-, treatments with polystyrene sleeves with and without UVB (Mylar-D); 50-UF3, treatment without UV; 50-340, treatment shielded from wavelengths < 330nm.

## Results

### Limnological conditions

A complete description of the limnological conditions of L. Erie in 1997 has been reported elsewhere (*see* Chapter 2). During the 1998 sampling cruises, 111 temperature and *in vivo* fluorescence water column profiles showed that in June, July and August only the East and Central basins stratified. The mean epilimnion depths were shallowest in July (11.9 ± 1.1 and 12.0 ± 1.6 m) and deepest in June (16.2 ± 1.6 and 15.8 ± 0.8 m) and August (17.5 ± 0.8 m and 13.0 ± 0.7 m). Among the lake stations sampled, no 'temporary' thermoclines were observed, in contrast to the stations surveyed in 1997. However, an inter-basin transparency gradient was again present in 1998, with seasonal median attenuation coefficients for PAR of 0.23 ± 0.12, 0.33 ± 0.12 and 0.59 ± 0.16 $m^{-1}$ in the East, Central and West basins, respectively.

The limnological conditions found at each station sampled throughout the summers of 1997 and 1998 are listed in Table 3.1 (*see* Chapter 2 for detailed description of the 1997 stations). Of the five stations sampled in 1998, stratified water columns were observed in the Central basin stations only. The East and West basin stations were uniformly mixed when sampled for experiments. In both 1997 and 1998, the *in vivo* fluorescence profiles of the sampled stations showed that the water samples collected at 5 m were generally representative of the mixed layer (Fig. 3.4) except on three occasions, station 23 sampled July 29/97 (*see* Chapter 2 cf. Fig. 2.5), stations 945 and 946 sampled June 9 and July 14/98, where chlorophyll *a* (chl *a*) increased with depth in the top 10 of the water column. Subsurface chlorophyll *a* (chl *a*) maxima were observed at some stations, including 945 (June 9/98). All these chl *a*

Table 3.1: Summary of limnological variables of the stations sampled for time-series experiments conducted on L. Erie between the months of May and August 1997 and June and August 1998.

| Date | Station | Basin | Epilimnion Depth (m) | | Temperature at 5 m (°C) | Chl *a* at 5 m ($\mu g \cdot L^{-1}$) | $K_{dPAR}$ ($m^{-1}$) | Mean PAR % of incident |
|---|---|---|---|---|---|---|---|---|
| 1997-7/5 | 946 | C | 22 | | 6.0 | 1.5 | 0.43 | 10.6 |
| 3/6 | 946 | C | 22 | (iso.) | 8.8 | 2.5 | 0.29 | 15.1 |
| 4/6 | 337 | W | 9 | (iso.) | 13.2 | 9.8 | 1.61 | 6.9 |
| 5/6 | 961 | C | 19 | (iso.) | 13.4 | 1.2 | 0.83[a] | 6.3 |
| 1/7 | 23 | E | 5 | | 20.3 | 0.7 | 0.36 | 46.4 |
| 2/7 | 967 | W | 8.5 | | 23.5 | 2.1 | 0.36 | 32.8 |
| 29/7 | 23 | E | 15 | | 22.0 | 3.5 * | 0.24 | 27.0 |
| 30/7 | 953 | C | 12 | | 22.2 | 1.4 | 0.32 | 25.5 |
| 31/7 | 962 | C | 11 | | 23.7 | 2.0 | 0.36[a] | 24.8 |
| 27/8 | 337 | W | 9 | (iso.) | 21.1 | 15.5 | 1.16 | 9.6 |
| 1998-8/6 | 932 | E | 21 | (iso.) | 15.0 | 1.3 | 0.19 | 24.6 |
| 9/6 | 945 | C | 10 | | 12.8 | 2.3 | 0.27 | 34.5 |
| 14/7 | 946 | C | 15 | | 22.5 | 1.1 | 0.19 | 33.1 |
| 12/8 | 337 | W | 9 | (iso.) | 24.8 | 4.7 | 0.63 | 17.6 |
| 13/8 | 961 | C | 9 | | 22.5 | 3.1 | 0.23[a] | 42.2 |

*Note that *in vivo* chl *a* fluorescence was not uniformly distributed with the mixed layer on this date (*see* Fig. 2.5)

[a] Value of $K_{dPAR}$ derived from the following relationship: $K_{dPAR} = -0.026 * \text{Transmission} + 2.258$

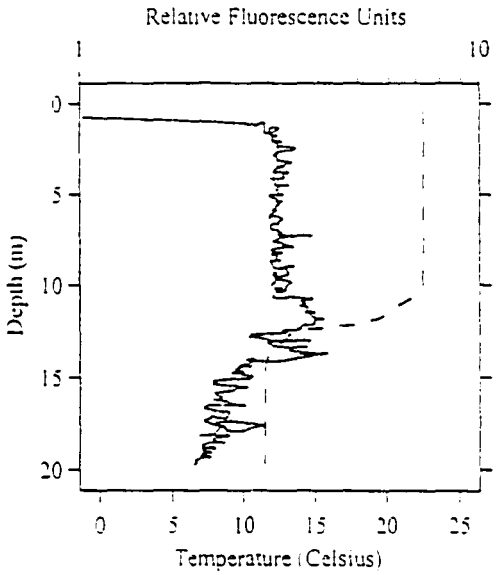



Figure 3.4: Temperature and *in vivo* fluorescence water column profile station 961 sampled August 13, 1998 indicating relatively well mixed epilimnion typical of the stations sampled. Dashed line: temperature; solid line: *in vivo* fluorescence.

peaks occurred in or near the seasonal thermocline, as described in more detail in Chapter 2. On average, chl *a* concentrations were higher in the West basin (8.0 ± 7.9 $\mu g \cdot L^{-1}$) although extensive variability was noted, while the East and Central basins had consistently lower chl *a* concentrations (1.8 ± 1.4 and 1.9 ± 0.5 $\mu g \cdot L^{-1}$).

*Performance of limiting case models in 1997*

The first order, irradiance-dependent (E), model was fitted to interval estimates of photosynthetic rates (normalized to estimated optimal rates) for each 1997 time-series experiment. The model was largely unsuccessful (e.g. Fig. 3.5a,b), as reflected in its refusal to converge in over half of the 10 experiments (Table 3.2) and in a pattern of systematic lack of fit even where parameter estimates could be obtained. Scatter plots of residuals vs exposure time (e.g. Fig. 3.5c) suggested the model systematically underestimated inhibition for longer exposures, especially in the 50% exposure treatments. Using paired t-tests of residuals for 1h exposures vs 8h exposures, significantly ($p < 0.05$) greater residuals were indeed found for the shorter exposures in three of the four experiments (except July 31; $p = 0.291$) for which the E model could be fitted. The plots also indicated consistently larger residuals for the 100% than the 50% exposure treatments, and this systematic difference was confirmed by paired t-tests.

The systematic variation of residuals from the E model thus indicated a time dependence of UVR photoinhibition, evidence for some dependence of photoinhibition on cumulative exposure, and not just irradiance. A dependence on cumulative exposure was reflected in the fit of the H model, which was, on average, a better predictor of photoinhibition than the E model. The H model did fail to converge in 2 of the 10 experiments (Table 3.2), however, and a systematic divergence between the 100% and 50% exposure treatments was

Figure 3.5: Irradiance (a, b) and cumulative exposure (d, e) worst and best model fits of the 1997 time series photosynthesis data using the *Phaeodactylum tricornutum* weighting function (Cullen et al. 1992) with residual plots (c, f) showing evidence of systematic lack of fit. Panel a: July 30 (worst E model fit; $r^2 = 0.080$) station 953. Panel b: June 3 (best E model fit; $r^2 = 0.416$) station 946. Panel c: Residuals of best fit to the E model (June 3) showing lack of independence with time and irradiance. Panel d: June 3 (worst H model fit; $r^2 = 0.109$) station 946. Panel e: June 4 (best H model fit; $r^2 = 0.561$) station 337. Panel f: Residuals of best fit to the H model (June 4) showing lack of independence with irradiance. Relative photosynthesis is the dimensionless ratio of the observed photosynthetic rate to the optimum photosynthetic rate respective to each date. Solid lines in panels a,b,d and e represent the predicted relative photosynthesis by each model. Dashed lines in panel c represent a LOWESS trend line (SYSTAT ver. 7). Legend panels a and b: x = 0.5 h; ○ = 1 h; △ = 2 h; □ = 3 h; ☆ = 4 h; ▽ = 6 h; ▷ = 8 h. Legend panels c, d, e and f: ● = 50% PAR exposures all treatments; ○ = 100% PAR exposures all treatments.

a
b
c
d
e
f
Relative Photosynthesis
Weighted Irradiance (W·m-2)
Residuals
Time (hours)
Weighted Exposure (kJ·m-2)
Model Estimates

Table 3.2: Nutrient status and light history/adaptation indicators for the algal assemblages sampled in 1997 and the amount of variance in photosynthesis explained by the E and H models. Nutrient status for the whole water sample was assessed using all nutrient deficiency indicators (*see* Chapter 2). The light saturation parameter ($I_k$; $\mu E \cdot m^{-2} \cdot s^{-1}$) values, calculated as $P^b_m : \alpha^b$, and mean PAR, calculated using Eq. 2.1 (*see* Chapter 2), are reported here as indicators of light history/adaptation indicators.

| Date | Station | Basin | Model Performance ($r^2$) | | Nutrient Status of Algal Assemblage | | Light History/Adaptation of Algal Assemblage | |
|---|---|---|---|---|---|---|---|---|
| | | | E | H | N deficiency[a] | P deficiciency[b] | Mean PAR (%) | $I_k$ |
| 7/5 | 946 | C | 0.210 | 0.183 | Y | N | 10.6 | 177.7 |
| 3/6 | 946 | C | 0.416 | 0.109 | Y | Y | 15.1 | 60.9 |
| 4/6 | 337 | E | - | 0.561 | N | N | 6.9 | 87.4 |
| 5/6 | 961 | C | - | 0.162 | Y | N | 6.3 | n.a. |
| 1/7 | 23 | E | - | 0.277 | Y | N | 46.4 | 122.8 |
| 2/7 | 967 | W | - | 0.545 | Y | Y | 32.8 | 126.2 |
| 29/7 | 23 | E | - | - | N | Y | 27.0 | 87.7 |
| 30/7 | 953 | C | 0.080 | 0.395 | Y | Y | 25.5 | 129.5 |
| 31/7 | 962 | C | 0.207 | - | Y | Y | 24.8 | 110.4 |
| 27/8 | 337 | W | - | 0.269 | N | Y | 9.6 | 270.0 |

regularly observed (e.g. Fig. 3.5d,e,f). The results of paired t-tests, show that in all but one experiment (June 4, 1997), the residuals for 100% exposures were significantly ($p < 0.00001$) different than those for 50% exposures, with negative residuals (model overestimation) in the 100% PAR treatments and positive residuals (model underestimation) in the 50% PAR treatments (Fig. 3.5f). While the H model was more successful in fitting the photosynthesis data (only two model fit failures), the percentage of explained variation was nonetheless lower than 50% in all but two experiments, and never higher than 56%, indicating substantial unexplained variation in addition to the systematic lack of fit.

The relative success of the two models was assessed relative to the variation in environmental conditions and physiological condition of the phytoplankton. The multiple r squared ($r^2$ or percent explained variation) values for E and H models were compared to the nutrient status of the algal assemblage, mean PAR and $I_k$ values (Table 3.2) to test whether nutrient deficiency or sufficiency, light history or photoadaptive state might influence how well the phytoplankton responses agreed with the models. Scatter plots and correlation analysis failed to identify any relationships between model performance and physiological status or light history of the phytoplankton, however.

### Calibration of the R model and BWF derivation

Fitted to the 1998 photosynthesis data, the R model accounted for ca. 86.2% (range 76.2 -93.0%) of the variance in UVR- and PAR-dependent photosynthesis (Table 3.3; Fig. 3.6). Although PAR inhibition was not noted in the short (1h) light gradient incubations in 1997 and 1998, it was a significant contributor to photoinhibition of primary production in three of the

Table 3.3: Summary of the statistical analysis of algal photoinhibition using the repair model for L. Erie phytoplankton. Photosynthetic parameters, maximum photosynthetic rates ($P^b_m$; μg C·μg Chl $a^{-1}$·$h^{-1}$) are the fitted values ± the asymptotic standard error of the estimate, and the light saturation parameter ($I_k$; μE·$m^{-2}$·$s^{-1}$) values calculated as $P^b_m/\alpha^b$ and are reported here as indicators of light adaptation status. Model parameters listed are $\varepsilon_{R(300)}$ $(W \cdot m^{-2})^{-1}$ represent the biological effectiveness coefficient values at 300 nm, $\varepsilon_{PAR}$ $(W \cdot m^{-2})^{-1}$ represent the PAR effectiveness coefficient acquired through PCA when the BWF were derived, and $k_1'$ and $k_2$ are the "damage" and repair constants ($s^{-1}$) fitted by the R model (*see* Materials and Methods section), respectively.

| Date | Station | Dominant Genera of Nano- and Microphytoplankton | $P^b_m$ | $I_k$ | $\varepsilon_{R(300)}$ x $10^{-4}$ | $r^2$ | $k_1'$ | $k_2$ x $10^{-4}$ | $\varepsilon_{PAR}$ x $10^{-7}$ |
|---|---|---|---|---|---|---|---|---|---|
| 8/6 | 932 | *Ochromonas* | 5.91 ± 0.20 | 227.3 | 1.12 | 0.930 | 1.06 ± 0.12 | 0.30 ± 0.30 [a] | 0.48 ± 0.16 |
| 9/6 | 945 | *Ochromonas/Asterionella* | 3.72 ± 0.16 | 169.1 | 5.41 | 0.762 | 0.83 ± 0.16 | 5.04 ± 1.54 | 24.10 ± 5.60 |
| 14/7 | 946 | *Franceia/Dynobryon/Anabaenopsis* | 2.18 ± 0.10 | 37.6 | 4.99 | 0.918 | 1.72 ± 0.18 | 2.57 ± 0.56 | 2.07 ± 0.67 |
| 12/8 | 337 | *Aphanothece/Selenastrum* | 4.76 ± 0.23 | 144.2 | 1.45 | 0.894 | 3.62 ± 1.02 | 6.26 ± 2.34 | 1.28 ± 0.86 [a] |
| 13/8 | 961 | *Cyclotella/Aphanothece* | 2.11 ± 0.10 | 84.4 | 5.14 | 0.809 | 3.71 ± 0.96 | 5.76 ± 2.27 | 1.72 ± 1.64 [a] |

[a] denotes that this estimated coefficient was not different from zero

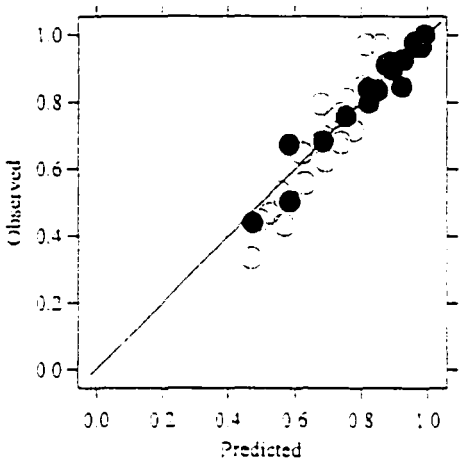



Figure 3.6: Repair kinetic model best and worst fits of the 1998 time series photosynthesis data using each respective biological weighting function derived. ● = Best fit June 8 station 932, $r^2 = 0.930$ ; ○ = Worst fit June 9 station 945, $r^2 = 0.762$.

five 1998 experiments in the longer (4h) spectral treatment experiments. The June 8 and 9 mixed assemblages were the least and most PAR sensitive, while the August phytoplankton communities showed no significant PAR inhibition ($\varepsilon_{PAR} = 0$).

The estimated recovery rate constants were variable between sample dates, ranging from non significantly different from zero (June 8) to $6.26 \times 10^{-4}$ $s^{-1}$ (Aug. 12) (Table 3.3). Regardless of the fluctuating recovery constants, however, the R model consistently performed well (Table 3.3; Fig. 3.6). This is in contrast to the irradiance (E) and cumulative exposure (H) kinetic models, which systematically showed a poorer fit to the UVR- and PAR-dependent photosynthetic rates observed. These model performances were more variable than the R model, with $r^2$ values ranging from 0.241 - 0.750 and 0.403 - 0.927 for the E and H model fits, respectively. Furthermore, paired partial *F*-tests determined that the R model significantly ($p < 0.000001$) improved the fit of the data compared to both the E and H models on all dates except on June 8, when the H and R model fits were not significantly different ($p = 0.309$; $F = 1.08_{1,26}$). On this date, the estimated recovery rate constant was not significantly different from zero, which follows the assumptions of the H model.

The predictability of the kinetics of photoinhibition by both the E and H kinetic models was conspicuously dependent on the estimates of the recovery rate constants. This was apparent when the R model estimates of recovery rate constants were plotted against the amount of variance explained ($r^2$) by both the E and H models (Fig. 3.7). There was a significant ($p < 0.05$; $r^2 = 0.977$) negative linear relationship between the H model performance ($r^2$) and the recovery rate constant estimates. Conversely, a significant ($p < 0.01$; $r^2 = 0.989$) positive linear relationship between the E model $r^2$ and the recovery rate constant was observed. Recovery rate

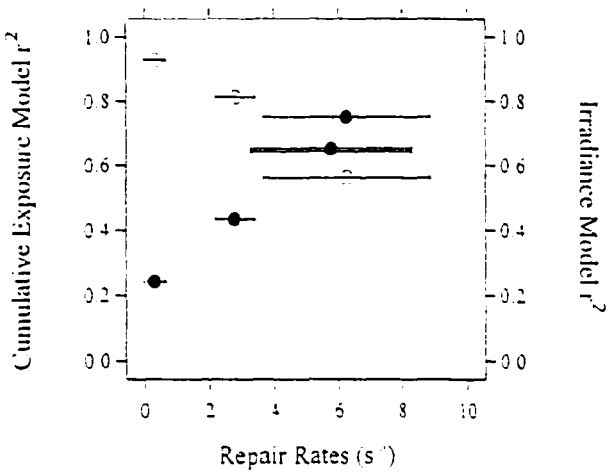



Figure 3.7: Irradiance (E) and cumulative exposure (H) model performances vs estimated recovery rate constants (R model) for the 1998 data. Legend: ○ H model performance; ● E model performance. Error bars represent asymptotic standard errors of the R model estimated recovery rate constants. The E and H model $r^2$ values for June 9 had high Studentized Residuals, consequently were deemed outliers and excluded from the analysis.

constants did not show any obvious relationships with dominant nano- and microphytoplankton groups, light adaptation indicator ($I_k$), light history (% mean PAR) or temperature. However, a significant negative relationship ($p < 0.001$; $r^2 = 0.985$) was noted between recovery rate constant estimates and epilimnion depth.

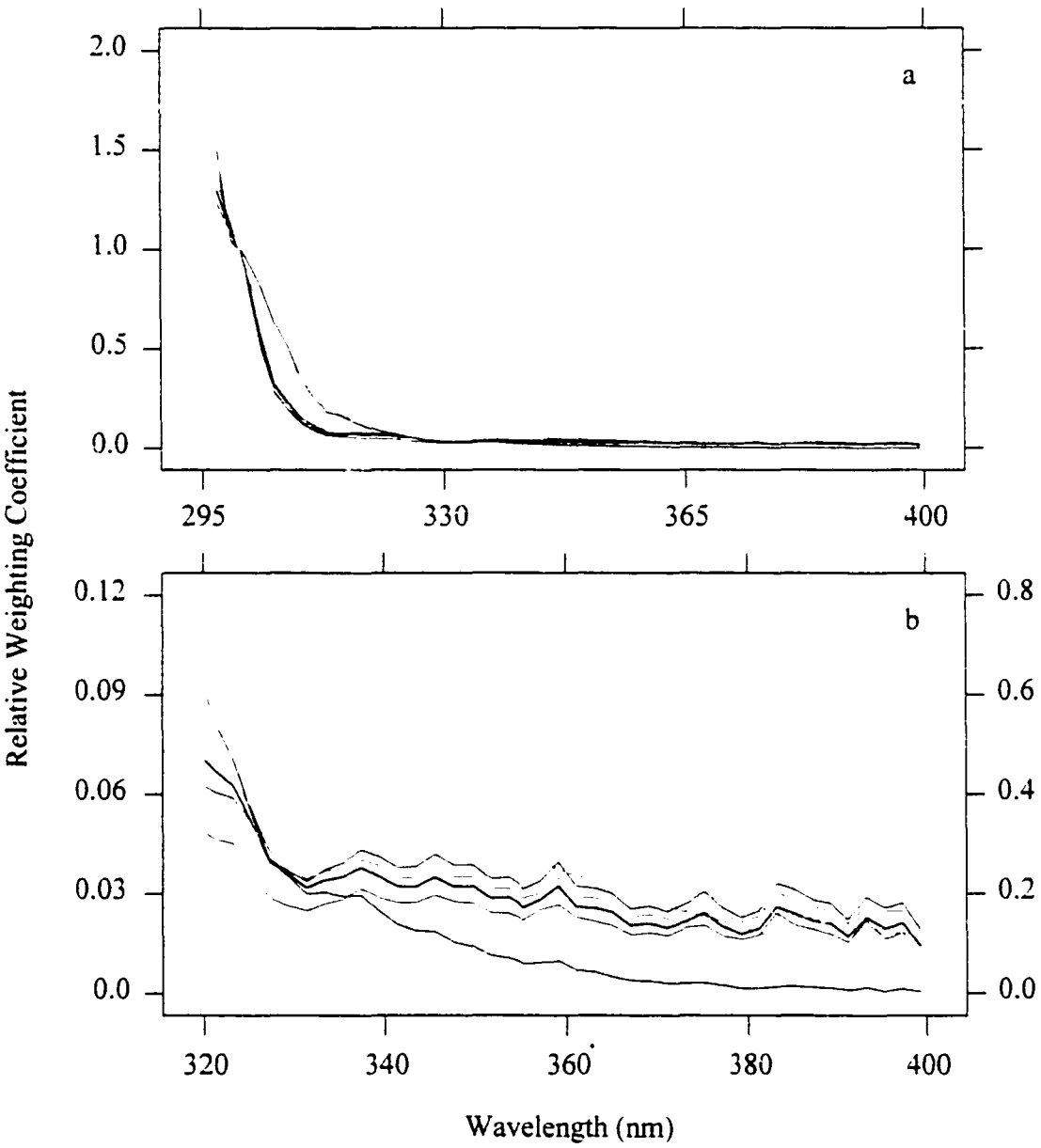
All the BWFs derived here showed significant inhibitory effects of UVB and UVA, although the weighting of each waveband varied between experimental dates (Fig. 3.8a). The BWFs are most easily compared by calculating the cross-product of the weighting coefficients with a representative incident radiation spectrum (Fig. 3.8b). By calculating the biologically effective radiation spectrum (dimensionless) in this manner for each BWF, three different patterns became clearly apparent. The BWF of June 8 and August 12 were not significantly different from each other, and had the lowest values of the weighting coefficients ($\varepsilon_{R(\lambda)}$). The BWF of June 9 and August 13 were similar to each other, with consistently higher $\varepsilon_{R(\lambda)}$. The BWF of July 14 had a different shape from all others, with significantly higher $\varepsilon_{R(\lambda)}$ in the short UVB range (305 - 315 nm) but low $\varepsilon_{R(\lambda)}$ in the 345 - 375 nm range. At longer wavelengths, the July 14 $\varepsilon_{R(\lambda)}$ were not significantly different from zero.

When normalized to the $\varepsilon_{R(300)}$ values (Fig. 3.9), all but one of the independently derived BWFs were nearly superimposed, emphasizing their similarity of shape despite variations in absolute value. The BWF estimated on July 14, however, differed by having relatively higher UVB and relatively lower UVA effectiveness coefficients (Fig. 3.9a,b). The shape of the previously-published *P. tricornutum* BWF, when similarly normalized, somewhat resembled those derived here, with a steep slope in the UVB. However, the L. Erie BWFs had lower normalized weighting coefficients for the long UVB and short UVA part of the spectrum

Figure 3.8: BWFs derived from PCA using the R kinetic model for all five 1998 experimental dates. Panel a: Absolute values of the effectiveness coefficients with standard errors (dashed lines). The BWF derived for July 14 has negative standard errors at wavelengths > 374 nm. Panel b: Biologically weighted radiation spectra (dimensionless) for each 1998 BWFs. The dimensionless cross-product of the biological effectiveness coefficients and a representative incident radiation spectra. The sum of the cross-product, i.e. indicator of overall UVR sensitivity, for each BWF is: 0.0140, 0.0784, 0.0470, 0.0200 and 0.0553 for June 8, June 9, July 14, August 12 and August 13, respectively. Legend: Black: June 8; red: June 9; blue: July 14; green: August 12; violet: August 13.

Biologically Weighted Radiation Spectra
Weighting Coefficient ((W•m-2)-1)
0.0010
0.0008
0.0006
0.0004
0.0002
0.0
a
b
295
330
365
400
Wavelength (nm)

Figure 3.9: Relative weighting coefficients for each 1998 BWFs. For each BWF, $\varepsilon_{R(\lambda)}$ are normalized to each respective $\varepsilon_{R(300)}$ value. Additionally, the Cullen et al. (1992) *Phaeodactylum tricornutum* and the Jones and Kok (1966) photoinhibition biological weighting functions are plotted for comparison. Panel a is for the entire UVR spectrum while the UVA portion of the spectrum is enlarged in panel b. The scale on the right of panel b applies to the Jones and Kok (1966) BWF only. Legend: Black: June 8 BWF; red: June 9 BWF; blue: July 14 BWF; green: August 12 BWF; violet: August 13 BWF; orange: *P. tricornutum* BWF; gray: chloroplast inhibition BWF.


a
b
2.0
1.5
1.0
0.5
0.0
295
330
365
400
0.12
0.09
0.06
0.03
0.0
0.8
0.6
0.4
0.2
0.0
320
340
360
380
400
Relative Weighting Coefficient
Wavelength (nm)

(Fig. 3.9a,b). The chloroplast inhibition BWF was very different in shape, when normalized, from those found here, with a relatively shallow slope and relatively high coefficients from 300 to 400 nm.

The algal assemblage with the highest overall UVR sensitivity, represented by the sum of the cross-products, i.e. $\Sigma(I \cdot \varepsilon_{R(\lambda)})$, (Fig. 3.8a; June 9), was dominated by a small chrysophyte and a large pennate diatom. The lowest sum was recorded for a community sampled the previous day (June 8) and dominated by the same small chrysophyte. The small data set in this study and the cursory evaluation of the taxonomic composition of algal assemblage limited the ability of identifying species specific sensitivities to total UVR. However, a borderline significant ($p = 0.054$; $r^2 = 0.680$) negative relationship was observed between maximum photosynthetic rates ($P^b_m$) estimated from the light gradient incubations and $\varepsilon_{R(300)}$. No further relationships could be identified between UVR sensitivity and light history/adaptation indicators or species composition in this small 1998 data set. No nutrient status indicators were available for the 1998 data.

### Application of the R model to 1997 observations

The ability of the R model and the BWFs derived from the 1998 calibration experiments to predict photoinhibition in other years and stations was tested against the 1997 experimental results. The BWF of June 9 1998 was selected as representative of the shape observed in 4 of the 5 experiments and combined with the radiation actually measured in 1997. In addition to the R-model, the limiting-case E and H models were also tested again against the 1997 data, with the 1998 L. Erie BWF rather than the *Phaeodactylum* BWF. The R model could be fitted to every experiment conducted in 1997 but it did not perform as well as in 1998. On average,

the R model accounted for 46.1% (range 38.1 - 59.8%) of the variance in UVR-dependent inhibition. Recovery rate constants were significantly greater than zero for six of the 10 experiments, ranging from 1.05 to 3.27 x $10^{-4}$ $s^{-1}$. Despite the modest success of the R model, in terms of explained variation, it significantly improved the fit compared to the E and H models. Once again, significant positive (E model: $p < 0.01$; $r^2 = 0.852$) and negative (H model: $p < 0.01$; $r^2 = 0.722$) relationships were observed between the amount of explained variation ($r^2$) by the E and H kinetic models and the estimated recovery rate constants (Fig. 3.10).

The relationship between recovery rate constants and epilimnion depth was marginally confirmed by the 1997 data when it was considered that station 23 sampled on July 1 was subjected to a shallow 'temporary' thermocline. Assuming that the seasonal thermocline on July 1 was closer to 12m (near the chl *a* maximum; *see* Fig. 2.5), the relationship between recovery rate constants and epilimnion depth using both the 1997 and 1998 data was borderline significant ($p = 0.066$; $r^2 = 0.253$) (Fig. 3.11).

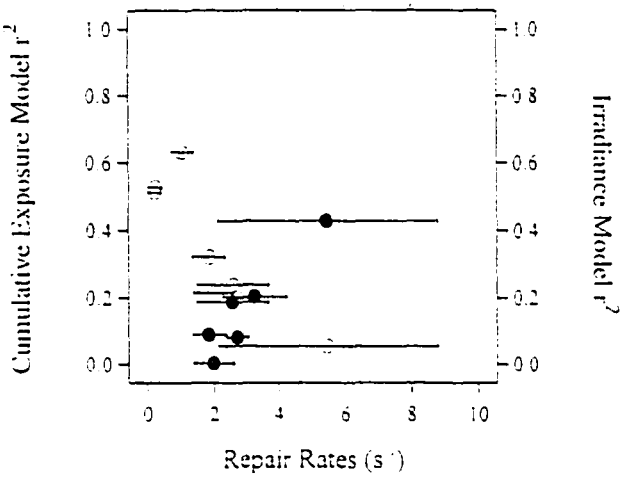



Figure 3.10: Irradiance (E) and cumulative exposure (H) model performances vs estimated recovery rate constants (R model) for the 1997 data. Radiation was weighted using the BWF derived for the June 9 algal assemblage and all three kinetic models were used to fit the photosynthetic data. Legend: ○ H model performance; ● E model performance. Error bars represent asymptotic standard errors of the R model estimated recovery rate constants.

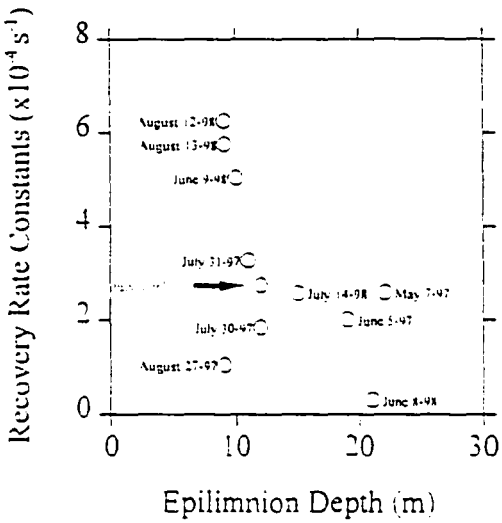



Figure 3.11: Recovery rate constants vs epilimnion depth for the 1997 and 1998 data. The linear regression was analysed with a 12m epilimnion depth on July 1 (*see* text).

## Discussion

The E and H models tested here are kinetic models with *a priori* assumptions about repair kinetics (Cullen et al. 1992, Neale et al. 1998b), with the E model embodying the assumption of rapid repair processes and the H model assuming no repair at all. The H model has been the most successful to date in describing the responses of natural communities in marine and fresh waters (Neale et al. 1998b, Smith et al. 1998). As first implemented here (1997), both models depended on a biological weighting function (BWF) derived from lab studies of a marine diatom (Cullen et al. 1992). Neither the E nor the H model so constituted was satisfactory for L. Erie phytoplankton in either 1997 or 1998. The lack of fit of the models was systematic, with residuals significantly related to both exposure period and irradiance level. The latter pattern is hard to explain as a consequence of an incorrect BWF because the spectral composition of radiation was virtually identical in both 50% and 100% irradiance treatments, and tests with an alternative BWF from the literature (Jones and Kok 1966), or a BWF derived for L. Erie phytoplankton in 1998, failed to improve the model fit. The apparent dependence of the response on both cumulative exposure and exposure rate is explicable if the idea of a finite repair rate, too fast to be ignored but too slow to attain equilibrium within the experimental period, is entertained. The interpretation would then be that the L. Erie phytoplankton sampled here maintained more rapid repair than did the Southern Ocean (Neale et al. 1998b,c) or L. Ontario (Smith et al. 1998) phytoplankton previously shown to follow the H model, but did not achieve a rapid equilibrium between damage and repair as seen in diatom cultures that follow the E model (Cullen et al. 1992). The relative success of the R model, the non-zero recovery rates it usually indicated and their relationship to the E and H model performances (in terms of

$r^2$), supported the idea that finite, but not instantaneous, rates of recovery are an important influence on phytoplankton response to UVR. There seems little doubt that models containing fixed assumptions about recovery rates will not generally be successful in L. Erie or, probably, other large lakes.

Incident radiation, mixing depths and rates, temperature, algal species composition and nutrient status may all influence the repair abilities of algal assemblages (Karentz et al. 1991a, Lesser et al. 1994, Neale et al. 1998b, Pang and Hays 1991). At no time was a L. Erie sample encountered that fitted the E model well enough to suggest a very rapid rate of repair, despite independent evidence that L. Erie phytoplankton do have effective and rapid recovery processes (Marwood et al. 2000). Marwood et al. (2000) found near-complete recovery of photosynthetic electron transport within 2 hours of recovery under dim light. Their exposures were <1h long, however, and inhibition was not as severe as that seen for carbon assimilation after prolonged exposures in the present study. The longer exposures used here may have resulted in longer-lasting damage (e.g. structural damage to membranes or RUBISCO), which would require lengthier recovery times. More moderate impacts, from shorter exposures, may be offset more effectively by short-term defence mechanisms such as energy dissipation via fluorescence (Ferris and Christian 1991), or repair of rapidly-cycled components such as the D1 protein of photosystem II (Greenberg et al. 1989). Additionally, carbon assimilation as measured here may reveal effects that would not be as evident in measures of electron transport, such as altered RUBISCO activity. The recovery rates estimated here for the shorter, and less severe, exposures were in fact not greatly different from those observed by Marwood et al. (2000). Over extended exposures, these quick responses will become overwhelmed and more extensive damage will

occur which will require more drastic counteracting measures (e.g. repair). The different time scale of the experimental exposures in these two L. Erie studies is likely the consequence for the differences in the inferred recovery abilities. On the other hand, the H model performed relatively well ($r^2 > 0.5$) on some occasions, suggesting slower than usual repair. Most of the measured environmental and physiological status variables failed to show any strong relationships with estimated recovery rates or the performance of E and H models. Nutrient limitation was slight or nonexistent on the two dates of best performance (June 4, July 2, 1997) but the model performed poorly on other dates with absent or slight nutrient limitation (e.g. June 5, July 1). $I_k$ was low to moderate on the two dates of best performance, but was equally low on other dates when the model did poorly (e.g. June 3, July 29). Both of the dates with good model performance were dominated by diatoms and/or chrysophyceans, but bad performance was seen on other dates with similar composition (e.g. May 7, July 31). No one environmental factor was clearly dominant in determining model performance or, by implication, recovery rates.

In aquatic systems, the physical and chemical environments vary both temporally and spatially and one physiological process that can change over time to facilitate adaptation to a dynamic environment is repair. In 1998, the various stations sampled in L. Erie changed from being dominated by small chrysophytes to being dominated by diatoms and cyanophytes. The community composition should influence the photoinhibitory response of an algal assemblage because the repair of UVR-induced DNA photoproducts and essential photosynthetic proteins (e.g. D1 protein) is species-specific (Boelen et al. 2000, Karentz et al. 1991a, Xiong et al. 1997), as is the ability to synthesise UVR screening compounds (Hannach and Sigleo 1998,

Sinha et al. 1998). In Lake Michigan, spring diatom and chrysophyte communities have been reported to be more susceptible to UVR than summer and fall cyanophyte communities, a phenomenon attributed to differences in protective pigments (Gala and Giesy 1991). However, as in 1997 (*see* Chapter 2), a particularly sensitive algal groups in L. Erie could not be identified in 1998. For example, communities dominated by small chrysophytes could be both tolerant of (June 8) or sensitive to (June 9) UVR (Table 3.3; Fig. 3.8b). Since two closely related species can exhibit very different UVR survival strategies, and show large differences in their photoinhibitory responses (Quesada and Vincent 1997), the level of taxonomic identification in this study may not have been detailed enough to attribute the observed differences in sensitivity to such a cursory community composition evaluation.

The overall sensitivity of algae to UVR will not only depend on algal physiology but also on the physical and optical characteristics of the water column. These parameters will affect the algal UVR-exposure, and hence influence their photoinhibitory response. While no relationship could be identified between mean PAR and UVR sensitivity or recovery rate constant estimates, a significant negative linear relationship between recovery rate constants and epilimnion depth (i.e. mixing depth). While the 1997 data only marginally supported the relationship noted in 1998, the highly significant linear regression observed and the large confidence intervals around the 1997 R model recovery rate estimates, preclude the dismissal of this relationship. It appeared that phytoplankton experiencing rapid changes in light climate within a relatively shallow and turbid mixing layer maintained low UVR sensitivity by manifesting vigorous recovery rates. On the other hand, phytoplankton experiencing slow exposure variations within a relatively deep and clear mixing water column reduced UVR

sensitivity by means other than vigorous recovery (e.g. pigments). It is proposed that overall UVR sensitivity should be considered as having two important components: 1) a susceptibility to damage component possibly influenced by the presence of photoprotective pigments and 2) an ability to recover component mediated by repair processes.

Adaptation through the synthesis of pigments can confer protection from damaging radiation. The dinoflagellate, *Gymnodinium sanguineum*, grown under high light increased its protective pigment concentrations, consequently, when repair was artificially inhibited via streptomycin, PSII efficiency remained relatively unchanged in the presence of inhibiting radiation (Neale et al. 1998a). Without a pigment analysis to support this claim, it is merely speculation that on June 8, the sampled algae were pre-adapted to high light conditions and photoprotective pigments conferred these algae a higher UVR tolerance in the absence of vigorous repair. On the other hand, it can be suggested that the variable light climate in the shallow turbid mixed water column sampled on August 12 stimulated repair (Table 3.3) which lead to the low UVR sensitivity.

Conceivably, the depth of the mixed layer as well as the rate at which the water is being mixed will determine the duration and extent of UVR exposure within a given water body. While mean PAR values will be indicative of the average light climate, epilimnion depth will be a surrogate of mixing strength (i.e. rate) in a lake (Wetzel 1983). No relationship between mean PAR and UVR sensitivity or recovery rates was observed. Mean PAR values, although similar for the June 8 and August 12 stations, the two extremes in recovery rates observed in 1998, these average light climate values were low for different reasons. Mean PAR values were low for station 932 (June 8) because the mixed layer was deep (21 m), whereas, mean PAR

values were low for station 337 (August 12) because PAR attenuation was high ($K_{dPAR}$ = 0.63 $m^{-1}$). While mean PAR is a good approximation of the amount of light algae are seeing within a given mixed water column, it does not take into account the rate at which cells are being mixed within this water body. This will invariably influence the magnitude and duration of the UVR exposure for a particular cell. The differences in water clarity between stations 932 and 337 imply that, given a similar mixing rate, phytoplankton at the deeply mixed clear water station will experience relatively slower rates of change in radiation than their counterparts at the relatively shallow mixed turbid station. The photoadaptative response of algae to a dynamic light climate depends both on the rate and magnitude of change in radiation, in addition to the direction (down- vs up-ward shifts in light) of the change (Cullen and Lewis 1988). The subsequent response to these variations in radiation will reflect the integrated action of different active photoadaptive processes, each of which proceed at various time scales (Ferris and Christian 1991). If different photoadaptive mechanisms have different cues or triggers, whether it be high PAR or a slow or rapid changing light climate, it would explain at least partially why algae adapted to similar mean light climate showed two completely different strategies for counteracting the effects of inhibiting UVR. Algae at the clear water station reduced their susceptibility to UVR damage, possibly by increasing their photoprotective pigment contents, while those at the more turbid site exhibited vigorous recovery.

The biological weighting functions derived in this study were very consistent in their relative weightings between experimental dates. While the relative shape of the BWFs derived in this study was similar to the *P. tricornutum* function, used to fit the E and H models with the 1997 data, they had notably lower biological weightings in the high UVB and low UVA range

of the spectrum. In this study, natural mixed assemblages adapted to solar radiation were used to derive the BWFs as opposed to a single species culture (e.g. *P. tricornutum*) reared under laboratory conditions. The shape of a BWF can be influenced by the light exposure regime (Neale et al. 1998a). Phytoplankton in natural systems have various UVR adaptation mechanisms, such as the synthesis of mycosporine-like amino acids, a series of photoprotective pigments, with high absorption in the 309 - 360 nm range (Roy 2000). The presence of these pigments in the natural assemblages may have resulted in the lower relative effectiveness coefficients of the BWFs in this part of the solar spectrum.

The normalized spectra of the BWFs showed that, on average, the different L. Erie phytoplankton assemblages had similar wavelength-dependent photoinhibition, although the BWF derived for the July 14 algal community distinguished itself from the rest (Fig. 3.8b). This weighting function had relatively higher UVB and relatively lower UVA effectiveness coefficients. The shape of the BWF reflects the sensitivity of the biological parameter of interest to various wavelengths. This sensitivity can depend on species size and composition, nutrient availability and the presence of photoprotective pigments (Boelen et al. 2000, Karentz et al. 1991a,b, Lesser et al. 1994, Roy 2000). To our knowledge, only one study has specifically investigated the effects of light adaptation/history on the shape of a BWF, a study with the dinoflagellate, *Gymnodinium sanguineum* (Neale et al. 1998a). Cells grown under high light demonstrated increased concentrations of mycosporine-like amino acids (MAAs; UVR 'sunscreens') compared to those grown under low light, consequently, these high light grown algae had lower effectiveness coefficients between 320 - 340 nm, the wavelengths of maximum MAAs absorption. Although, the algal assemblage of July 14 was relatively more sensitive to

UVB, at wavelengths > 330 nm the weights of the effectiveness coefficients were relatively lower than those of the other BWF. Pigments with specific absorption at these longer UVA wavelengths may have prevailed in these algae.

The short UVB wavelengths are strongly absorbed by aromatic amino acids (Tevini 1993), consequently, proteins can be readily photomodified by these wavelengths. Maximum rates of photosynthesis ($P^b_m$) under saturating light conditions reflect among other things the concentration of the carbon fixing enzyme Rubisco (Lesser 1996 and references therein). The negative relationship observed in 1998 between algal UVB sensitivity (i.e. $\varepsilon_{R(300)}$) and $P^b_m$ may suggest that light-saturated photosynthetic rates were inhibited to a greater extent in the more sensitive algal assemblages. UVR-associated damage is known to decrease light-saturated photosynthetic rates (cf. Ferris and Christian 1991, Hazzard et al. 1997), a possible consequence of the photomodification of Rubisco known to occur following UVB radiation exposure (Wilson et al. 1995). Alternatively, if Rubisco concentrations or activities are low, for example, due to low light adaptation, UVB sensitivity may be enhanced in these algae by a limited capacity to further withstand any losses of this critical enzyme. In 1997, a similar relationship was not observed between an index of UVB sensitivity ($UVB_{inh\ eff}$; *see* Chapter 2) and maximum photosynthetic potential. This index, based on a linear exposure response curve, may not have reflected the UVB sensitivity as accurately as the $\varepsilon_{R(300)}$ from the individual BWFs.

What the repercussions of photoinhibition will mean to an aquatic ecosystem as a whole will depend on the physicochemical and biological characteristics of that water body. While the kinetics of photoinhibition will be influenced by the overall sensitivity of the algal community,

the transmission properties as well as the rate and depth of mixing of the water column will likely have a greater influence on the relevant extent of photoinhibition, i.e. the inhibition on integrated primary production. These parameters will control the extent and duration of exposure to inhibiting radiation. In the following chapter the R model is validated with experimentally measured recovery rates and use this model for some predictive modelling to assess the impacts of present day and forecasted levels UVB on integrated primary production in L. Erie.

# Chapter 4

## The impact of ultraviolet radiation on vertically-integrated primary production in L. Erie: The role of recovery and mixing processes

## Abstract

A model of ultraviolet and visible radiation-dependent photoinhibition, developed for L. Erie phytoplankton, was used to calculate losses of daily production under mixing and water transparency scenarios that spanned the common range of conditions in the lake. The model's predictions of rates of recovery from photoinhibition were also tested against direct measurements of recovery following varied spectral exposures. Consistent with model predictions, notable recovery of photosynthesis, even when inhibited 80% by prior exposure to damaging radiation, occurred following transfer to benign, and relatively low irradiance, conditions. Measured recovery rate constants were independent of pre-exposure treatment, with a median of 0.49 x $10^{-4}$ $s^{-1}$. Recovery rate constants estimated from the photoinhibition model under higher radiation fluxes were significantly larger than the rate constants measured in recovery experiments, possibly reflecting differences in availability of PAR and long-UVA wavelengths involved in photoenzymatic repair. Both estimates of recovery rates indicated that near-full recovery would occur within one photoperiod under most conditions. Integrated photoinhibition ($PI_{int}$), i.e. the daily loss of production throughout the photic zone, predicted by the model was little affected by mixing rate variations, except that all scenarios with finite mixing rates experienced more inhibition than those with no mixing. The contribution of different wavebands to total photoinhibition also varied little with mixing rate. In a mixed water column, PAR-, UVA- and UVB-attributed inhibition under typical mid-summer, clear-sky, conditions, averaged 2.2, 9.9 and 1.2% for the entire lake. $PI_{int}$ was always highest in the relatively turbid, but shallow, West basin, regardless of the mixing scenario. Shallow 'temporary' thermoclines in the West basin led to the highest $PI_{int}$ predictions (2.6 and 15.8%

PAR and UVR inhibition, respectively). A forecasted 20% decrease in stratospheric ozone concentrations resulted in a minimal increase of 1.2% of $PI_{int}$ in the West basin, and would have a similarly minor effect in the other basins. Variations of phytoplankton susceptibility to UVR, and of their recovery rates, over the ranges observed to date in L. Erie, could lead to extremes of 5% to 20% loss of production under normal mixing conditions. UVA, rather than UVB or PAR, appears to be the major waveband responsible for photoinhibition of primary production in L. Erie. The impacts of climate change and human activity on transmission of UVA are therefore more of a concern than ozone-related variations of UVB in the Laurentian Great Lakes.

## Introduction

The main targets of UV radiation in phytoplankton are DNA and photosystem II structural proteins (D1), therefore recovery from exposure likely involves 1) the repair of damaged DNA; and 2) *de novo* synthesis of chloroplast proteins. Some of the enzymes involved in repairing damaged DNA are inducible. The transcription of photolyase is under light control and is inducible by UVB in plants; in addition, there is evidence that DNA polymerase β and DNA ligase are inducible (Greenberg et al. 1997, Pang and Hays 1991). The control of transcription of these different enzymes is under regulatory control by kinases which are involved in signal transduction and are themselves inducible by growth arrest and DNA damage (Pang and Hays 1994). Evidence for the necessity of *de novo* chloroplast protein synthesis for recovery of photosynthetic activity, comes from experiments specifically inhibiting chloroplast protein synthesis by the use of streptomycin (Ihle 1997, Lesser et al. 1994). In the presence of this protein synthesis inhibitor, recovery does not occur.

Results from photosynthetic recovery studies are ambiguous, ranging from evidence for complete recovery potential within a few hours to incomplete recovery after > 20h (e.g. Hermann et al. 1997, Larkum and Wood 1993). The seemingly contradictory results are due to different endpoints measured (DNA photoproduct removal, oxygen evolution, quantum yield, photosynthesis), different exposure conditions used (short (<1h) vs long (>1h) exposures, natural vs artificial irradiance, spectral treatments) and the variety of species used to test recovery potential (Buma et al. 1996, Hanelt et al. 1997, Hazzard et al. 1997, Karentz et al. 1991a, Schofield et al. 1995). For example, full recovery of optimal quantum yield (measured as $F_v/F_m$) and $O_2$ evolution in *Dunaliella salina* was achieved following short exposures (30

min) to natural solar radiation, but recovery was still incomplete after 21 h when the exposure was 3h long and included mainly UVB and short UVA radiation (Hermann et al. 1997). Wavelength dependence of recovery was also observed in a macroalga, *Palmaria palmata*, for which exposure to progressively shorter wavelengths increased the degree of photoinhibition and delayed the onset of recovery in the field (natural photoperiod; Hanelt et al. 1997).

Quantifying the relative impacts of UVR under natural conditions is complicated by the difficulty of measuring or modelling the spectral conditions and exposure regimes in the natural environment (Buma et al. 1996). While the spectral transmission properties of a water body can be measured, mixing in aquatic systems continuously changes the radiation exposure of phytoplankton cells, complicating the attempts at forecasting impacts. Not only does the presence or absence of mixing influence integrated photoinhibition but the strength of mixing (i.e. mixing rates) and depth of mixing are also controlling factors (Franks and Marra 1994). Few studies have attempted to quantify the effects of mixing on integrated primary production. Two approaches have been reported in the literature. The first involves a physical simulation of mixing, either mechanically (e.g Zagarese et al. 1998) or by rotating optical filters over a fixed sample (e.g. Helbling et al. 1994). The second approach employs models that incorporate quantitative functions to describe the biological responses together with additional functions to simulate the mixing and optical regime in the water column (e.g. Franks and Marra 1994, Neale et al. 1998c). The influence of mixing on the extent of photoinhibition has been related to sensitivity of the organisms to UVR (Boelen et al. 2000, Neale et al. 1998c, Zagarese et al. 1998) and the kinetics of photoadaptation with respect to the mixing and optical characteristics of the water column (Cullen and Lewis 1988, Franks and Marra 1994). Because

vertical mixing will invariably cause different phytoplankton cells within a same water column to possess different light histories, biological weighting functions and knowledge of the kinetics of UVR-associated damage and repair become particularly important when modelling of impacts in a mixed water column are attempted (Cullen and Lesser 1991, Lesser et al. 1994, Neale et al. 1998c).

In the previous chapter the importance of considering repair processes when modelling primary production was clearly demonstrated. A new kinetic model, which incorporates a finite recovery term as well as the first known biological weighting functions for freshwater phytoplankton, was shown to be applicable to L. Erie phytoplankton. The model provides the tools necessary to make realistic predictions about the impacts of UVR in Lake Erie. This chapter begins by evaluating the R model (*see* Chapter 3) further by comparing its estimates of recovery rate constants to experimentally measured recovery rates. Then, the model is combined with information about the optical conditions in the lake to calculate the impact of present day and future levels of UVR on primary production in Lake Erie, all within the realistic context of a mixed water column.

## Methods and Materials

### Theory

In the presence of inhibiting radiation, photosynthesis will be a function of both damage and repair kinetics (*see* Eq. 3.1). If cells are removed from the presence of any inhibiting radiation, photosynthesis will recover and may obey first-order kinetics in the following manner:

$$\frac{dP'_{(t)}}{dt} = k_2(1 - P'_{(t)}) \tag{4.1a}$$

Equation 4.1a integrated over time becomes.

$$P'_{(t)} = 1 - \left[\left(1 - P'_{(0)}\right)e^{-k_2 t}\right] \tag{4.1b}$$

where $P'_{(t)}$ is the photosynthetic rate at time t after transfer to non-inhibiting conditions, and $P'_{(0)}$ is the photosynthetic rate when first transferred to the non-inhibiting conditions. $P'_{(t)}$ and $P'_{(0)}$ express photosynthetic rates normalized to the uninhibited rate expected for the given irradiance conditions. $k_2$ is the recovery rate constant ($h^{-1}$).

Using the recovery rate constant estimates calculated from Eq. 4.1b, expected time of recovery to 95% full capacity can be calculated as follows:

$$t_{95} = \frac{\ln(1 - P'_{(0)}) - \ln(1 - P'_{Recovered})}{k_2} \tag{4.2}$$

where $P'_{Recovered}$ is the normalized photosynthetic rate at 95% recovery, i.e. 0.95.

Equations 4.1-4.2 deal with the case of phytoplankton transferred to non-inhibiting conditions, but $k_2$ can also be estimated simultaneously with inhibition, as done for the 8h time series experiments in Chapter 3. Such estimates are less direct, but may give a more accurate measure of recovery rates under the higher irradiance conditions in which the damage actually occurs. The two types of recovery rate estimates will be compared here.

### Experimental Procedures

The water sampling and experimental protocols for the first 2h of exposure for the 1997 and 1998 recovery experiments were as described in Chapter 2 and 3. Briefly, in 1997 and 1998, eight and two recovery experiments were conducted, respectively. In 1997, quartz tubes were pre-exposed for 2h in different spectral treatments (100 and 50% PAR full spectrum (all experiments) and 100 and 50% PAR and UVA without UVB (July (4 dates) and August (1 date) experiments)) and sampled at 0.5h (when appropriate), 1h and 2h. The tubes were then transferred to a benign 5 (May 7, June 4 and 5) or 10% (all other experiments) recovery box which transmitted 5 or 10% of the incident solar radiation at all wavelengths. Carbon incorporation was further monitored over time and samples were taken at 2h, 4h and 6h of benign light conditions. In 1998, the experimental design was essentially the same, however, two additional spectral treatments were used, 100 and 50% PAR only, and an extra sampling time was included, 1h after transfer.

### Modelling of Lake Erie

Using the modelling package Stella® (version 5.1.1 for Windows™), the R kinetic model was used to forecast the inhibition of integrated primary production in the three L. Erie basins. The purpose was to determine the extent to which UVR- and PAR-dependent

photoinhibition reduced primary production in the entire water column over the course of one day.

Photoinhibition was modelled for an algal community with typical L. Erie photosynthetic parameter values ($P^b_m$ = 4.35 C·Chl $a$·$h^{-1}$, $\alpha^b$ = 7.67 C·Chl $a^{-1}$·$E^{-1}$·$m^2$). These values are averages from 46 light gradient incubations performed in 1997 (11, 21 and 14 in the East, Central and West basins, respectively). These values were accepted as reasonable representative estimates of L. Erie phytoplankton photosynthetic performance since 74 and 56% of the $P^b_m$ and $\alpha^b$ values measured in 1997, fell within one standard deviation (±1.80 and ±2.51, $P^b_m$ and $\alpha^b$, respectively) of the mean. A representative, clear-sky, diurnal radiation spectrum (June 4 1997) with incident radiation measurements at 20 min intervals (9h40 to 19h20) was used to model integrated primary production. While summer days can be as long as 16h, the 10h photoperiod modelled here was centred around the maximum UVR photoperiod. Radiation before 9h40 and after 19h20 is unlikely to result in photoinhibition. However, photosynthesis will continue during this time likely unabated by inhibiting levels of UVR or PAR. Since times of the day when only recovery and/or uninhibited primary production is occurring are ignored, integrated photoinhibition is probably overestimated. Integrated primary production estimates were modelled for each basin assuming various mixing depth scenarios: 1) a 10 m epilimnion layer; 2) unstratified water column using basin-specific mean depth; 3) stratified water column using basin-specific typical epilimnion depth; and 4) shallow (1m) 'temporary' thermocline (for the West basin only). An organized water motion, a Langmuir circulation pattern (Fig. 4.1) was assumed to be the dominant mixing process and mixing rates

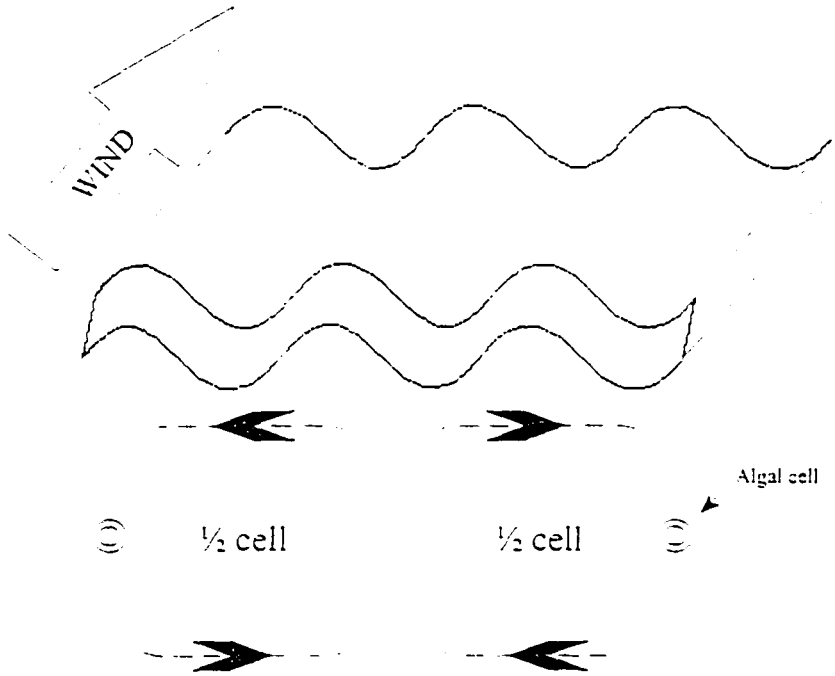



Figure 4.1: Organized circulation pattern, Langmuir circulation, used in the modelling of the inhibition of integrated primary production. Primary production was calculated for algae within ½ Langmuir cell with different starting depths and mixing at different rates.

were varied between no motion (i.e. static water column) to 20 $m \cdot h^{-1}$, a theoretical upper limit for vertical displacement within an organized circulating cell (Denman and Gargett 1983).

Integrated primary production was calculated for the 10 h photoperiod, by predicting relative photosynthetic rates at 15 min. intervals, according to the kinetic model and calculating cumulative photosynthesis. This was done for four conditions: 1) full spectrum (PAR+UVA+UVB); 2) PAR+UVA; 3) PAR only and 4) optimum predicted from the photosynthetic parameters $P^b_m$ and $\alpha^b$, i.e. no UVR or PAR-attributed photoinhibition. The first three conditions allowed for photoinhibition from each waveband, and the estimates were compared to the theoretical optimum (condition 4) to determine the percent inhibition of integrated primary production ($PI_{int}$) attributed to PAR, UVA and UVB. This was done for 48 theoretical algal cells either remaining at one point within the water column for the entire photoperiod (static scenario) or cycling at different rates and starting the day at different depths within a ½ Langmuir cell (Fig. 4.1). The kinetics of damage and recovery were assumed constant throughout the day, and algal biomass was assumed to be uniformly distributed throughout the water column. PAR availability was calculated using basin-specific attenuation coefficients, representing median values observed in five separate cruises in spring and summer of 1997 (0.26, 0.32 and 0.64 $m^{-1}$, for the East, Central and West basins, respectively). Wavelength specific attenuation coefficients ($K_{d\lambda}$) for UVR were predicted from previously-derived models for L. Erie which best predicted UVR attenuation coefficients (Smith et al. 1999). The first relationship was used to predict the attenuation coefficient at 320 nm ($K_{d320}$):

$$K_{d320} = 1.378 + 0.218 \cdot TSS + 0.804 \cdot K_{dPAR} \qquad (4.3)$$

using total suspended solids concentrations (TSS) and vertical attenuation coefficient for PAR

($K_{dPAR}$). The second relationship then used predicted $K_{d320}$ (Eq. 4.3) to calculate attenuation coefficients for other wavelengths ($K_{d\lambda}$):

$$K_{d\lambda} = K_{d320} \cdot e^{3.288-0.011\lambda} \quad (4.4)$$

Radiation at each depth interval was calculated with incident spectral radiation weighted with the biological weighting function derived for the algal assemblage sampled on June 9/98. This BWF was chosen because it was derived from algae demonstrating high UVR sensitivity ($\varepsilon_{R(300)}$ and $\Sigma\varepsilon_{R(\lambda)}$; *see* Table 3.3 and Fig. 3.8b), yet the overall shape of the BWF seemed representative of the relative biological effectiveness of different UVR wavelengths on L. Erie phytoplankton (*see* Fig. 3.9b,c). Using the weighted radiation, the R kinetic model was applied to predict photosynthesis, assuming median 1998 values of recovery rate constants ($5.04 \times 10^{-4}$ $s^{-1}$) and PAR effectiveness coefficients ($1.72 \times 10^{-7}$ $(W \cdot m^{-2})^{-1}$). By using a high-sensitivity BWF it was intended to illustrate the maximum UVR-inhibition that might be expected, but sensitivity analysis was also done to explore the implications of different assumptions regarding BWF and recovery rate constants.

Variations in the incident radiation spectra were calculated for 'normal' ozone levels (300 Dobson Units(DU)) and a 20% reduction in ozone concentration (240 DU), using published wavelength specific ozone absorption values (Molina and Molina 1986). A 20% reduction in ozone layer is an upper limit of ozone depletion encountered in southern Canada during spring months (Meteorological Service of Canada 1999). While not as severe as ozone thinning observed in the Arctic (up to 45%) and Antarctic (50%), an average 3.4% decrease of total ozone occurred between 1979 and 1997 over North America and assuming this trend is

maintained, a further 20% decrease could be expected over the next century (Meteorological Service of Canada 1999).

The unweighted UVB irradiance spectrum for 300 and 240 DU is illustrated in Fig. 4.2. The inhibition of integrated primary production under 'normal' ozone levels was modelled for each basin and all mixing scenarios, while the forecasted effects associated with a 20% reduction in stratospheric ozone concentrations were modelled for the West basin only. Furthermore, sensitivity analysis was performed on this basin, under complete mixing conditions (mixing depth of 7.6m), for four different combinations of low ($0.30 \times 10^{-4}$ $s^{-1}$) and high ($6.26 \times 10^{-4}$ $s^{-1}$) recovery rate constants and low ($1.12 \times 10^{-4}$ $(W \cdot m^{-2})^{-1}$) and high ($5.41 \times 10^{-4}$ $(W \cdot m^{-2})^{-1}$) UVR sensitivity (i.e. $\varepsilon_{R(300)}$). This additional modelling was performed for the West basin only because it seemed to show the greatest response to UVR (*see* Results) and would be expected to show the strongest response to ozone depletion, and to variable recovery rates and phytoplankton sensitivity.

## Statistical Analysis

Analysis of variance (ANOVA) was used to investigate the dependence of relative cumulative photosynthesis and the measured recovery rates as a function of pre-exposure treatments. Frequent (3 out of 4) failure of non-linear regression modelling for the UVR excluded treatments allowed only one estimate of $k_2$ for this spectral quality treatment, therefore, the effect of total UVR exclusion on recovery rate constants could not be assessed. While the $k_2$ and $P'_{final}$ satisfied the ANOVA assumptions, the $P'_{(0)}$ were not normally distributed and therefore these values were natural logarithm transformed. Wilcoxon's test, a non-parametric, two sample paired t-test, was used to assess the differences between the

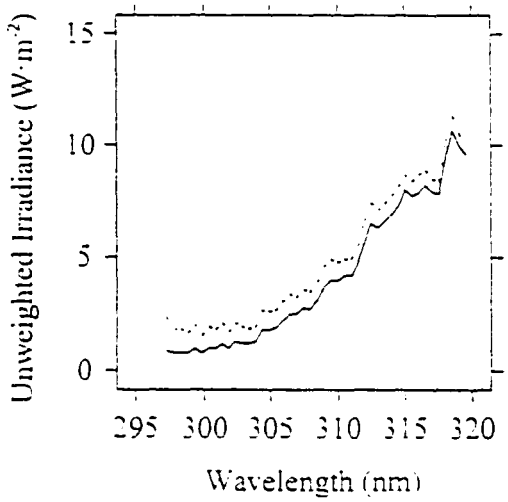



Figure 4.2: UVB irradiance spectra under 'normal' (300 DU) and 'depleted' (240 DU) stratospheric ozone concentration. Solid line: 300 DU; dashed line: 240 DU.

directly measured (recovery experiments) and inferred (R model) recovery rate constants.

## Results

### Limnological Conditions

A total of ten stations were sampled for recovery experiments, eight in 1997 and two in 1998. The limnological conditions found at each station sampled are listed in Table 4.1 (*see* Chapter 2 for detailed description of the stations sampled in 1997). The two stations sampled from the Central basin in 1998 were stratified and chl *a* was uniformly distributed within the top mixed layer. At stations 945 on July 16, a subsurface chl *a* maximum was observed between 6 and 14m, near the thermocline and the kinetics of recovery were investigated for the algal community sampled at 10m. Chl *a* vertical distribution was, however, uniform at station 946 on August 11 and the 5m water sample was representative of the mixed layer. There was no evidence of shallow 'temporary' thermoclines at either of these stations.

### UVR-Dependent Inhibition and Recovery of Photosynthesis

In all experiments, two hours of exposure resulted in a notable reduction of relative cumulative photosynthesis ($P'_{(0)}$; *see* Materials and Methods) and meaningful recovery occurred when the samples were transferred to benign, low-light, recovery boxes (Fig. 4.3). On average, the harshest treatment (100% PAR full spectrum) suppressed photosynthesis by as much as 80% in 2h relative to the optimum photosynthetic rate. Conversely, the mildest treatment (50% PAR only) resulted in minimal inhibition, ca. 4% (Fig. 4.3b). While exposure to UVB did diminish photosynthesis, the bulk of the photoinhibition was attributed to UVA (Fig. 4.3b). Analysis of variance (ANOVA) showed that the $P'_{(0)}$ values (Table 4.2) were significantly ($p < 0.00001$) lower in the UVR-exposed (UVA and/or UVB) treatments than the

Table 4.1: Summary of the limnological variables of the stations sampled for time-series recovery experiments conducted on L. Erie in the summers of 1997 and 1998.

| Date | Station | Basin | Epilimnion Depth (m) | | Temperature at 5 m (°C) | Chl *a* at 5 m ($\mu g \cdot L^{-1}$) | $K_{dPAR}$ ($m^{-1}$) | Mean PAR % of incident |
|---|---|---|---|---|---|---|---|---|
| 1997-7/5 | 946 | C | 22 | | 6 | 1.5 | 0.43 | 10.6 |
| 3/6 | 946 | C | 22 | (iso.) | 8.8 | 2.5 | 0.29 | 15.1 |
| 4/6 | 337 | W | 9 | (iso.) | 13.2 | 9.8 | 1.61 | 6.9 |
| 5/6 | 961 | C | 19 | (iso.) | 13.4 | 1.2 | 0.83[a] | 6.3 |
| 29/7 | 23 | E | 15 | | 22 | 3.5 * | 0.24 | 27 |
| 30/7 | 953 | C | 12 | | 22.2 | 1.4 | 0.32 | 25.5 |
| 31/7 | 962 | C | 11 | | 23.7 | 2 | 0.36[a] | 24.8 |
| 27/8 | 337 | W | 9 | (iso.) | 21.1 | 15.5 | 1.16 | 9.6 |
| 1998-16/7 | 945 | C | 10 | | 22.9 | 4.6 | 0.33 | 29.2 |
| 11/8 | 946 | C | 17.5 | | 23.6 | 4.9 | 0.25 | 22.6 |

*Note that *in vivo* chl *a* fluorescence was not uniformly distributed with the mixed layer on this date (*see* Fig. 2.5)

[a] Value of $K_{dPAR}$ derived from the following relationship: $K_{dPAR} = -0.026 * \text{Transmission} + 2.258$

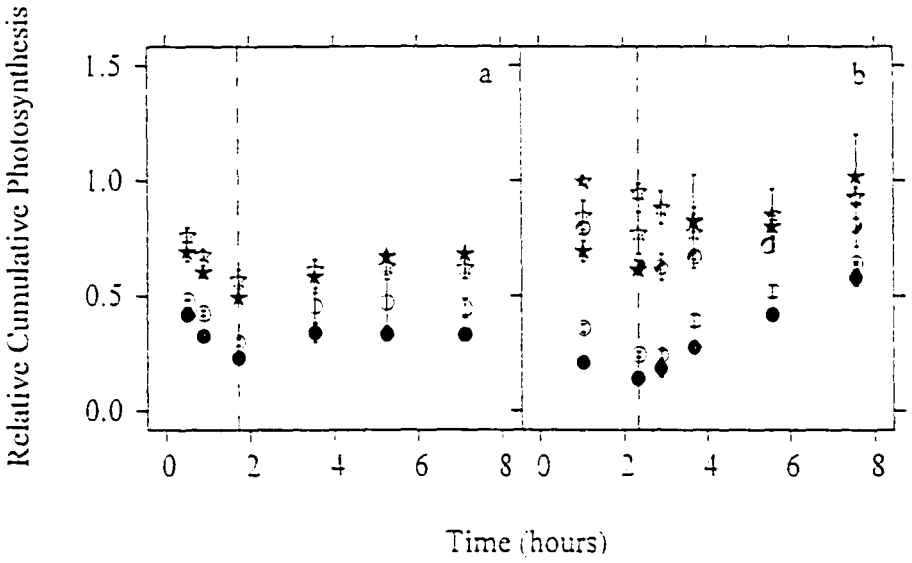



Figure 4.3: Temporal change in relative cumulative photosynthesis for the various 2h pre-exposure spectral quality treatments (a) July 29/97 and (b) August 11/98. Vertical dashed lines represent the time samples were transferred to benign recovery deck boxes. Legend: ● = 100% PAR full spectrum; ○ = 100% PAR + UVA; = 100% PAR only; ★ = 50% PAR full spectrum; ☆ = 50% PAR + UVA; = 50% PAR only.

Table 4.2: Relative cumulative photosynthesis for each spectral treatment following 2h of exposure just before being transferred to the benign recovery deck boxes (initial) and following 6h of recovery (final). Averages (over all experimental dates) ± 1SE; subscript denotes sample size; values in parentheses represent the range of observed values.

| Relative Photosynthesis | 100% PAR full spectrum | 100% PAR UVB-shielded | 100% PAR only | 50% PAR full spectrum | 50% PAR UVB-shielded | 50% PAR only |
|---|---|---|---|---|---|---|
| $P'_{(0)}$ | $0.21 \pm 0.02_{11}$ | $0.29 \pm 0.01_{7}$ | $0.74 \pm 0.11_{2}$ | $0.55 \pm 0.03_{11}$ | $0.65 \pm 0.03_{7}$ | $0.96 \pm 0.01_{2}$ |
| | (0.12 - 0.31) | (0.24 - 0.32) | (0.63 - 0.85) | (0.41 - 0.70) | (0.53 - 0.77) | (0.95 - 0.97) |
| $P'_{(final)}$ | $0.58 \pm 0.07_{10}$ | $0.59 \pm 0.10_{7}$ | $1.11 \pm 0.30_{2}$ | $0.69 \pm 0.09_{10}$ | $0.91 \pm 0.10_{5}$ | $1.02 \pm 0.10_{2}$ |
| | (0.23 - 0.89) | (0.18 - 0.99) | (0.80 - 1.41) | (0.16 - 1.07) | (0.62 - 1.16) | (0.93 - 1.12) |

UVR- shielded treatments within each PAR level. After 6h of recovery, however, $P'_{(t)}$ (i.e. $P'_{final}$) were no longer significantly different between spectral treatments in either PAR treatment level ($p > 0.05$) (Table 4.2).

Recovery of photosynthetic rates was observed following all spectral exposure treatments (Table 4.2). After 6h, the samples subjected to the harshest treatment (100% full spectrum) had recovered to ca. 60% of the low-light control, while those exposed to the mildest treatments (100 and 50% PAR only) no longer showed any signs of inhibition. While a trend towards lower $P'_{(final)}$ values in the harshest treatments compared to milder treatments was evident, these differences were not significant.

### Recovery Rate Constants and Associated Recovery Times

Recovery rate constants were estimated by fitting Eq. 4.1b for each spectral treatment to ascertain whether recovery rates were dependent on the nature of the pre-exposure radiation treatment. In the UVR shielded (PAR only) treatments little damage was observed within the 2h of exposure (Table 4.2), so there was little scope for recovery, and rate constants could not be estimated in 3 out of the 4 experiments. Thus, the effect of total UVR exclusion on recovery rate constants could not be properly assessed. Among UVR-exposed treatments, estimated recovery rate constants did not significantly differ between the UVB exposed and shielded treatments ($p > 0.90$, Table 4.3). In the absence of pre-exposure treatment effects, all treatments were pooled and an average recovery rate constant was estimated for each sample date (Table 4.4). These recovery rates ranged from 0.11 (June 4/97) to $1.25 \times 10^{-4}$ $s^{-1}$ (July 16/98), and had a median of $0.49 \times 10^{-4}$ $s^{-1}$ (Table 4.4). The highest recovery rate was observed on July 16/98 for the 10m sample from the metalimnetic chlorophyll fluorescence maximum.

Table 4.3: Experimentally determined recovery rates for the different spectral treatments averaged over all sample dates.

| Spectral Treatment | Recovery Rate ($h^{-1}$) |
|---|---|
| 100PAB | $0.17 \pm 0.04_{11}$ |
| | (-0.02 - 0.47) |
| 100PA | $0.15 \pm 0.06)_{7}$ |
| | (-0.03 - 0.48) |
| 50PAB | $0.18 \pm 0.07_{9}$ |
| | (-0.07 - 0.57) |
| 50PA | $0.18 \pm 0.11_{7}$ |
| | (-0.24 - 0.71) |

Table 4.4: Measured and modelled estimates of recovery rate constants for each experimental date. Estimates (or median) ± the asymptotic standard error of the estimate (or standard error).

| Date | Exponential fit | | Repair (R) model | |
|---|---|---|---|---|
| | $k_2$ | $r^2$ | $k_2$ | $r^2$ |
| | (x $10^{-4}$ $s^{-1}$) | | (x $10^{-4}$ $s^{-1}$) | |
| 1997 - 7/5 | 0.11 ± 0.04 | 0.993 | 2.58 ± 1.00 | 0.443 |
| 3/6 | 0.63 ± 0.04 | 0.978 | 5.46 ± 2.99 * | 0.481 |
| 4/6 | 0.11 ± 0.04 | 0.81 | 0.24 ± 0.19 * | 0.604 |
| 5/6 | 1.09 ± 0.41 | 0.748 | 2.00 ± 0.57 | 0.441 |
| 29/7 | 0.41 ± 0.02 | 0.874 | 11.30 ± 6.29 * | 0.144 |
| 30/7 | 0.65 ± 0.07 | 0.923 | 1.84 ± 0.45 | 0.598 |
| 31/7 | 0.56 ± 0.06 | 0.882 | 3.27 ± 0.89 | 0.381 |
| 27/8 | 0.29 ± 0.04 | 0.802 | 1.05 ± 0.30 | 0.446 |
| 1998 - 8/6 | - | - | 0.30 ± 0.30 *[a] | 0.93 |
| 9/6 | - | - | 5.04 ± 1.54 [a] | 0.762 |
| 14/7 | - | - | 2.57 ± 0.56 [a] | 0.918 |
| 16/7 | 1.25 ± 0.10 | 0.945 | - | - |
| 11/8 | 0.40 ± 0.04 | 0.932 | - | - |
| 12/8 | - | - | 6.26 ± 2.34 [a] | 0.894 |
| 13/8 | - | - | 5.76 ± 2.27 [a] | 0.809 |
| Median | 0.49 ± 0.12 | - | 2.58 ± 0.82 | - |

*Recovery rate constant estimate was not significantly different from zero.

[a]No direct recovery measurements available.

Recovery rate constants estimated by the photoinhibition model for samples exposed to higher, and damaging, irradiance ranged from non-significantly different from zero (e.g. June 4/97) to 11.30 x $10^{-4}$ $s^{-1}$ (July 29/97), and the median was 2.58 x $10^{-4}$ $s^{-1}$ (Table 4.4). Wilcoxon's nonparametric paired t-test showed that recovery rate constant estimates from the photoinhibition model were significantly larger than those measured directly in the recovery treatments ($p < 0.05$).

Using the median measured and inferred recovery rate constants, 95% recovery times were calculated for severe (80%) and mild (20%) levels of inhibition. Recovery times were calculated assuming no further exposure to inhibiting radiation. For severe inhibition, 15.7 to 3.0h was required for 95% recovery, using median values of the directly measured (low irradiance) and inferred (higher irradiance) recovery rate constants, respectively. Recovery from mild inhibition would by comparison require, on average, 7.9 to 1.5h.

### Modelling Inhibition of Integrated Primary Production in a Mixed Water Column

For each L. Erie basin, various water column circulation scenarios were simulated to investigate the effects of mixing rate and mixing depth on the inhibition of integrated primary production ($PI_{int}$). Fig. 4.4 shows the $PI_{int}$ results for typical summer epilimnion depths as a function of mixing rates for the two basins that differ most in depth and transparency. The East (Fig. 4.4a) and Central (not shown) basins showed similar patterns of photoinhibition, that is lower $PI_{int}$ for a static water column (1.7, 5.0 and 0.5%, PAR, UVA and UVB inhibition) and essentially no variation under the different mixing rates. Averaged among the different mixing rates, the relative proportion of $PI_{int}$ attributed to PAR, UVA and UVB was 2.2 ± 0.0, 8.7 ± 0.1 and 1.1 ± 0.0%, respectively, in the East basin. The West basin also showed little or no effect of

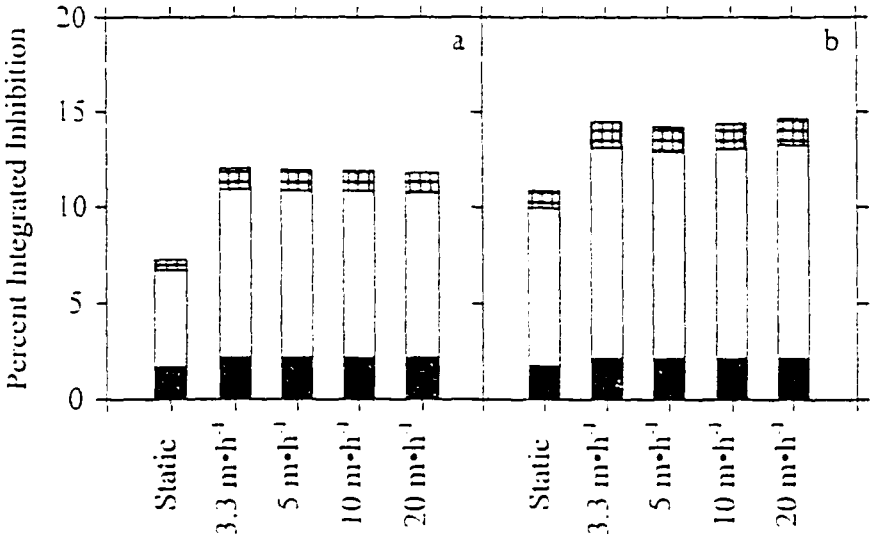



Figure 4.4: Inhibition of integrated primary production predictions for typical summer stratification events in the (a) Eastern and (b) West basins for different mixing rates. The mixing depths were 16m and 5m for the Eastern and West basins, respectively. Legend: solid bars: PAR inhibition; open bar: UVA inhibition; hatched bar: UVB inhibition.

mixing rate on total $PI_{int}$ estimates and lowest inhibition when a static water column was simulated. In the absence of any mixing rate effects on the $PI_{int}$ estimates all subsequent model predictions presented here were performed for a water column mixing at a rate of 10 $m \cdot h^{-1}$.

In Chapter 2, it was suggested that the radiation transmission properties and the stratification pattern of the West basin rendered this part of L. Erie most vulnerable to UVR, and Fig. 4.4 tended to confirm this suggestion. To further compare the basin-specific $PI_{int}$, the effects of PAR, UVA and UVB were modelled for a 10 m water column (Fig. 4.5a), an unstratified water column using mean basin depth (Fig. 4.5b), and a typical basin-specific epilimnion depth (Fig. 4.5c). As for the different mixing rate simulations, PAR inhibition was relatively constant among mixing depths scenarios and between basins (2.2 ± 0.1, 2.2 ± 0.1 and 2.3 ± 0.6%, E, C and W basin, respectively; Fig. 4.5). Most of the inter-basin variation was due to UVA (8.8 ± 0.5, 9.3 ± 0.3 and 11.7 ± 4.4%, E, C and W basin, respectively), although inhibition by UVB was somewhat greater for the West than the other basins (1.1 ± 0.1, 1.1 ± 0.0 and 1.4 ± 0.7%, E, C and W basin, respectively; Fig. 4.5). Assuming a 10 m mixing depth for each basin, the East and Central basins showed similar patterns of inhibition, whereas the West basin suffered great inhibition by UVA and UVB. While the inter-basin differences in inhibition were greatest under this mixing scenario, the pattern of higher $PI_{int}$ in the West basin was also manifested under the stratified and unstratified conditions (Fig. 4.5). The absolute $PI_{int}$ did not vary greatly between mixing scenarios, although deep mixing in the East and Central basins showed potential for more UVR attributed inhibition (Fig. 4.5b).

The West basin was thus the most susceptible to UVR inhibition under fairly typical lake mixing processes. However, the West basin also tends to develop shallow 'temporary'

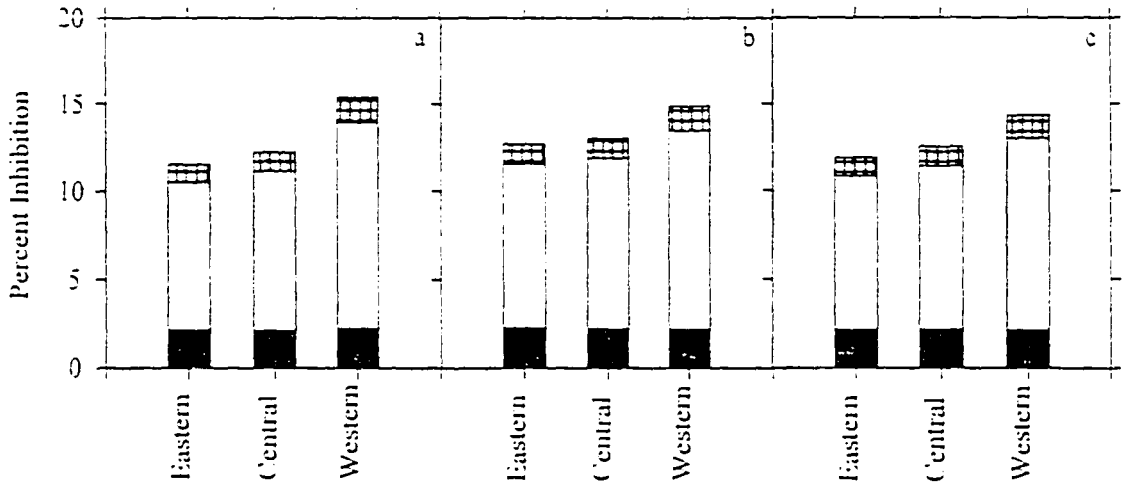



Figure 4.5: Basin-specific inhibition of integrated primary production predictions for (a) a 10m mixed layer, (b) complete mixing and (c) typical summer epilimnion depths for a water column with an average vertical displacement speed of $10 m \cdot h^{-1}$. Photosynthesis was integrated to 27, 17.8 and 7.6m for the E, C and W basins, respectively, for the complete mixing simulation and to 16, 13 and 5m for the E, C, and W basins, respectively, for the typical summer epilimnion depth simulations. Although the West basin is commonly uniformly mixed, it does stratify on occasion and of the stations we sampled, the median epilimnion depth was 5m. Legend: solid bars: PAR inhibition; open bar: UVA inhibition; hatched bar: UVB inhibition.

thermoclines more frequently than the East or Central basins (*see* Chapter 2), which may further sensitize this basin to UVR inhibition. To explore this issue, $PI_{int}$ was modelled for a 7.6m water column (mean depth for the West basin) under a shallow 'temporary' thermocline scenario. $PI_{int}$ was calculated for algae trapped in the first metre of the water column, for those in the remaining 6.6m and finally for the entire water column (Fig. 4.6). In the top metre of the water column, total $PI_{int}$ was estimated at ca. 23% with 20% attributed to UVR (17.8 and 2.3% UVA and UVB inhibition, respectively), while the bottom 6.6 m showed a mere 4.7% UVR-attributed inhibition. However, when the production of the entire water column was integrated, a total $PI_{int}$ of 18.4% (2.6, 14.0 and 1.8% PAR, UVA and UVB inhibition, respectively) was estimated, an approximate increase of 4% UVR inhibition compared to the typical stratified and unstratified conditions (Fig. 4.5). Since the West basin was observed to be the most UVR vulnerable, the effects of a 20% ozone depletion on $PI_{int}$ in this basin were forecasted (Fig. 4.6). The associated added flux of UVB resulted in a mere 0.8, 1.9 and 1.2% increased $PI_{int}$, for the top 1m, the bottom 6.6m and the entire water column, respectively.

Sensitivity analysis was also performed for the West basin, using the extremes for recovery rate constants and sensitivity (i.e., BWF values) observed. Under the worst case scenario, i.e. low recovery rates and high sensitivity, PAR and UVR caused 6.1 ± 0.0 and 21.2 ± 0.4% inhibition respectively (Fig. 4.7). Under the best case scenario, i.e. high recovery rates and low sensitivity, inhibition was 1.9 ± 0.0 and 3.0 ± 0.0% by PAR and UVR, respectively. Variations of both recovery constant and sensitivity between the observed extremes were of approximately equal importance in determining the total inhibition. While the PAR inhibition changes were strictly a function of recovery rate variations, UVR was affected

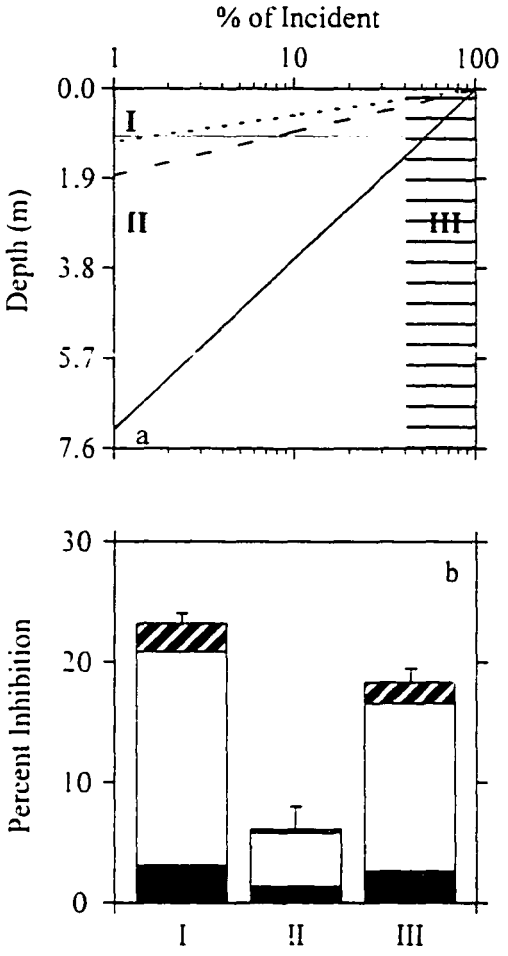



Figure 4.6: Solar radiation transmission properties (a) and inhibition of integrated primary production predictions (b) for the West basin (used mean depth of 7.6m) during a shallow (1m) 'temporary' thermocline event. Legend: I: $PI_{int}$ integrated over top 1m; II: $PI_{int}$ integrated for the remaining 6.6m; III: $PI_{int}$ integrated over the entire water column, i.e. 7.6m. Solid bars: PAR inhibition; open bar: UVA inhibition; hatched bar: UVB inhibition. Error bars represent the additional inhibition due to 20% ozone depletion.

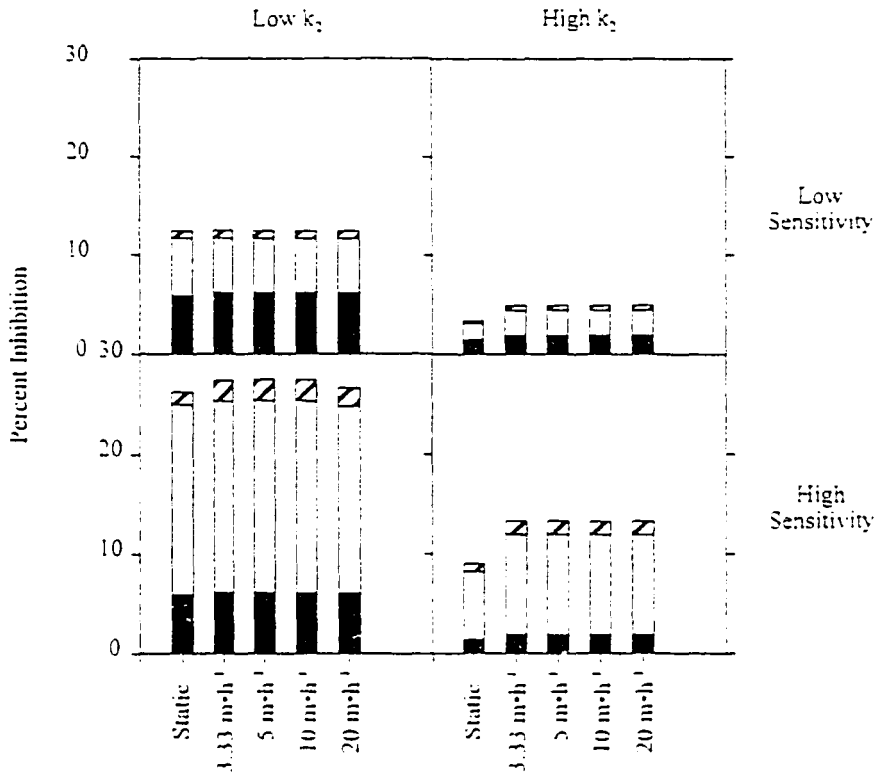



Figure 4.7: Sensitivity analysis of integrated photoinhibition predictions using two levels of recovery rate constants and overall UVR sensitivity under different mixing scenarios. Low and high $k_2$ values: 0.30 and 6.26 x $10^{-4}$ $s^{-1}$. Low and high sensitivity: $\varepsilon_{R(300)}$: 1.12 and 5.41 x $10^{-4}$ $((W \cdot m^{-2})^{-1})$. Solid bars: PAR inhibition; open bars: UVA inhibition; hatched bars: UVB inhibition.

both by recovery and sensitivity and consequently showed a 7 fold difference in inhibition under the two extreme sensitivity scenarios. As noted in the previous modelling scenarios, water column mixing rate did not affect $PI_{int}$, while a static water column showed less photoinhibition than any of the mixed conditions, particularly when recovery rates were high. Given the same UVR sensitivity, the high PAR and UVR, particularly UVA, in the top 2m of the water column resulted in as much as 50% more inhibition when recovery rates were low than high (Fig. 4.8).

Of all the different mixing scenarios that were modelled for the three L. Erie basins, the most severe $PI_{int}$ predictions were for the West basin when shallow 'temporary' thermoclines were simulated. Integrating the top 1m of the water column, this can be viewed as an upper limit of severity of inhibition *in situ* within one photoperiod. Under these conditions, a total of 20% photoinhibition could be attributed to UVR and associated recovery times of 1.5h for 95% recovery were then calculated using the higher R model estimates of average recovery rates. By comparison, 'normal' mixing scenarios would likely result in lower damage severity and recovery times. Based on these calculations, the R kinetic model predictions were considered reliable indicators of day to day effects of UVR on integrated photoinhibition.

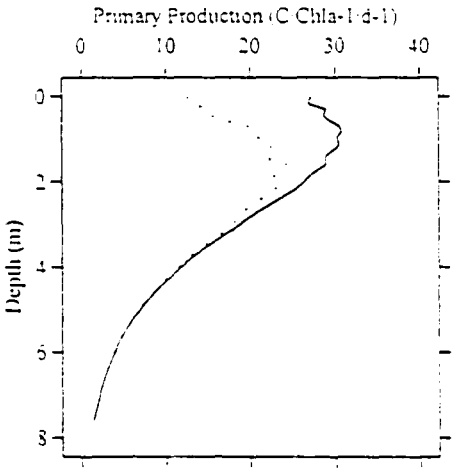



Figure 4.8: Comparison of the impact of low vs high recovery rate constants on primary production inhibition in a static water column. Solid line: high repair; dotted line: low repair.

## Discussion

The susceptibility of photosynthesis to damage by UVR is comprised of at least two important and distinct components: 1) a sensitivity to damage component partly influenced by the presence of photoprotective pigments (Schofield et al. 1995) and 2) an ability to recover component mediated by repair processes (Chapter 3). The first component of UVR susceptibility has been studied by numerous researchers mostly investigating the presence and/or induction of mycosporine-like amino acids (MAAs), a category of pigments typically associated with UVR photoprotection in microalgae (Roy 2000). The second component of UVR susceptibility, the ability to recover, has received comparatively limited attention despite its obvious importance in the integrated response of primary producers to damaging UVR. The R model for photoinhibition predicted active recovery in most of the L. Erie phytoplankton communities sampled, and direct measurements of recovery supported the prediction.

L. Erie phytoplankton demonstrated meaningful recovery of photosynthesis following 2h of exposure to damaging radiation (UVR and PAR). As noted in Chapter 2, suppression of photosynthesis in the UVR exposed samples could be extensive and rapid, particularly in simulated surface water samples, for which ca. 80% photoinhibition was observed on average. Rapid kinetics of photoinhibition by UVR have repeatedly been demonstrated with 30 min full spectrum exposures capable of eliciting up to 90% inhibition (Lesser et al. 1994, Herrmann et al. 1997, Marwood et al. 2000). While these and other studies (e.g. Kinzie et al. 1998) have observed severe inhibition of phytoplankton photosynthesis, the exposures were rather extreme. Natural aquatic systems are usually subject to vertical mixing, preventing long term residence of phytoplankton in high UVR surface waters. Nevertheless, notable recovery of algal

photosynthesis was observed even after relatively harsh exposures. L. Erie phytoplankton have also shown the ability to recover the efficiency of electron transport and the steady-state quantum yield of photosystem II following short (≤ 30 min) exposures to high incident solar radiation (Marwood et al. 2000).

One of the few other recovery studies carried out, using methods similar to those of the present study, found no recovery of photosynthesis in Antarctic (Southern Ocean) phytoplankton following short (≤1h) exposures to solar radiation (Neale et al. 1998b). The Antarctic waters were cold and were mixing down to 50 or 100m when sampled; and the phytoplankton were shade adapted and showed high UVR sensitivity (Neale et al. 1998b). By comparison, L. Erie has a maximum depth of 64m and a mean depth of only 18.6m (Burns 1985), while summer thermocline depths are typically between 10 and 20m (*see* Chapter 2). Instantaneous incident irradiance is also higher during summer at L. Erie than at the Antarctic sites. Consequently, light history should differ between these two systems, and the light saturation parameters of L. Erie phytoplankton were indeed higher than those of the Antarctic (*see* Chapter 2; Neale et al. 1998b). In addition, time scales of adaptation to a changing light environment can depend both on the magnitude and direction of change in photosynthetically active photon fluence density (PPFD), with large increases of incident light requiring longer adjustment periods than small, presumably due to unbalanced growth (Cullen and Lewis 1988). The low light adapted Antarctic phytoplankton, were probably confronted with a much larger change in mean irradiance than were the L. Erie algae when transferred to the experimental conditions, and low temperatures may have slowed the necessary biosynthetic responses. Time scales of photoadaptation outlasting the experimental time frame (3h of monitored recovery

rates) may therefore have contributed to the absence of measurable recovery in the Antarctic algae.

At the onset of exposure to damaging radiation, phytoplankton have short term (seconds to minutes) mechanisms available to offset photoinhibition, such as energy dissipation via fluorescence or state transitions (Ferris and Christian 1991). When these protective mechanisms are overwhelmed by longer exposures, more destructive outcomes can occur, such as protein photomodification or membrane lipid peroxidation (Girotti 1985, Wilson et al. 1995) for which counteracting measures will likely require longer time scales (minutes to hours). Because different wavelengths have different molecular targets, and possibly different short and long term consequences, spectral quality of exposure may influence recovery rates. Consistent with such spectral quality influences, recovery was slower when Antarctic phytoplankton were exposed to full spectrum radiation than to PAR plus UVA only (Schofield et al. 1995). No comparable effect was observed in the L. Erie phytoplankton studied here, suggesting that the principal sites or mechanisms of action were similar for UVB and UVA. However, recovery times were dependent on total exposure, because the extent of damage varied accordingly.

Recovery rates for L. Erie phytoplankton were higher when estimated from the R model than when measured experimentally. This disparity may be a consequence of availability and spectral quality of radiation. The measured recovery rates were estimated from samples transferred to much lower irradiance, with a deficiency of UVA, while R model estimates were derived from samples exposed to higher, and more spectrally-complete, radiation. In the latter case, phytoplankton may have received more of the radiation required in photoenzymatic repair, i.e. PAR and UVA, allowing higher recovery rates. In addition, comparison of irradiance in the

recovery boxes with the light-saturation parameters, derived from the PAR-only light gradient incubator experiments, showed that photosynthesis was probably light-limited for most of the recovery experiments. Active protein synthesis is essential in mitigating the effects of PAR photoinhibition (Ohad et al. 1984), and is involved in alleviating UVR-dependent photoinhibition (Lesser et al. 1994, Ihle 1997). Protein synthesis, and other repair processes, require energy supplied in the form of ATP (Raven and Samuelsson 1986). Increased energetic demands during repair may limit the recovery of photosynthetic C fixation in energy-limiting conditions, as a significant part of the ATP produced in the electron transport chain may be diverted to these energy requiring repair processes and not towards the Calvin-Benson cycle (Hanelt et al. 1997). Furthermore, if newly synthesized macromolecules are favoured as rapidly accessible energy sources, significant recycling of the $^{14}$C-label may have been occurring in the 'recovery' boxes, and the radiocarbon method used here may have underestimated gross photosynthesis. In any case, the discrepancy in recovery rates probably reflected real differences, driven by differing availability of useful radiation, in the rate of recovery of net C fixation. Moreover, even in the light-limited 'recovery' boxes, phytoplankton managed recovery rates that would largely restore their photosynthetic ability, under most exposure conditions, before the beginning of the next photoperiod. The photoinhibitory losses of primary production rates estimated here are therefore probably not cumulative between days, i.e. productive potential ($P_{opt}$) will be largely restored before the next period of high irradiance and renewed photoinhibition.

The inhibition of integrated primary production was modelled for both a static and a mixed water column in L. Erie. It can be argued that inhibition by UVR can either be reduced

or increased in a mixed, as compared to a static, water column (Helbling et al. 1994, Cullen and Lewiss 1988). Previous work with bacterio- and phytoplankton has given examples of both directions of effect (Boelen et al. 2000, Neale et al. 1998c). The direction of effect depends not only on the rate of mixing through the vertical radiation gradient, but also on the kinetics of both damage and recovery. On an individual basis, production of one algal cell will most likely be increased compared to a cell which remains for example just below the surface, since mixing will provide some shelter from damaging UVR. For the entire water column, however, mixing has the disadvantage of exposing more of the algal biomass to damaging surface conditions, which can be particularly detrimental to low-light adapted algae and/or those with slow rates of repair (Neale et al. 1998b). Our results showed that mixing in L. Erie consistently induces more inhibition than static conditions despite the substantial recovery abilities of the phytoplankton. Mixing rate, however, had little effect, so estimates of column-integrated inhibition do not seem to require very precise knowledge of mixing energy or processes.

Only one study has mechanically simulated mixing, by appropriate variation of the radiation regime, to determine effects on UVR-dependent inhibition (Helbing et al. 1994). As in the present case, column-integrated inhibition was greater with, than without, mixing. This, however, was only observed on sunny days, opposite results were observed under low irradiance days. This contrasts with older studies, involving exposure to PAR only, which indicated higher integrated production rates by marine phytoplankton when vertical mixing motions were included. Franks and Marra (1994) demonstrated that integrated primary production depends on light extinction, the extent of wind stress and the thickness of the mixing layer. Turbid, deeply and rapidly mixing water columns tend to support higher

integrated primary production. However, these authors recognized that large short term fluctuations in incident light, due to clouds for example, can make the beneficial effects of mixing (depth and rates) negligible, a conclusion supported by previous studies (Franks and Marra 1994 and references therein). The critical difference with our data may be in the efficiency and speed with which UVR promotes photoinhibition, as compared to PAR.

The rate at which cells are mixed within a water column may also influence the extent of $PI_{int}$. The only study to model this effect, as far as we know, was again for an Antarctic phytoplankton community (Neale et al. 1998c). Fast (50 $m \cdot h^{-1}$) and deep (100m) mixing resulted in comparatively lower $PI_{int}$ than slow (21 $m \cdot h^{-1}$) and shallow (21m) mixing for the Antarctic phytoplankton. While information on the mixing dynamics in L. Erie is unknown, an upper limit for mixing rates cited in the literature was used (Denman and Gargett 1983). This, combined with water column and/or epilimnion depths constrained the scales of light climate variability that could be expected in the lake. No effects of mixing rate on $PI_{int}$ were observable over the possible range, so defined. The contrast with the results of the Antarctic study may, again, be related to the differing photoadaptive status and recovery rates of the phytoplankton in the two systems. In addition, however, the Antarctic study applied a kinetic model, that assumed no repair capabilities, so that photoinhibition was strictly a function of cumulative exposure to inhibiting radiation (*see* Chapter 3; Neale et al. 1998b). While the assumption of negligible recovery was justified for the Antarctic phytoplankton, L. Erie phytoplankton behave differently and are less sensitive to variations in mixing rate.

The extent of column-integrated inhibition will depend greatly on the spectral transmission properties of a given water body, especially in the damaging UVR waveband.

Generally, light attenuation will depend on light scattering and light absorption by water itself, dissolved organic matter and particulate organic (e.g. phytoplankton) and inorganic matter (Kirk 1994). Specific to UVR, dissolved organic matter seems to be particularly influential (Scully and Lean 1994) although total suspended solids can also be important (Smith et al. 1999). The three basins of L. Erie differ systematically in their transmission properties (*see* Chapter 2), so to demonstrate the dependence of predicted UVR impacts on transmission properties, without confounding effects of varying mixing depths, $PI_{int}$ was modelled for a 10m water column in each basin. The East and Central basins have relatively similar spectral transmission properties on average (Smith et al. 1999), and accordingly they had similar $PI_{int}$ predictions. The West basin, on the other hand, consistently showed higher $PI_{int}$ than the both East and Central basins.

The relatively greater inhibition in the turbid West basin may seem counter-intuitive, since less transparent waters might be expected to suffer less UVR-dependent inhibition. However, most studies have emphasized the role of dissolved organic matter in the attenuation of UVR and protection against inhibition (e.g. Granéli et al. 1996, Lindell et al. 1996, Williamson et al 1996), whereas, L. Erie is an example of a system in which suspended solids are an important influence on UVR transmission (e.g. Smith et al. 1999). The high concentration of total suspended solids in the West basin is associated with relatively shallow mean euphotic depths, but a relatively high proportion of the photic zone (1% PAR depth) receiving potentially significant UVR exposure (>1% surface incident). The pathlength that a photon will travel in water will depend partly on how it is scattered, which in turn will depend largely on its wavelength and on the characteristic dimensions of the scattering agents. While

the suspended particles size distribution in L. Erie is unknown, it has been shown that particles larger than photon wavelengths generally scatter light in the forward direction (Kirk 1994). Short UVR (295-400nm) wavelengths may be forward scattered more consistently than the longer wavelength PAR (400-700nm) photons in the West basin, thereby, proportionately increasing the UVR photic depth in this basin.

More realistic predictions of integrated photoinhibition, were made using basin-specific maximum depths and stratification patterns typical of spring and fall, i.e. complete uniform mixing, and the summer, i.e. thermal stratification. Given representative incident radiation spectra, two different stratification scenarios did not significantly alter the basin-specific pattern of $PI_{int}$ compared to the 10m mixed layer scenarios. The West basin was again the most vulnerable of the three. All three basins, however, showed slightly higher $PI_{int}$ predictions when the water column was completely mixed (spring and fall turnover). This may have important consequences for spring algal bloom production, since ozone losses over southern Canada are highest in the spring (Meteorological Service of Canada, 1999). Diatoms, which constitute a large proportion of the spring algal biomass, are not noted accumulators of UV-absorbing pigments (particularly the mycosporine-like amino acids, or MAAs; Davidson et al. 1994) but rather seem to use alternate mechanisms of UVR protection (Davidson and Marchant 1994). If diatoms have limited protection capabilities from UVR, the small modelled differences in integrated photoinhibition may actually be accentuated during the period of seasonal UVR enhancement.

The West basin not only differs in its spectral transmission properties but also in its thermal stratification structure (*see* Chapter 2). This basin commonly established shallow

'temporary' thermoclines on relatively calm and sunny days. Within a 1m 'shallow' thermocline, $PI_{int}$ attributed to UVR could be as much as 20%. Inhibition integrated over the entire water column for such situations was 16%, only a 4% increase of inhibition relative to an unstratified water column. Furthermore, under this same mixing scenario a simulated 20% decrease of stratospheric ozone increased $PI_{int}$ by only 1.2%. Ozone dependent increases in surface incident UVB fluxes had a minimal impact on our modelled $PI_{int}$ estimates. The only other study which used a similar kinetic and mixed water column approach showed similar minimal effects of ozone depletion, although, this response varied with algal UVR sensitivity (Neale et al. 1998c). Due to the non-linear nature of the kinetic model used, highly sensitive algal assemblages showed less additional inhibition due to ozone depletion.

The response of column-integrated inhibition to variations of sensitivity and recovery potential over the range observed in L. Erie phytoplankton showed that both are important determining factors in the overall response of these phytoplankton communities. Variations in recovery rates could cause a two-fold range in inhibition, while variations in sensitivity caused larger differences (approximately 3.5-fold). The importance of recovery rates was greatest in the simulated static water column, where phytoplankton were constrained to high PAR and UVR, especially UVA, exposures. Just below the surface, photoinhibition of primary production reached 67 and 38% of the optimum when recovery rates were low and high, respectively. Without any appreciable recovery potential or relief from high inhibiting radiation exposures via mixing processes, inhibition of primary production was maximal in the shallow surface waters. However, it should be noted that integrated photoinhibition in the low recovery rate and static water column scenario did not exceed that of any of the mixing scenarios. The

highest integrated cumulative photoinhibition recorded for a completely mixed water column was ca. 27% (PAR and UVR) (worst case scenario), yet at the end of the day, the lowest relative photosynthetic rate recorded was 0.93. Even at the slowest rates of recovery, photosynthetic potential would reach 95% full capacity within 3.4h. Although extensive (ca. 27%) production could be lost throughout the day, the ability to repair photosynthesis allowed for near complete recovery by the end of the simulated photoperiod. The predictions of integrated photoinhibition modelled using the R kinetic model are, therefore, reliable indicators of day to day effects of damaging UVR.

Constant across all simulations was the relatively minor PAR and UVB-attributed inhibition and the significant UVA-attributed inhibition, which confirms findings in several other aquatic systems (Bühlmann et al. 1987, Helbling et al. 1992, Neale et al. 1994). UVA has much lower photoinhibition efficiency than UVB because of its lower energetic content (e.g. Ghetti et al. 1998) but the flux of incident UVA is much greater than that of UVB. While the incident flux of UVA is not significantly altered by ozone depletion, its penetration into lakes is strongly influenced by dissolved organic carbon (DOC) content (Scully and Lean 1994) and suspended particle concentration (Smith et al. 1999), factors which are subject to significant anthropogenic disturbance. Increased air temperatures and lower precipitations due to global climate change, for example, have been linked to reduced DOC contents in temperate lakes (Schindler et al. 1992). Such influences may be more important in controlling UVR exposure and damage than is ozone depletion.

# Chapter 5

Conclusions

## General Conclusions

The primary goal of this study was to characterize the effects of UVR on the natural phytoplankton communities of Lake Erie. L. Erie is of interest because in recent years it has experienced increased water clarity due to nutrient input restrictions and the invasion of *Dreissena* sp. The possible increased penetration of UVR, coupled with the decreasing levels of stratospheric ozone and the associated increases in UVB radiation occurring in the northern mid-latitudes, have raised concerns over the possible consequences to primary production in this large lake.

As a first approach, a qualitative evaluation of the effects of UVB was conducted to determine if this waveband controls primary production in L. Erie. Time-series experiments revealed that indeed UVB could inhibit primary production in near-surface waters. In 8h simulated near-surface incubations, UVB exposure could suppress cumulative photosynthesis by as much as 58% (average 36%) and half of that inhibition was realized in the first hour of exposure. The rapid kinetics of UVB inhibition were underscored by the significantly higher UVB inhibition efficiency ($UVB_{inh\,eff}$) indices observed after 1h compared to 8h incubations. Inhibition of cumulative photosynthesis was milder in the 50% UVB (as well as PAR and UVA) showing 8.7 and 15.5% inhibition in the 1h and 8h incubations, respectively. Unfortunately, no relationship could be established between UVB inhibition and environmental parameters such as algal light history/adaptation and phytoplankton taxonomic composition. However, a higher susceptibility to UVB inhibition was noted for phosphorus (P) deficient mixed algal assemblages.

Inhibition by UVA was also investigated and while only partial UVA (short UVA)

effects could be quantified, in the absence of a UVA specific optical filter, suppression of cumulative photosynthesis by 21.6% and 12.4% in 1h and 8h exposures, respectively, could be attributed to UVA. In contrast to UVB inhibition, partial UVA effects decreased over time approximately by half. Furthermore, UVA inhibition remained appreciable in the 50% irradiance exposures (PAR and UVA), with cumulative inhibition maintained at ca. 20% and 10% in the 1h and 8h incubations, respectively.

These experiments showed that UVB can significantly inhibit photosynthesis in near-surface waters whereas its role at depth is relatively reduced. In addition, UVA emerged as a potentially important inhibitor of primary production even at depths where irradiance of this spectral waveband is reduced by half. Furthermore, the different kinetics of UVB and UVA photoinhibition suggests there are fundamental differences in their respective photosynthesis inactivation mechanisms. Alternatively, the various short term acclimation processes available to phytoplankton may be more effective in dealing with UVA than UVB damage.

The effect of UVR on production ($^{14}$C-labelled) in the dissolved (DOC) and particulate (POC) (<2 μm and >2 μm) organic carbon fractions was quantified after 8h incubations. The proportion of labelled DOC was significantly increased by exposure to UVB. The production in the picoplankton fraction of the POC pool was negatively impacted by both UVB and UVA, whereas the POC production in the larger phytoplankton was relatively higher in the presence of UVB. These effects were notable only at the higher exposure levels, that is, the treatment representative of near-surface incubations. The DOC and size specific (POC) effects observed in this study indicate that UVR exposure may have repercussions on aquatic food webs.

In L. Erie, PAR and UVR transmission properties are not homogeneous across the lake,

a rather distinct east-west spatial gradient exists, and inhibition of photosynthesis may indeed vary between basins. In fact, the turbid West basin was deemed more susceptible to UVR-attributed photoinhibition because the proportion of euphotic zone occupied by damaging UVR was found to be 50-60% higher in this part of the lake.

Having observed a significant effect of UVR in L. Erie, characterization of the kinetics of this inhibition was carried out to ultimately make reliable predictions of UVR-photoinhibition in the different basins of L. Erie. A first attempt at describing the kinetics of UVR photoinhibition was performed by applying known biological weighting functions (BWF) and using simple kinetic models available in the literature. The BWF used were derived from a marine diatom culture or from *in vitro* chloroplasts isolated from spinach, and the kinetic models used, one dependent on irradiance (E model) and the other on cumulative exposure (H model), had *a priori* assumptions about repair, either repair was in equilibrium with damage or it was assumed to be inactive.

These simpler models failed to adequately describe the kinetics of UVR-dependent photoinhibition, explaining in most cases less than 50% of the variance in the photosynthetic response. Examination of the residuals of the nonlinear regression fit of both the irradiance dependent and cumulative exposure models revealed that both irradiance and cumulative dose are important radiation parameters involved in the algal photoinhibitory response. The lack of fit of the photosynthetic data to these models was not attributable to the BWF used, since the application of two separate BWF of dissimilar shape did not change the trends in the residuals of the two models. This failure of conformity lead to the derivation of the first known BWFs specific to freshwater phytoplankton assemblages and the development of a new, more

applicable, kinetic model with explicit damage and repair components, the R model. This model explained, on average, 86% of variance in the photosynthetic response and in all but one instance, the R model indicated active recovery processes. The importance of considering rates of recovery when describing the kinetics of photoinhibition was demonstrated by the strong significant relationships observed between the estimated recovery rates (R model) and the amount of variance explained ($r^2$) by both the E and H models. As recovery rates increased so did the $r^2$ of the E model and the reverse relationship was true for the H model. All BWFs derived for L. Erie natural phytoplankton communities showed significant inhibition in the UVB and UVA portion of the spectrum, and 4 of these 5 derived showed a strong commonality in their relative shape when normalized to $\varepsilon_{R(300)}$.

The variability in both the recovery rate constants and the sensitivity to UVB of the different phytoplankton communities, indicated that overall sensitivity to UVB can be considered as having at least two components: 1) a susceptibility to damage component possibly influenced by the presence of photoprotective pigments and 2) an ability to recover component mediated by repair processes.

With the proper tools in hand, that is BWF specific to L. Erie phytoplankton assemblages and a kinetic model with no *a priori* assumption about repair, predictions of UVR- and PAR-dependent daily losses of integrated primary production in L. Erie could be made. The recovery rate estimates suggested complete recovery potential for phytoplankton in a mixed water column. Modelling various mixing scenarios revealed that integrated photoinhibition was relatively insensitive to mixing rates but rather water transmission properties were more important factors controlling UVR-dependent photoinhibition. The model

predicted higher integrated photoinhibition in the turbid West basin of L. Erie compared to the clearer East and Central basins. UVR inhibition in the West basin could potentially be exacerbated by the more frequent occurrence of shallow 'temporary' thermoclines in this basin. Under these severe conditions of exposure, total water column integrated UVR-photoinhibition was ca. 16%. Furthermore, inhibition due to a 20% ozone depletion resulted in a minimal 1.2% increased inhibition in integrated primary production. Inhibition of primary production due to UVR will likely fall within the range of 5-20% in natural freshwater ecosystems.

In conclusion, the role of UVB in photoinhibition is relatively minor compared to the inhibition potential of UVA. This latter waveband plays a dual role, that of photoinhibitor and as an inducer of photoenzymatic repair processes. The larger involvement of UVA in photoinhibition is due to its higher flux than UVB in the natural environment. Since it is UVB that is most significantly altered by ozone depletion, it is the transparency of aquatic systems to UVA which will likely influence integrated primary production. UVR transparency is greatly dependent on the dissolved organic carbon content of aquatic systems, and any changes to the input of DOC due, for example, to global climate change may be more important in controlling UVR-dependent photoinhibition that ozone depletion.

## Future Directions

The results of this study suggested that progress toward reliable predictions of the impacts of UVR on primary production is linked to improved knowledge of phytoplankton recovery kinetics. The shape of BWF, an indicator of damage at each UVR wavelength, was showed to be relatively constant between phytoplankton assemblages, and while the absolute magnitude of the effectiveness coefficients ($\varepsilon_{R(\lambda)}$) was variable, this could be accounted for by

estimating a damage constant ($k_1$) through non-linear regression. Variability in the recovery rate constants, however, are not as easily account for. While repetition of these experiments is feasible, they are labour intensive. More efforts should be directed towards developing simple and rapid tools as surrogate measures of recovery rates. For example, quantifying messenger RNA as an indicator of *de novo* protein synthesis (important process in repair) and relating that to photosynthetic recovery rate constants which can then be used in the R model. Similarly, the use of PAM fluorescence to quantify recovery rates of photosystem II could also be related to photosynthetic recovery rate constants. The availability of the BWF derived in this study and the possibility of easy measures of recovery rate constants suggest that relatively few spectral exposure treatments would be required to make reliable predictions of the effects of UVR on primary production.

# Chapter 6

Reference List

Armstrong, D. A. and Buchanan, J. D. 1978. Reactions of O2.-, H2O2 and other oxidants with sulfhydryl enzymes. *Photochemistry and Photobiology* 28: 743-755.

Asada, K. and Takahashi, M. 1987. Production and scavenging of active oxygen in photosynthesis. In *Photoinhibition*, ed. D.J. Kyle, C.B. Osmond and C.J. Arntzen, pp. 227-287. Elsevier Science Publishing.

Barnes, R. S. K. and Hughes, R. N. 1988. *An Introduction to Marine Ecology*. Blackwell Scientific Pub., London.

Bartish, T. 1987. A review of exchange processes among the three basins of Lake Erie. *Journal of Great Lakes Research* 13: 607-618.

Beaver, J. R. and Crisman, T. L. 1991. Temporal variability in algal biomass and primary productivity in Florida lakes relative to latitudinal gradients, organic color and trophic state. *Hydrobiologia* 224: 89-97.

Behrenfeld, M. J., Chapman, J. W., Hardy, J. T. and Lee II, H. 1993. Is there a common response to ultraviolet-B radiation by marine phytoplankton? *Marine Ecology Progress Series* 102: 59-68.

Bjørsen, P. K. 1988. Phytoplankton exudation of organic matter: *Why* do healthy cells do it? *Limnology and Oceanography* 33: 151-154.

Boelen, P., de Boer, M. K., Kraay, G. W., Veldhuis, M. J. W. and Buma, A. G. J. 2000. UVBR-induced DNA damage in natural marine picoplankton assemblages in the tropical Atlantic Ocean. *Marine Ecology Progress Series* 193: 1-9.

Bolsenga, S. J. and Herdendorf, C. E. 1993. Lake Erie and Lake St-Clair handbook. Detroit, Wayne State University Press.

Bothwell, M. L., Sherbot, D., Roberge, A. C. and Daley, R. J. 1993. Influence of natural

ultraviolet radiation on lotic periphyton diatom community growth, biomass accrual, and species composition: Short-tern versus long-term effects. *Journal of Phycology* 29: 24-35.

Boucher, N. P. and Prézelin, B. B. 1996. Spectral modeling of UV inhibition of *in situ* Antarctic primary production using a field-derived biological weighting function. *Photochemistry and Photobiology* 64: 407-418.

Buhlmann, B., Bossard, P. and Uehlinger, U. 1987. The influence of longwave ultraviolet radiation (u.v.-A) on the photosynthetic activity (14C-assimilation) of phytoplankton. *Journal of Plankton Research* 9: 935-943.

Buma, A. G. J., Zemmelink, H. J., Sjollema, K. and Gieskes, W. W. C. 1996. UVB radiation modifies protein and photosynthetic pigment content, volume and ultrastructure of marine diatoms. *Marine Ecology Progress Series* 142: 47-54.

Burns, N. M. 1985. Erie: the lake that survived. Totowa, Rowan and Allanheld.

Chamberlain, J. and Moss, S. H. 1987. Lipid peroxidation and other membrane damage produced in *Escherichia coli* K1060 by near-UV radiation and deuterium oxide. *Photochemistry and Photobiology* 45: 625-630.

Charlton, M. N., Milne, J. E., Booth, W. G. and Chiocchio, F. 1993. Lake Erie offshore in 1990: Restoration and resilience in the central basin. *Journal of Great Lakes Research* 19: 291-309.

Coohill, T. P. 1997. UV action spectra for marine phytoplankton. *Photochemistry and Photobiology* 65: 259-260.

Cullen, J. J. and Lesser, M. P. 1991. Inhibition of photosynthesis by ultraviolet radiation as a function of dose and dosage rate: results for a marine diatom. *Marine Biology* 111:

183-190.

Cullen, J. J. and Lewis, M. R. 1988. The kinetics of algal photoadaptation in the context of vertical mixing. *Journal of Plankton Research* 10: 1039-1063.

Cullen, J. J. and Neale, P. J. 1997. Biological weighting functions for describing the effects of ultraviolet radiation on aquatic systems. In *The Effects of Ozone Depletion on Aquatic Ecosystems*, ed. D.-P. Häder, pp. 97-118 R.G. Landes Company.

Cullen, J. J., Neale, P. J. and Lesser, M. P. 1992. Biological weighting function for the inhibition of phytoplankton photosynthesis by ultraviolet radiation. *Science* 258: 646-650.

Dahl, J. A., Graham, D. M., Dermott, R., Johannsson, O. E., Millard, E. S. and Myles, D. D. 1995. Lake Erie 1993, western, west central and eastern basins: Change in trophic status, and assessment of the abundance, biomass and production of the lower trophic levels . *Canadian Technical Report of Fisheries and Aquatic Sciences No. 2070* 118.

Davidson, A. T., Bramich, D., Marchant, H. J. and McMinn, A. 1994. Effects of UV-B irradiation on growth and survival of Antarctic marine diatoms. *Marine Biology* 119: 507-515.

Davidson, A. T. and Marchant, H. J. 1994. The impact of ultraviolet radiation on *Phaeocystis* and selected species of Antarctic marine diatoms. In *Ultraviolet Radiation in Antarctica: Measurements and Biological Effects. Antarctic Research Series, Volume 62*, ed. C.S. Weiler and P.A. Penhale, pp.187-205 Washington D.C., American Geophysical Union.

Denman, K. L. and Gargett, A. E. 1983. Time and space scales of vertical mixing and advection of phytoplankton in the upper ocean. *Limnology and Oceanography* 28: 801-

815.

Döhler, G. 1994. UV-effects on the nitrogen metabolism of marine phytoplankton and adaptation to UV radiation. In *Stratospheric Ozone Depletion/UV-B Radiation in the Biosphere*, ed. R.H. Biggs and M.E.B. Joyner. pp. 163-174. Berlin, Springer-Verlag.

Döhler, G., Worrest, R. C., Biermann, I. and Zink, J. 1987. Photosynthetic $^{14}CO_2$ fixation and [$^{15}$N]-ammonia assimilation during UV-B radiation of *Lithodesmium variabile*. *Physiologia Plantarum* 70: 511-515.

Fahnensteil, G. L., Chandler, J. F., Carrick, H. J. and Scavia, D. 1989. Photosynthetic characteristics of phytoplankton communities in Lakes Huron and Michigan: P-I parameters and end-products. *Journal of Great Lakes Research* 15: 394-407.

Fahnenstiel, G. L., Krause, A. E., McCormick, M. J., Carrick, H. J. and Schelske, C. L. 1998. The structure of the planktonic food-web in the St. Lawrence Great Lakes. *Journal of Great Lakes Research* 24: 531-554.

Falkowski, P. G. and Raven, J. A. 1997. *Aquatic Photosynthesis*. Oxford, Blackwell Science Ltd.

Fee, E. J., Hecky, R. E. and Welch, H. A. 1987. Phytoplankton photosynthesis parameters in central Canadian lakes. *Journal of Plankton Research* 9: 305-316.

Ferris, J. M. and Christian, R. 1991. Aquatic primary production in relation to microalgal responses to changing light: a review. *Aquatic Sciences* 53: 187-217.

Figueroa, F. L., Blanco, J. M., Jiménez-Gómez, F. and Rodriguez, J. 1997. Effects of ultraviolet radiation on carbon fixation in Antarctic nanophytoflagellates. *Photochemistry and Photobiology* 66: 185-189.

Franks, P. J. S. and Marra, J. 1994. A simple new formulation for phytoplankton

photoresponse and an application in a wind-driven mixed-layer model. *Marine Ecology Progress Series* 111: 143-153.

Furgal, J. A. and Smith, R. E. H. 1997. Ultraviolet radiation and photosynthesis by Georgian Bay phytoplankton of varying nutrient and photoadaptive status. *Canadian Journal of Fisheries and Aquatic Sciences* 54: 1659-1667.

Gala, W. R. and Giesy, J. P. 1991. Effects of ultraviolet radiation on the primary production of natural phytoplankton assemblages in Lake Michigan. *Ecotoxicology and Environmental Safety* 22: 345-361.

Gallegos, C. L., Platt, T., Harrison, W. G. and Irwin, B. 1983. Photosynthetic parameters of arctic marine phytoplankton: Vertical variations and time scales of adaptation. *Limnology and Oceanography* 28: 698-708.

Garcia-Pichel, F. 1994. A model for internal self-shading in planktonic organisms and its implications for the usefulness of ultraviolet sunscreens. *Limnology and Oceanography* 39: 1704-1717.

Ghetti, F., Fuoco, S. and Checcucci, G. 1998. UVB monochromatic action spectrum for the inhibition of photosynthetic oxygen production in the green alga *Dunaliella salina*. *Photochemistry and Photobiology* 68: 276-280.

Girotti, A. W. 1985. Mechanisms of lipid peroxidation. *Journal of Free Radicals in Biology and Medicine* 1: 87-95.

Goes, J. I., Handa, N., Taguchi, S. and Hama, T. 1994. Effect of UV-B radiation on the fatty acid composition of the marine phytoplankter *Tetraselmis* sp.: relationship to cellular pigments. *Marine Ecology Progress Series* 114: 259-274.

Graham, D. M., Dahl, J. A., Millard, E. S., Johannsson, O. E. and White, L. L. 1996.

Assessment of abundance, biomass and production of the lower trophic levels in the eastern basin of Lake Erie, 1994. *Canadian Technical Report of Fisheries and Aquatic Sciences* No. 2110: X+104 P.

Granéli, W., Lindell, M. J. and Tranvik, L. 1996. Photo-oxidative production of dissolved inorganic carbon in lakes of different humic content. *Limnology and Oceanography* 41: 698-706.

Greenberg, B. M., Gaba, V., Canaani, O., Malkin, S., Mattoo, A. K. and Edelman, M. 1989. Separate photosensitizers mediate degradation of the 32-kDa photosystem II reaction center protein in the visible and UV spectral regions. *Proceedings of the National Academy of Science USA* 86: 6617-6620.

Greenberg, B. M., Wilson, M. I., Huang, X.-D., Duxbury, C. L., Gerhardt, K. E. and Gensemer, R. W. 1997. The effects of ultraviolet-B radiation on higher plants. In *Plants for Environmental Studies,* ed. W. Wang, J.W. Gorsuch and J.S. Hughes, pp. 1-35. Boca Raton FL., CRC Press LLC.

Guildford, S. J., Hendzel, L. L., Kling, H. J., Fee, E. J., Robinson, G. G. C., Hecky, R. E. and Kasian, S. E. M. 1994. Effects of lake size on phytoplankton nutrient status. *Canadian Journal of Fisheries and Aquatic Sciences* 51: 2769-2783.

Häder, D. P. 1986. Effects of solar and artificial UV irradiation on motility and phototaxis in the flagellate, *Euglena gracilis*. *Photochemistry and Photobiology* 44: 651-656.

Häder, D.-P. 1994. UV-B effects on aquatic systems. In *Stratospheric Ozone Depletion/UV-B Radiation in the Biosphere,* ed. R.H. Biggs and M.E.B. Joyner pp. 155-161. Berlin, Springer-Verlag.

Häder, D.-P. and Tevini, M. 1987. General Photobiology. pp. 293-309. Great Britain,

Pergamon Press.

Halac, S., Felip, M., Camarero, L., Sommaruga-Wögrath, S., Psenner, R., Catalan, J. and Sommaruga, R. 1997. An *in situ* enclosure experiment to test the solar UVB impact on plankton in a high-altitude mountain lake. I. Lack of effect on phytoplankton species composition and growth. *Journal of Plankton Research* 19: 1671-1686.

Hanelt, D., Wiencke, C. and Nultsch, W. 1997. Influence of UV radiation on the photosynthesis of Arctic macroalgae in the field. *Journal of Photochemistry and Photobiology B: Biology* 38: 40-47.

Hannach, G. and Sigleo, A. C. 1998. Photoinduction of UV-absorbing compounds in six species of marine phytoplankton. *Marine Ecology Progress Series* 174: 207-222.

Harris, G. P. 1986. *Phytoplankton Ecology: Structure, Function and Fluctuation* Chapman and Hall, London.

Hays, J. B. & Pang, Q. 1994. UV-B-inducible and constitutive genes that mediate repair and toleration of UV-damaged DNA in the plant *Arabidopsis thaliana*. In *Stratospheric Ozone Depletion/UV-B Radiation in the Biosphere*, (Ed.) R.H. Biggs and M.E.B. Joyner. Berlin, Springer-Verlag, pp. 107-122..

Hazzard, C., Lesser, M. P. and Kinzie III, R. A. 1997. Effects of ultraviolet radiation on photosynthesis in the subtropical marine diatom, *Chaetoceros gracilis* (Bacillariophyceae). *Journal of Phycology* 33: 960-968.

Healey, F. P. and Hendzel, L. L. 1979. Indicators of phosphorus and nitrogen deficiency in five algae in culture. *Journal of the Fisheries Research Board of Canada* 36: 1364-1369.

Helbling, E. W., Villafañe, V., Ferrario, M. and Holm-Hansen, O. 1992. Impact of natural ultraviolet radiation on rates of photosynthesis and on specific marine phytoplankton

species. *Marine Ecology Progress Series* 80: 89-100.

Helbling, E. W., Villafañe, V. and Holm-Hansen, O. 1994. Effects of ultraviolet radiation on Antarctic marine phytoplankton photosynthesis with particular attention to the influence of mixing. In *Ultraviolet Radiation in Antarctica: Measurements and Biological Effects. Antarctic Research Series, Volume 62*, ed. C.S. Weiler and P.A. Penhale, pp.207-227. Washington D.C., American Geophysical Union.

Herrmann, H., Häder, D.-P. and Ghetti, F. 1997. Inhibition of photosynthesis by solar radiation in *Dunaliella salina*: Relative efficiencies of UV-B, UV-A and PAR. *Plant Cell and Environment* 20: 359-365.

Hessen, D. O., De Lange, H. J. and Van Donk, E. 1997. Uv-induced changes in phytoplankton cells and its effects on grazers. *Freshwater Biology* 38: 513-524.

Holland, R. E. 1993. Changes in planktonic diatoms and water transparency in Hatchery Bat, Bass Island area, Western Lake Erie since the establishment of the zebra mussel. *Journal of Great Lakes Research* 19: 617-624.

HPS Inc. 1998. Stella® Version 5.1.1 for Windows™.

Ihle, C. 1997. Degradation and release from the thylakoid membrane of Photosystem II subunits after UV-B irradiation of the liverwort *Conocephalum conicum*. *Photosynthesis Research* 54: 73-78.

Jewson, D. H. 1976. The interaction of components controlling net phytoplankton photosynthesis in a well-mixed lake (Lough Neagh, Northern Ireland). *Freshwater Biology* 6: 551-576.

Jones, L. W. and Kok, B. 1966. Photoinhibition of chloroplast reactions. I. Kinetics and action spectra. *Plant Physiology* 41: 1037-1043.

Karentz, D. 1999. Evolution and ultraviolet light tolerance in algae. *Journal of Phycology* 35: 629-630.

Karentz, D., Bothwell, M. L., Coffin, R. B., Hanson, A., Herndl, G. J., Kilhamn, S. S., Lesser, M. P., Lindell, M., Moeller, R. E., Morris, D. P., Neale, P. J., Sanders, R. W., Weiler, C. S. and Wetzel, R. G. 1994. Impact of UV-B radiation on pelagic freshwater ecosystems: Report of working group on bacteria and phytoplankton. *Arch. Hydrobiol. Beiht Ergebn. Limnol.* 43: 31-69.

Karentz, D., Cleaver, J. E. and Mitchell, D. L. 1991a. Cell survival characteristics and molecular responses of Antarctic phytoplankton to ultraviolet-B radiation. *Journal of Phycology* 27: 326-341.

Karentz, D., McEuen, F. S., Land, M. C. and Dunlap, W. C. 1991b. Survey of mycosporine-like amino acid compounds in Antarctic marine organisms: potential protection from ultraviolet exposure. *Marine Biology* 108: 157-166.

Karentz, D. and Spero, H. J. 1995. Response of a natural *Phaeocystis* population to ambient fluctuations of UVB radiation caused by Antarctic ozone depletion. *Journal of Plankton Research* 17: 1771-1789.

Kerr, J. B. and McElroy, C. T. 1993. Evidence for large upward trends of ultraviolet-B radiation linked to ozone depletion. *Science* 262: 1032-1034.

Kim, D.-S. and Watanabe, Y. 1993. The effect of long wave ultraviolet radiation (UV-A) on the photosynthetic activity of natural population of freshwater phytoplankton. *Ecological Research* 8: 225-234.

Kinzie III, R. A., Banaszak, A. T. and Lesser, M. P. 1998. Effects of ultraviolet radiation on primary productivity in a high altitude tropical lake. *Hydrobiologia* 385: 23-32.

Kirk, J. T. O. 1994. Optics of UV-B radiation in natural waters. *Arch. Hydrobiol. Beih. Ergebn. Limnol.* 43: 1-16.

Kondratyev, K. Y. and Varotsos, C. A. 1996. Impact of surface solar ultraviolet radiation variability and ecosystems. *Environmental Science and Pollution Research* 3: 153-157.

Kramer, G. F., Norman, H. A., Krizek, D. T. and Mirecki, R. M. 1991. Influence of UV-B radiation on polyamines, lipid peroxidation and membrane lipids in cucumber. *Phytochemistry* 30: 2101-2108.

Lampert, W. and Sommer, U. 1997. *Limnoecology: The Ecology of Lakes and Streams.* Oxford University Press, New York.

Larkum, A. W. D. and Wood, W. F. 1993. The effect of UV-B radiation on photosynthesis and respiration of phytoplankton, benthic macroalgae and seagrasses. *Photosynthesis Research* 36: 17-23.

Laurion, I. and Vincent, W. F. 1998. Cell size versus taxonomic composition as determinants of UV-sensitivity in natural phytoplankton communities. *Limnology and Oceanography* 43: 1774-1779.

Lesser, M. P. 1996. Acclimation of phytoplankton to UV-B radiation: Oxidative stress and photoinhibition of photosynthesis are not prevented by UV-absorbing compounds in the dinoflagellate *Prorocentrum micans*. *Marine Ecology Progress Series* 132: 287-297.

Lesser, M. P., Cullen, J. J. and Neale, P. J. 1994. Carbon uptake in a marine diatom during acute exposure to ultraviolet B radiation: relative importance of damage and repair. *Journal of Phycology* 30: 183-192.

Lesser, M. P. and Shick, J. M. 1989. Effects of irradiance and ultraviolet radiation on

photoadaptation in the zooxanthellae of *Aiptasia pallida*: Primary production, photoinhibition and enzymic defenses against oxygen toxicity. *Marine Biology* 102: 243-255.

Lignell, R. 1990. Excretion of organic carbon by phytoplankton: its relation to algal biomass, primary productivity and bacterial secondary productivity in the Baltic Sea. *Marine Ecology Progress Series* 68: 85-99.

Lindell, M. J., Granéli, H. W. and Tranvik, L. J. 1996. Effects of sunlight on bacterial growth in lakes of different humic content. *Aquatic Microbial Ecology* 11: 135-141.

Lindell, M. J., Granéli, W. and Tranvik, L. J. 1995. Enhanced bacterial growth in response to photochemical transformation of dissolved organic matter. *Limnology and Oceanography* 40: 195-199.

Lubin, D., Frederick, J. E., Booth, C. R., Lucas, T. and Neuschuler, D. 1989. Measurements of enhanced springtime ultraviolet radiation at Palmer Station, Antarctica. *Geophysical Research Letters* 16: 783-785.

Madariaga, I. and Joint, I. 1994. Photosynthesis and carbon metabolism by size-fractionated phytoplankton in the southern North Sea in early summer. *Continental Shelf Research* 14: 295-311.

Mague, T. H., Friberg, E., Hughes, D. J. and Morris, I. 1980. Extracellular release of carbon by marine phytoplankton; a physiological approach. *Limnology and Oceanography* 25: 262-279.

Makarewicz, J. C. 1991. Photosynthetic parameters as indicators of ecosystem health. *Journal of Great Lakes Research* 17: 333-343.

Marwood, C. A., Smith, R. E. H., Furgal, J. A., Charlton, M. N., Solomon, K. R. and

Greenberg, B. M. 2000. Photoinhibition of natural phytoplankton populations in Lake Erie exposed to solar ultraviolet radiation. *Canadian Journal of Fisheries and Aquatic Sciences*.

Meteorological Service of Canada. 1999. The ozone layer. *Environment Canada World Wide Web Site, Url: Cd/factsheets/ozone/*.

Mishra, R. K. and Singhal, G. S. 1992. Function of photosynthetic apparatus of intact wheat leaves under high light and heat stress and its relationship with peroxidation of thylakoid lipids. *Plant Physiology* 98: 1-6.

Mitchell, D. L. and Karentz, D. 1993. The induction and repair of DNA photodamage in the environment. In *Environmental UV Photobiology*. ed. A.R. Young et al. Plenum Press, New York, pp. 345-377.

Miyake, C., Michihata, F. and Asada, K. 1991. Scavenging of hydrogen peroxide in prokaryotic and eukaryotic algae: Acquisition of ascorbate peroxidase during the evolution of cyanobacteria. *Plant Cell Physiology* 32: 33-43.

Molina, L. T. and Molina, M. J. 1986. Absolute absorption cross sections of ozone in the 185- to 350-nm wavelength range. *Journal of Geophysical Research* 91: 14501-14508.

Molina, M. & Rowland, F. S. 1974. Stratospheric sink for chlorofluoromethanes: chlorine atom-catalysed destruction of ozone. *Nature* 249: 810-812.

Mopper, K. & Kieber, D. J. 2000. Marine photochemistry and its impact on carbon cycling. In *The Effects of UV Radiation in the Marine Environment*, Ed. S. J. De Mora, S. Demers and M. Vernet, pp. 101-129. Cambridge University Press, Cambridge.

Morris, I. 1980. The Physiological Ecology of Phytoplankton. London, Blackwell Scientific Publications, pp.625.

Mortimer, C. H. 1987. Fifty years of physical investigations and related limnological studies on Lake Erie, 1928-1977. *Journal of Great Lakes Research* 13: 407-435.

Mostajir, B., Demers, S., de Mora, S., Belzile, C., Chanut, J.-P., Gosselin, M., Roy, S., Zulema Villegas, P., Fauchot, J., Bouchard, J., Bird, D., Monfort, P. and Levasseur, M. 1999. Experimental test of the effect of ultraviolet-B radiation in a planktonic community. *Limnology and Oceanography* 44: 586-596.

Neale, P. J. 2000. Spectral weighting functions for quantifying effects of UV radiation in marine ecosystems. In *The Effects of UV Radiation in the Marine Environment*, ed. S. J. De Mora, S. Demers and M. Vernet, pp. 72-100. Cambridge University Press, Cambridge.

Neale, P. J., Banaszak, A. T. and Jarriel, C. R. 1998a. Ultraviolet sunscreens in *Gymnodinium sanguineum* (Dinophyceae): Mycosporine-like amino acids protect against inhibition of photosynthesis. *Journal of Phycology* 34: 928-938.

Neale, P. J., Cullen, J. J. and Davis, R. F. 1998b. Inhibition of marine photosynthesis by ultraviolet radiation: Variable sensitivity of phytoplankton in the Weddell-Scotia Confluence during the austral spring. *Limnology and Oceanography* 43: 433-448.

Neale, P. J., Davis, R. F. and Cullen, J. J. 1998c. Interactive effects of ozone depletion and vertical mixing on photosynthesis of Antarctic phytoplankton. *Nature(London)* 392: 585-589.

Neale, P. J., Lesser, M. P. and Cullen, J. J. 1994. Effects of ultraviolet radiation on the photosynthesis of phytoplankton in the vicinity of McMurdo Station, Antarctica. In *Ultraviolet Radiation in Antarctica: Measurements and Biological Effects. Antarctic Research Series, Volume 62*, ed. C.S. Weiler and P.A. Penhale, Washington D.C.,

American Geophysical Union. pp.125-142.

Norrman, B., Zweifel, U. L., Hopkinson Jr., C. S. and Fry, B. 1995. Production and utilization of dissolved organic carbon during an experimental diatom bloom. *Limnology and Oceanography* 40: 898-907.

Ohad, I., Kyle, D. J. & Arntzen, C. J. 1984. Membrane protein damage and repair: Removal and replacement of inactivated 32-kilodalton polypeptides in chloroplast membranes. *Journal of Cell Biology* 99: 481-485.

Palenik, B., Price, N. M. and Morel, F. M. M. 1991. Potential effects of UV-B on the chemical environmental of marine organisms: A review. *Environmental Pollution* 70: 117-130.

Pang, Q. and Hays, J. B. 1991. UV-B inducible and temperature-sensitive photoreactivation of cyclobutane pyrimidine dimers in *Arabidopsis thaliana*. *Plant Physiology* 95: 536-543.

Pausz, C. and Herndl, G. J. 1999. Role of ultraviolet radiation on phytoplankton extracellular release and its subsequent utilization by marine bacterioplankton. *Aquatic Microbial Ecology* 18: 85-93.

Platt, T., Gallegos, C. L. and Harrison, W. G. 1980. Photoinhibition of photosynthesis in natural assemblages of marine phytoplankton. *Journal of Marine Research* 38: 687-701.

Prézelin, B. B. and Boucher, N. P. 1994. Marine primary production under the influence of the Antarctic ozone hole: Icecolors '90. In *Ultraviolet Radiation in Antarctica: Measurements and Biological Effects. Antarctic Research Series, Volume 62*, ed. C.S. Weiler and P.A. Penhale pp.159-186. Washington D.C., American Geophysical Union.

Prézelin, B. B., Boucher, N. P. and Schofield, O. 1994. Evaluation of field studies of UVB radiation effects on Antarctic marine primary productivity. In *Stratospheric Ozone*

*Depletion/UV-B Radiation in the Biosphere*, ed. R.H. Biggs and M.E.B. Joyner, pp. 181-194. Berlin, Springer-Verlag.

Quesada, A., Mouget, J.-L. and Vincent, W. F. 1995. Growth of antarctic cyanobacteria under ultraviolet radiation: UVA counteracts UVB inhibition. *Journal of Phycology* 31: 242-248.

Quesada, A. and Vincent, W. F. 1997. Strategies of adaptation by Antarctic cyanobacteria to ultraviolet radiation. *European Journal of Phycology* 32: 335-342.

Raven, J. A. and Samuelson, G. 1986. Repair of photoinhibitory damage in *Anacystis nidulans* 625 (*Synechococcus* 6301): Relation to catalytic capacity for, and energy supply to, protein synthesis, and implications for $\mu_{max}$ and the efficiency of light-limited growth. *New Phytologist* 103: 625-643.

Reynolds, C. S. 1989. Physical determinants of phytoplankton succession. In *Plankton Ecology: Succession in Plankton Communities*, ed. U. Sommer, pp. 9-56. Springer-Verlag, Berlin.

------. 1984. Phytoplankton periodicity: The interactions of form, function and environmental variability. *Freshwater Biology* 14: 111-142.

Roy, S. 2000. Strategies for the minimisation of UV-induced damage. In *The Effects of UV Radiation in the Marine Environment*, ed. S. J. De Mora, S. Demers and M. Vernet, pp. 177-205. Cambridge University Press, Cambridge.

Rüdiger, W. and López-Figueroa, F. 1992. Photoreceptors in algae. *Photochemistry and Photobiology* 55: 949-954.

Schindler, D. W., Bayley, S. E., Curtis, P. J., Parker, B. R., Stainton, M. P. and Kelly, C. A. 1992. Dissolved organic matter in lacustrine ecosystems: Energy source and system

regulator. *Hydrobiologia* 229: 1-21.

Schindler, D. W., Curtis, P. J., Parker, B. R. and Stainton, M. P. 1996. Consequences of climate warming and lake acidification for UV-B penetration in North American boreal lakes. *Nature* 379: 705-708.

Schofield, O., Kroon, B. M. A. and Prézelin, B. B. 1995. Impact of ultraviolet-B radiation on photosystem II activity and its relationship to the inhibition of carbon fixation rates for antarctic ice algae communities. *Journal of Phycology* 31: 703-715.

Scully, N. M. and Lean, D. R. S. 1994. The attenuation of ultraviolet radiation in temperate lakes. *Arch. Hydrobiol. Beih. Ergebn. Limnol.* 43: 135-144.

Senft, W. H. 1978. Dependence of light-saturated rates of algal photosynthesis on intracellular concentrations of phosphorus. *Limnology and Oceanography* 23: 709-718.

Setlow, R. B. 1974. The wavelengths in sunlight effective in producing skin cancer: A theoretical analysis. *Proceedings of the National Academy of Science USA* 71: 3363-3366.

Shirley, B. W. 1996. Flavonoid biosynthesis: 'new' functions for an 'old' pathway. *Trends in Plant Science* 1: 377-382.

Sinha, R. P., Klisch, M., Gröniger, A. and Häder, D.-P. 1998. Ultraviolet-absorbing/screening substances in cyanobacteria, phytoplankton and macroalgae. *Journal of Photochemistry and Photobiology B: Biology* 47: 83-94.

Smetacek, V. and Passow, U. 1990. Spring bloom initiation and Sverdrup's critical depth model. *Limnology and Oceanography* 35: 228-232.

Smith, R. C. and Cullen, J. J. 1995. Effects of UV radiation on phytoplankton. *Reviews of Geophysics* 33: 1211-1223.

Smith, R. C., Prézelin, B. B., Baker, K. S., Bidigare, R. R., Boucher, N. P., Coley, T., Karentz, D., MacIntyre, S., Matlick, H. A., Menzies, D., Ondrusek, M., Wan, Z. and Waters, K. J. 1992. Ozone depletion: Ultraviolet radiation and phytoplankton biology in Antarctic waters. *Science* 255: 953-959.

Smith, R. E. H., Furgal, J. A., Charlton, M. N., Greenberg, B. M., Hiriart, V. and Marwood, C. 1999. The attenuation of ultraviolet radiation in a large lake with low dissolved organic matter concentrations. *Canadian Journal of Fisheries and Aquatic Sciences*.

Smith, R. E. H., Furgal, J. A. and Lean, D. R. S. 1998. The short-term effects of solar ultraviolet radiation on phytoplankton photosynthesis and photosynthate allocation under contrasting mixing regimes in Lake Ontario. *Journal of Great Lakes Research* 24: 427-441.

Smith, R. E. H. and Maly, J. A. 1993. Photosynthetic carbon assimilation and allocation by surface and deep phytoplankton in Colpoys Bay (western Georgian Bay). *Canadian Journal of Fisheries and Aquatic Sciences* 50: 2235-2244.

Smith, R. E. H. and Platt, T. 1984. Carbon exchange and $^{14}C$ tracer methods in a nitrogen-limited diatom, *Thalassiosira pseudonana*. *Marine Ecology Progress Series* 16: 75-87.

Sommaruga, R., Sattler, B., Oberleiter, A., Wille, A., Wögrath-Sommaruga, S., Psenner, R., Felip, M., Camarero, L., Oina, S., Gironés, R. and Catalán, J. 1999. An *in situ* enclosure experiment to test the solar UVB impact on plankton in a high-altitude mountain lake. II. Effects on the microbial food web. *Journal of Plankton Research* 21: 859-876.

SPSS Inc. 1997. Systat® 7.0 for Windows®. Standard Version.

Stolarski, R., Bojkov, R., Bishop, L., Zerefos, C., Staehelin, J. and Zawodny, J. 1992.

Measured trends in stratospheric ozone. *Science* 256: 342-349.

Tevini, M. 1993. Molecular biological effects of ultraviolet radiation. *Book* Lewis Publishers.

Thingstad, T. F., Hagström, Å. and Rassoulzadegan, F. 1997. Accumulation of degradable DOC in surface waters: Is it caused by a malfunctioning microbial loop? *Limnology and Oceanography* 42: 398-404.

Tilzer, M. M. 1990. Environmental and physiological control of phytoplankton productivity in large lakes. In *Large Lakes: Ecological Structure and Function,* ed. M.M. Tilzer and C. Serruya, pp. 339-367. Springer-Verlag, Berlin.

Tilzer, M. M. and Beese, B. 1988. The seasonal productivity cycle of phytoplankton and controlling factors in Lake Constance. *Schweiz. Z. Hydrol.* 50: 1-45.

Tranvik, L. and Kokalj, S. 1998. Decreased biodegradability of algal DOC due to interactive effects of UV radiation and humic matter. *Aquatic Microbial Ecology* 14: 301-307.

U.S. EPA. 1998. 1997 National Air Quality: Status and Trends. *U.S. EPA World Wide Web Site. Url: Www.Epa.Gov/Oar/Aqtrnd97/Brochure/Glblwrm.Html.*

Valiela, I. 1984. *Marine Ecology Processes. Springer-Verlag, Berlin.*

Vernet, M. 2000. Effects of UV radiation on the physiology and ecology of marine phytoplankton. In *The Effects of UV Radiation in the Marine Environment,* ed. S. J. De Mora, S. Demers and M. Vernet, pp. 237-278. Cambridge University Press, Cambridge.

Villafañe, V. E., Helbling, E. W., Holm-Hansen, O. and Chalker, B. E. 1995. Acclimatization of Antarctic natural phytoplankton assemblages when exposed to solar ultraviolet radiation. *Journal of Plankton Research* 17: 2295-2306.

Vincent, W. F. and Neale, P. J. 2000. Mechanisms of UV damage to aquatic organisms. In *The Effects of UV Radiation in the Marine Environment,* ed. S. J. De Mora, S. Demers and

M. Vernet, pp. 149-176. Cambridge University Press, Cambridge.

Vincent, W. F. and Quesada, A. 1994. Ultraviolet radiation effects on cyanobacteria: Implications for antarctic microbial ecosystems. In *Ultraviolet Radiation in Antarctica: Measurements and Biological Effects Antarctic Research Series, Volume 62*. ed. C.S. Weiler and P.A. Penhale pp. 111-124. American Geophysical Union.

Vincent, W. F. and Roy, S. 1993. Solar ultraviolet-B radiation and aquatic primary production: damage, protection, and recovery. *Environment Review* 1: 1-12.

Wang, K. S. and Chai, T. 1994. Reduction of omega-3 fatty acids by UV-B irradiation in microalgae. *Journal of Applied Phycology* 6: 415-421.

Wängberg, S.-Å., Selmer, J.-S. and Gustavson, K. 1996. Effects of UV-B radiation on biomass and composition in marine phytoplankton communities. *Scientia Marina* 60: 81-88.

Weiler, C. S. and Penhale, P. A. 1994. Ultraviolet radiation in Antarctica: Measurements and biological effects. Washington, D.C., American Geophysical Union.

Wetzel, R. G. 1992. Gradient-dominated ecosystems: Sources and regulatory functions of dissolved organic matter in freshwater ecosystems. *Hydrobiologia* 229: 181-198.

Whitehead, R. F., de Mora, S. J. and Demers, S. 2000. Enhanced UV radiation - a new problem for the marine environment. In *The Effects of UV Radiation in the Marine Environment*, ed. S. J. De Mora, S. Demers and M. Vernet, pp. 1-34. Cambridge University Press, Cambridge.

Wilhelm, S. W. and Smith, R. E. H. 2000. Bacterial carbon production in Lake Erie is influenced by viruses and solar radiation. *Canadian Journal of Fisheries and Aquatic Sciences* 57: 317-26.

Williams, P. J. l. B. 1990. The importance of losses during microbial growth: commentary on

the physiology, measurement and ecology of the release of dissolved organic material. *Marine Microbial Food Webs* 4: 175-206.

Williamson, C. E. 1995. What role does UV-B radiation play in freshwater ecosystems? *Limnology and Oceanography* 40: 386-392.

Williamson, C. E., Stemberger, R. S., Morris, D. P., Frost, T. M. and Paulsen, S. G. 1996. Ultraviolet radiation in North American lakes: Attenuation estimates from DOC measurements and implications for plankton communities. *Limnology and Oceanography* 41: 1024-1034.

Wilson, M. I., Ghosh, S., Gerhardt, K. E., Holland, N., Babu, T. S., Edelman, M., Dumbroff, E. B. and Greenberg, B. M. 1995. *In vivo* photomodification of ribulose-1,5-bisphosphate carboxylase/oxygenase holoenzyme by ultraviolet-B radiation. *Plant Physiology* 109: 221-229.

Worrest, R. C., Thomson, B. E. and Van Dyke, H. 1981. Impact of UV-B radiation upon estuarine microcosms. *Photochemistry and Photobiology* 33: 861-867.

Xenopoulos, M. A., Prairie, Y. T. and Bird, D. F. 2000. Influence of ultraviolet-B radiation, stratospheric ozone variability, and thermal stratification on the phytoplankton biomass dynamics in a mesohumic lake. *Canadian Journal of Fisheries and Aquatic Sciences* 57: 600-609.

Xiong, F., Komenda, J., Kopecky, J. and Nedbal, L. 1997. Strategies of ultraviolet-B protection in microscopic algae. *Physiologia Plantarum* 100: 378-388.

Yan, N. D., Keller, W., Scully, N. M., Lean, D. R. S. and Dillon, P. J. 1996. Increased UV-B penetration in a lake owing to drought-induced acidification. *Nature* 381: 141-143.

Zagarese, H. E., Tartarotti, B., Cravero, W. and Gonzalez, P. 1998. UV damage in shallow

lakes: The implications of water mixing. *Journal of Plankton Research* 20: 1423-1433.